Naval Surface Warfare Center
Carderock Division
West Bethesda, Maryland 20817- 5700

NSWCCD-50-TR-2012/035 July 2012
Hydromechanics Department Report

Model-Scale Experiment of the Seakeeping Performance for R/V *Melville, Model 5720*

By

Lisa M. Minnick
Lauren. W. Hanyok
Heather A. Tomaszek
Mark P. Melendez
Charles R. Turner
Joel T. Park
Vadim Belenky
Christopher C. Bassler

REPORT DOCUMENTATION PAGE

Form Approved
OMB No. 0704-0188

1. REPORT DATE *(DD/MM/YYYY)*	**2. REPORT TYPE**	**3. DATES COVERED** *(From - To)*
30-06-2012	Final	1-Oct-2011 – 31-May-2012

4. TITLE AND SUBTITLE
Model-Scale Experiment of the Seakeeping Performance for R/V Melville, Model 5720

5a. CONTRACT NUMBER

5b. GRANT NUMBER

5c. PROGRAM ELEMENT NUMBER
0602236N

6. AUTHOR(S)

Lisa M. Minnick, Lauren W. Hanyok, Mark P. Melendez, Heather A. Tomaszek, Charles R. Turner, Joel T. Park, Vadim Belenky, and Christopher C. Bassler

5d. PROJECT NUMBER

5e. TASK NUMBER

5f. WORK UNIT NUMBER
100000539505/0010,0110,0120

7. PERFORMING ORGANIZATION NAME(S) AND ADDRESS(ES) AND ADDRESS(ES)

Naval Surface Warfare Center
Carderock Division
9500 Macarthur Boulevard
West Bethesda, MD 20817-5700

8. PERFORMING ORGANIZATION REPORT NUMBER

NSWCCD-50-TR-2012/035

9. SPONSORING / MONITORING AGENCY NAME(S) AND ADDRESS(ES)

Dr. Paul Hess
Office of Naval Research, ONR 331
Ballston Center Tower One
800 North Quincy Street
Arlington, VA 22217-5660

10. SPONSOR/MONITOR'S ACRONYM(S)
ONR

11. SPONSOR/MONITOR'S REPORT NUMBER(S)

12. DISTRIBUTION / AVAILABILITY STATEMENT
Approved for public release; distribution is unlimited.

13. SUPPLEMENTARY NOTES

14. ABSTRACT

An experiment was performed in the Maneuvering and Seakeeping (MASK) basin at the Naval Surface Warfare Center Carderock Division (NSWCCD) to provide time-synchronized model ship motion and wave measurement data, at moderate speeds, of the R/V Melville. Model 5720, representing R/V Melville, was designed and constructed at NSWCCD and experiments were performed to assess seakeeping in regular and uni-directional irregular waves. This report details the data obtained from this experiment and presents some analysis, including standard time-series statistical parameters and Response Amplitude Operators (RAOs) for both regular and irregular wave conditions. A comprehensive data set, analysis, and supporting documentation accompanies this report in the form of a data CD.

15. SUBJECT TERMS
Ship Motions, Seakeeping, Environmental Forecasting, Wave Measurements, Time-Domain Predictions, Deterministic Ship Motions

16. SECURITY CLASSIFICATION OF:			**17. LIMITATION OF ABSTRACT**	**18. NUMBER OF PAGES**	**19a. NAME OF RESPONSIBLE PERSON**
a. REPORT	**b. ABSTRACT**	**c. THIS PAGE**			Christopher C. Bassler
UNCLASSIFIED	UNCLASSIFIED	UNCLASSIFIED	UL	109	**19b. TELEPHONE NUMBER** *(include area code)* (301) 227-5926

CONTENTS

ABSTRACT 1

ADMINISTRATIVE INFORMATION 1

ACKNOWLEDGEMENTS 1

INTRODUCTION AND BACKGROUND 1

Objectives 2

FACILITIES 2

MASK Basin 2

Wave Generation 4

Tracking System 4

MODEL DESCRIPTION 4

Hull Geometry 5

Model Geometry Modifications Made During Testing 9

Model Propulsion 10

Model Control 12

MASK Carriage Operations with a Tethered Model 12

Model Ballasting 12

INSTRUMENTATION 16

Model Motion Sensors 20

Vertical Gyro 20

Microstrain Gyro Enhanced Orientation Sensor 20

Rate Gyro 20

Accelerometer 21

Model Control Sensors 21

Shaft Speed 21

Steering Angle 21

Compass 21

Speed Through Water 21

Speed Over Ground 22

Model Tracking System 22

Wave Environment Sensors 23

Data Acquisition 24

Video 25

EXPERIMENTAL METHODS 25
Wave-maker Settings 25
Roll Decay 25
Speed Calibration 26
Seakeeping in Regular Waves 26
Seakeeping in Irregular Waves 27
MEASUREMENT UNCERTAINTY ANALYSIS 30
Model Instrumentation Summary 30
Wave Height 31
Correction for Zeroes 32
DATA INTERPRETATION 35
Data Files 35
Model and Carriage Data (*.tmq Files) 35
Tracker Data (.TTQ Files) 36
Bridge Wave Data (.TWQ Files) 36
Coordinate Systems 39
Relative Wave Heading 45
EXPERIMENTAL RESULTS AND DATA ANALYSIS 45
Wave-maker Settings 45
Roll Decay 47
Seakeeping in Regular Waves 48
Standard Runs vs. Transient Runs 49
Statistical Analysis 50
Response Amplitude Operators (RAOs) 51
Seakeeping in Irregular Waves 54
Statistical Analysis 54
Achieved Wave Spectra 56
Response Amplitude Operators (RAOs) 59
Statistical Uncertainty 60
SUMMARY 61
APPENDIX A: MEASUREMENT UNCERTAINTY THEORY AND DETAILS 63
Theory 63
Accelerations 65
Tilt Table 65
Acceleration Calibration by Inclination 65

Uncertainty in Acceleration 66
Columbia Triaxial Accelerometer 66
Local Acceleration of Gravity 67
Pitch and Roll Angle 67
Rosemount/Goodrich 67
MicroStrain 67
Pod Steering Angle 68
Shaft Speed and Signet Paddlewheel Flow Sensor 68
Shaft Speed 68
Speed through Water (STW) 69
Model Speed from Shaft Speed 70
MASK Carriage Speed 70
Rate Sensors 71
Battery Voltage Monitors 71
APPENDIX B: DATA CD FILE SRUCTURE 83
APPENDIX C: EXAMPLE DATA SETS 85
APPENDIX D: IRREGULAR WAVE ROLL AND PITCH RAOs 89
APPENDIX E: STATISTICAL UNCERTAINTY ANALYSIS 95
General Considerations 95
Estimate of the Autocorrelation Function 95
Averaged Spectrum 97
Cut-Off Procedure for Estimate of Autocorrelation Function 98
Comparison of Spectra 100
Calculation of Autocorrelation Function from Spectrum 100
Statistical Uncertainty of the Average and Variance of a Record 101
Statistical Uncertainty of Average and Variance of an Ensemble 104
REFERENCES 107

This page intentionally left blank

FIGURES

Figure 1. Photograph of the R/V Melville. 2
Figure 2. Maneuvering and Seakeeping basin (MASK) at NSWCCD. 3
Figure 3. Laser scan results of Model 5720. Red and blue coloring show areas outside of the set tolerance, ±1.57mm (±1/16 inch). 6
Figure 4. Renderings of Model 5720. 7
Figure 5. Model 5720 tethered to the MASK carriage. 8
Figure 6. Model 5720 with port bilge keel shown, from forward to aft (left to right). 8
Figure 7. Model 5720 with turbulence stud spacing shown, forward of station 6 (left) and aft of station 2 (right). 8
Figure 8. Model 5720 with chimney installed at the tether cable pass-through on the starboard side deck. 9
Figure 9. Model 5720 with backsplash shield on the stern shown. 9
Figure 10. R/V Melville propulsion system. 10
Figure 11. Model 5720 propulsion pods. 11
Figure 12. Side by side comparison of R/V Melville propeller and rendering of designed model propeller. 11
Figure 13. Model 5720 suspended from the A-frame. 14
Figure 14. Mounting apparatus for model attachment to the pivot gear. 15
Figure 15. Example of an Inclining Test Rig. 16
Figure 16. Schematic of model and carriage based wave probes for a head seas condition. 23
Figure 17. Histogram of model and wave data file duration difference 37
Figure 18. MASK basin coordinate system definition. 40
Figure 19. Location of bridge wave height sensors in the global coordinate system for two bridge settings: 0 and 45 degrees. The (0,0) point coincides with the origin of the global coordinate system. All locations given in full scale units. 41
Figure 20. Top view of the local coordinate system. 42
Figure 21. Plot of carriage wave height sensors, moonpool perimeter, and camera locations in the carriage/local coordinate system. The (0,0) point coincides with the origin of the local coordinate system. All locations given in full scale units. 44
Figure 22. Definition of relative wave heading, μ. 45
Figure 23. Example of roll decay time history. 47
Figure 24. Roll decay coefficients for 0 (blue), 8 (red), and 12 (green) knots full scale. 48
Figure 25. Example data from a regular waves transient run. 50
Figure 26. Regular wave roll RAOs for all headings and speeds, 1/60 wave steepness 51
Figure 27. Regular wave pitch RAOs for all headings and speeds, 1/60 wave steepness. 52

Figure 28. Example of achieved versus target wave spectra. Condition: BS-SS3, 8 knots, following seas. 57
Figure 29. Roll RAOs for SS3, all headings, 8 knots. 59
Figure 30. Pitch RAOs for SS3, all headings, 8 knots. 60
Figure 31. Example of statistical uncertainty analysis results. SS3, Beam Seas, 8 knots, estimate of the variance for roll and pitch. 61

TABLES

Table 1. Principal Particulars for the Full-Scale R/V Melville and Model 5720. 5
Table 2. Comparison of R/V Melville and Model 5720 propulsion system measurements. All measurements are in model scale dimensions. 11
Table 3. Summary of Load Condition 1: Design Payload, 100% Fuel. 14
Table 4. Achieved mass and inertial characteristics for Model 5720, as tested 3/2012. 15
Table 5. Table of instrument locations. 17
Table 6. Model Data Channel list. 18
Table 7. Bridge Data Channel List. 20
Table 8.Summary of data collection software. 24
Table 9. Details of the regular wave conditions. 27
Table 10. Summary of the irregular wave conditions. 28
Table 11. Summary of Irregular Wave Seakeeping runs and required run time. 29
Table 12. Calibration summary of Model 5720 instrumentation 33
Table 13. Summary of Uncertainty in Model 5720 Instrument Calibration. 34
Table 14. Calibration Summary of Model 5720 Voltage Monitors. 34
Table 15. Calibration Summary of MASK Bridge Probe Wave Height Transducers. 34
Table 16. Calibration Summary of MASK Carriage Probe Wave Height Transducers. 34
Table 17. Table of histogram bin data. 38
Table 18. Location of bridge wave height probes measured relative to the global/MASK origin. 42
Table 19. Carriage wave height sensors and camera locations in the carriage/local coordinate system. 43
Table 20. Wave condition settings for regular wave seakeeping. 46
Table 21. Wave condition settings for irregular wave seakeeping. 46
Table 22. Summary of planned and achieved regular wave conditions. 49
Table 23. Summary of regular wave roll and pitch RAOs. 53
Table 24. Summary of achieved irregular wave seakeeping conditions. 54
Table 25. Excerpt of irregular wave seakeeping conditions statistical summary. 55
Table 26. Summary of achieved significant wave height (H_s) and modal period (T_m) for each irregular wave condition. 58

This page intentionally left blank

ABSTRACT

An experiment was performed in the Maneuvering and Seakeeping (MASK) basin at the Naval Surface Warfare Center Carderock Division (NSWCCD) to provide time-synchronized model ship motion and wave measurement data, at moderate speeds, of R/V Melville. Model 5720, representing R/V Melville, was designed and constructed at NSWCCD and experiments were performed to assess seakeeping in regular and uni-directional irregular waves. This report details the data obtained from this experiment and presents some analysis, including standard time-series statistical parameters and Response Amplitude Operators (RAOs) for both regular and irregular wave conditions. A comprehensive data set, analysis, and supporting documentation accompanies this report in the form of a data CD.

ADMINISTRATIVE INFORMATION

The work described in this report was performed by the Seakeeping Division (Code 5500) of the Hydromechanics Department at the Naval Surface Warfare Center, Carderock Division (NSWCCD). The work was funded by the Office of Naval Research, Code 331, as part of the Environmental and Ship Motions Forecasting (ESMF) Future Naval Capabilities (FNC) Program (NWAs 100000539505/0010, 0110, 0120), under the direction of Dr. Paul Hess.

ACKNOWLEDGEMENTS

The authors would like to thank Brian Chirozzi, Keo Chum, David Fry, Demetrius Govotsos, Anthony Haglar, Joe Kim, Calvin Krishen, Anthony Lopez, Lloyd McCoy, Matt Powell, Howard Reynolds, and Donnie Walker for their support on the experimental set-up, instrumentation, and data collection; Ryan Hanyok and Devin Pisner for the video support; and Joe Klamo, and Sang Soo Lee for their support of data analysis. The authors would also like to thank Todd Carrico, Dan Hayden, and Martin Dipper for their guidance.

INTRODUCTION AND BACKGROUND

The Office of Naval Research (ONR) Environmental and Ship Motion Forecasting (ESMF) Future Naval Capability (FNC) Program is developing technologies to support Sea Basing initiatives. To support ESMF, ONR is using full-scale measurements from R/V Melville, in conjunction with model experiments, to investigate Science and Technology (S&T) to enable and improve real-time prediction of ship motions.

R/V Melville (T-AGOR 14) (Figure 1) is a research vessel operated by Scripps Institute of Oceanography (SIO) University of California. This 85m, 3000 tonne (279 ft, 2955 lton) vessel has been in service for more than four decades as an ocean going science platform. This report details model-scale experimentation to characterize the seakeeping performance of R/V Melville over a range of sea state conditions, at moderate speeds. The data from this model test will be used to support the development and testing of ESMF systems, to predict real-time ship motions in moderate sea states, as well as

support future numerical code development to deterministically assess ship seakeeping performance.

Figure 1. Photograph of the R/V Melville.

Objectives

The ESMF FNC program is developing technologies to provide environmental and ship motion forecasting, in order to predict windows of opportunity for sea basing operations. These include inter/intraship material, personnel, and vehicle movement, skin-to-skin operations, wet-deck operations, and launch and recovery of manned and unmanned vehicles. The objective of this model test was to provide a controlled data set of measured model ship motion and wave environment data to support the development and testing of proposed ESMF technologies.

The primary objective of the experiment was to provide time-synchronized model ship motion and wave measurement data, for moderate speeds, in both regular and irregular uni-directional wave conditions. This capability is expected to aid in creating additional ship motion validation data sets, as well as assist in the development of numerical ship motion prediction tools.

FACILITIES

MASK Basin

This experiment was conducted in the Maneuvering and Seakeeping basin (MASK) at Naval Surface Warfare Center, Carderock Division (NSWCCD) located in Bethesda, Maryland.

The MASK is an indoor basin and has an overall length of 110 m (360 ft), width of 73 m (240 ft), and depth of 6.1 m (20ft), except for a 10.7 m (35 ft) wide trench parallel to the long side of the basin (Figure 2). A 114.6-m (376 ft) bridge supported on a rail system spans the basin. The rail system permits the bridge to traverse half the width of the basin and to rotate up to 45 degrees from the longitudinal centerline. Models can be towed at all headings relative to the waves. A 6.1m (20 ft) wide by 6.6 m (21.8 ft) long

by 2 m (6 ft) high towing carriage is hung from the bridge. The carriage has a maximum speed of 7.7 m/sec (15 knots) and is driven by a pair of opposing traction wheels powered by two electric motors through a worm gear drive. Suspended from the bridge are six active wave probes to measure the wave-field. There are four additional wave probes mounted on the towing carriage. The major dimensions and capabilities of the MASK Basin are displayed in Figure 2.

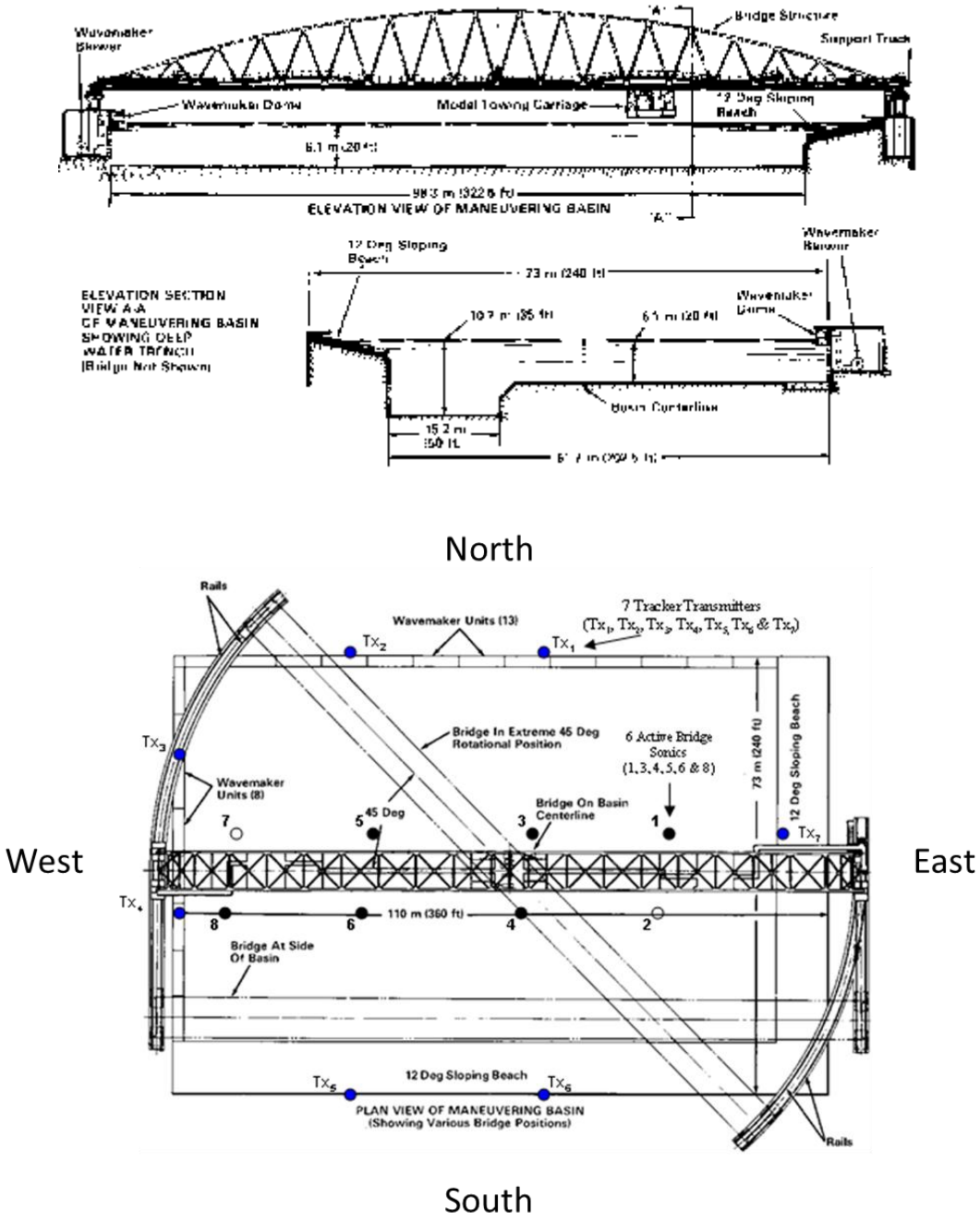

Figure 2. Maneuvering and Seakeeping basin (MASK) at NSWCCD.

Wave Generation

Eight pneumatic wave-maker units are located along the 73m (240 ft) west side of the basin and thirteen units along the 110m (360 ft) north side of the MASK basin (Figure 2). The two perpendicular banks of wave-makers can be operated individually to produce long-crested waves, or simultaneously to generate a bi-directional wave-field. Each wave-maker unit includes an inverted U-shaped dome, which is partially submerged in the water. Wave generation takes place using an electrically driven blower. The flow controlled by an electro-hydraulic actuator, which delivers pressurized air to the top of the dome. The wave-makers have a frequency range between 0.3 to 2.0 Hz. Irregular waves can be produced for a spectral distribution up to 0.4-m (1.3 ft) in significant wave height over the 0.3 to 2.0 hertz frequency range. Opposite each wave-maker bank is a constant slope beach designed to absorb waves and minimize reflections. Beach absorption is on average 97 percent effective, with the worst case being 92 percent at 0.3 hertz.

Tracking System

Model and carriage position in the MASK basin were tracked using a Nikon Metrology Indoor Global Positioning System (iGPS). The theory of operation and components of the onboard sensors and tracking system are described in the Instrumentation section of this report. The model was fitted with four detectors (two per vector bar, details are given in the Model section) that receive laser and infrared (IR) pulses from transmitters set up along the sides of the basin, as represented by the blue dots in Figure 2. The carriage was fitted with one tracker iJavelin station, which also received laser and IR pulses from the basin transmitters.

MODEL DESCRIPTION

A 1/23rd scale model of the R/V Melville, in its current configuration, was designed and constructed by the NSWCCD model shop (Model 5720). This scale ratio was chosen to enable coverage of a desired range of sea states and wave conditions in the MASK basin. The following simplifications were made in the design of the model:

- Roll stabilization systems (roll tanks) were neglected
- Bow thrusters were neglected
- A simplified superstructure, with major features, was included (all details of the topside were not represented)
- Propeller geometry was not modeled exactly

The roll tanks were neglected due to the complexity and difficulty of scale effects of these devices. A bow thruster that is present on the full-scale ship was neglected, as it is typically retracted for underway operations. It was necessary to model major features of the superstructure to aid in future model tests of Model 5720; however, the structure was simplified for construction purposes. The primary objective of this test was to collect time-synchronized model ship motion data. Therefore, the ability to provide the thrust needed to meet speed requirements was of primary concern. It was assumed that the

differences in propulsor geometry, compared to the full-scale propulsors, had a negligible effect on ship motions.

Hull Geometry

The model was built of fiberglass with stainless steel bilge keels. A summary of model particulars, in full and model scale, is provided in Table 1. The hull geometry was verified using NSWCCD's laser scan system. The hull was within the standard accuracy required for seakeeping experiments, ±1.57mm (±1/16 inch), except for two areas aft of amidships near the top of the bulwark. This out of tolerance area was due to the manufacturing processes and was high above the waterline, and therefore, does not affect the seakeeping performance of the model (see Figure 3). The hull thickness was set at 4.76 mm.

Table 1. Principal Particulars for the Full-Scale R/V Melville and Model 5720.

Full Scale (salt water)			Model Scale (fresh water)	
max speed (kts)	16.0		max speed (m/s)	1.716
LOA (m)	85.0		LOA (m)	3.695
LBP (m)	77.4		LBP (m)	3.366
disp full load (kN)	29451.6		disp full load (N)	2360.1
disp design payload (kN)	28674.0		disp design payload (N)	2299.2
disp lightship (kN)	22177.8		disp lightship (N)	1777.2
Max beam (m)	14.0		Max beam (m)	0.610
propulsor stock (m)	0.4		propulsor stock (m)	0.016
ducted prop diameter (m)	2.7		ducted prop diameter (m)	0.119
ducted prop hub diameter (m)	0.9		ducted prop hub diameter (m)	0.040

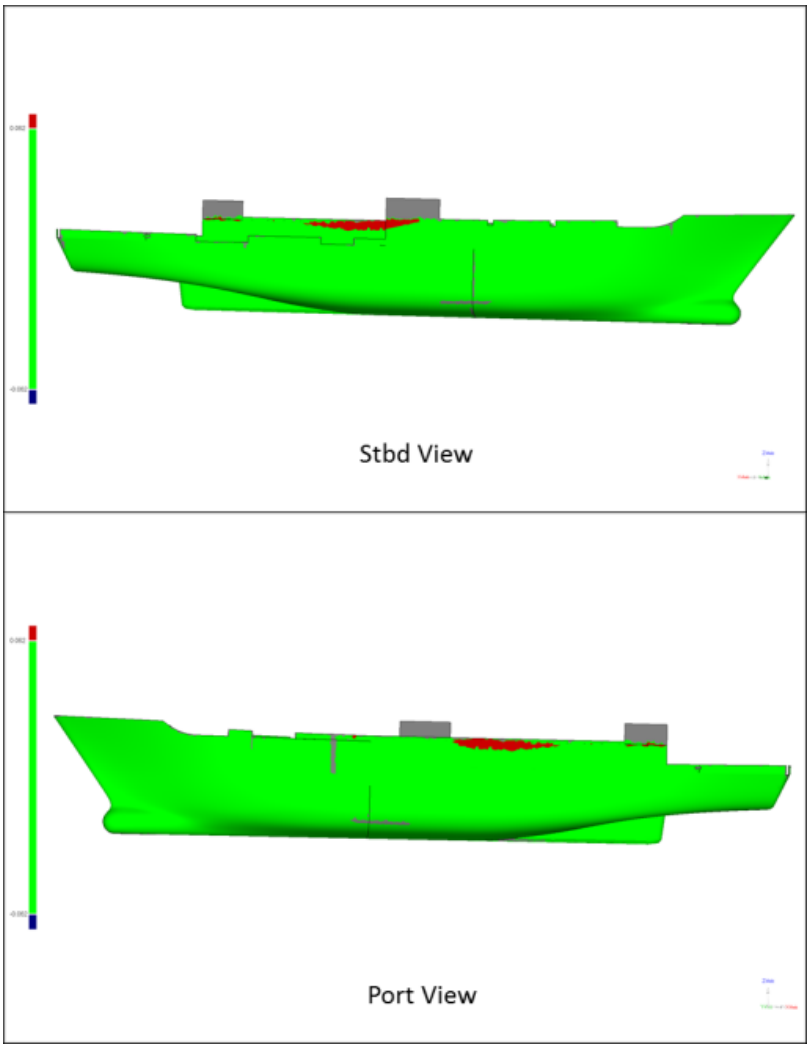

Figure 3. Laser scan results of Model 5720. Red and blue coloring show areas outside of the set tolerance, ±1.57mm (±1/16 inch).

Figure 4 shows a rendering of Model 5720 and Figure 5 provides pictures of the model tethered to the MASK carriage during testing. The model was constructed in two pieces, as noted in Figure 4, by the parting line along the parallel midbody. An aluminum bulkhead with an o-ring seal was located at the model split The aim of constructing the model in two pieces was to aid in the process used to determine the model center of gravity (CG) and moments of inertia. The forward-most section of the bow, as well as the skeg, was filled with epoxy foam to prevent significant damage to the model, in the case of a collision with the wave-maker or the beach in the MASK basin. Two internal fiberglass bulkheads provided stiffening. Figure 4 also shows the locations of the tracker detectors/vector bars on the model. Internal platforms were installed to house the necessary instrumentation. The deck camber and shear w modeled, as well as the bow and stern bulwark. The superstructure was constructed of high density foam. The bilge keels were constructed of stainless steel and fit to match the bilge keel trace from the ship drawings (Figure 6). A weight post that extended through the forward superstructure was

installed to aid in the process to set the metacentric height. All communication cables were gathered in the model and run through a single opening in the model located in the deck on the starboard side (Figure 8). A chimney made of PVC piping was installed to provide structure to the cable bundle and to provide waterproofing at the deck opening.

Turbulence stimulation for the model was provided by a series of studs placed along the circumference of the bow bulb, 25.4mm aft of station 2, and 25.4mm forward of the station 6, just ahead of the bilge keels, as shown in Figure 7. Turbulence stimulation was needed to trip the boundary layer and ensure turbulent flow.

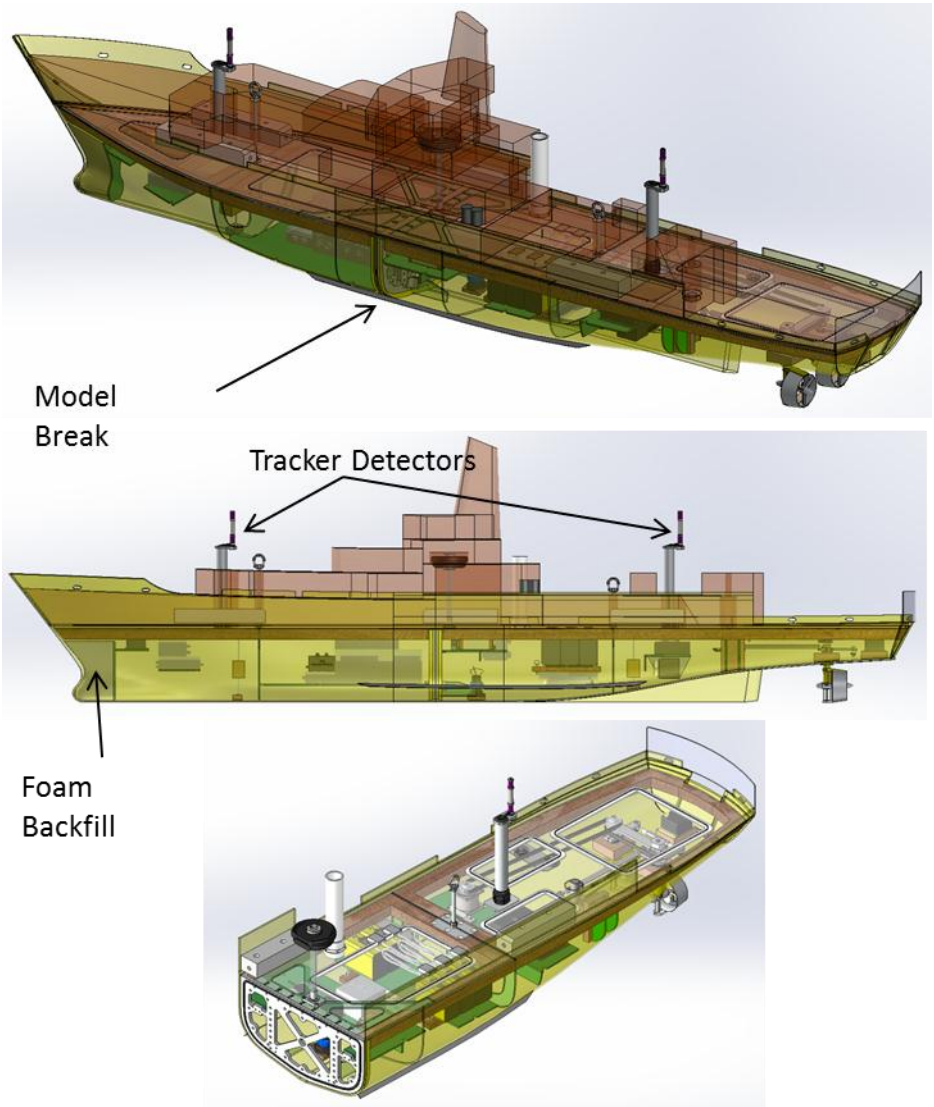

Figure 4. Renderings of Model 5720.

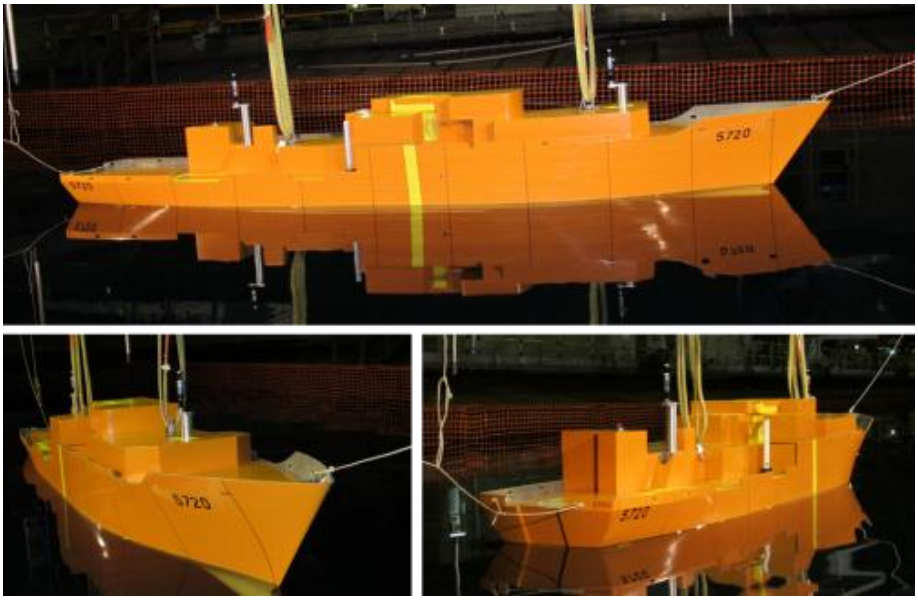

Figure 5. Model 5720 tethered to the MASK carriage.

Figure 6. Model 5720 with port bilge keel shown, from forward to aft (left to right).

Figure 7. Model 5720 with turbulence stud spacing shown, forward of station 6 (left) and aft of station 2 (right).

Model Geometry Modifications Made During Testing

Some modifications were made to the model during testing to troubleshoot unanticipated events. This section details those modifications. A post incline test (described in the Model Ballasting section) was performed to quantify the impact of these modifications on the model mass properties.

Chimney

All communication cables were gathered in the model and run through a single opening in the model located in the deck on the starboard side (Figure 8). A chimney made of PVC piping was installed to provide structure to the cable bundle and to provide waterproofing at the deck opening. The chimney was added to the model late during the first week of testing, when observations were made that better waterproofing was necessary at the cable pass-through location on the deck.

Figure 8. Model 5720 with chimney installed at the tether cable pass-through on the starboard side deck.

Backsplash Shield

At the end of each run, the carriage towed the model back to its initial starting point to prepare for the next run. During back-up operations in following and quartering seas at the higher regular wave wave steepness conditions and higher sea states a significant amount of water was washed over the aft deck. To minimize the amount of deck wash a pulley system was rigged to partially lift the stern out of the water. In addition, a backsplash shield was installed as shown in Figure 9.

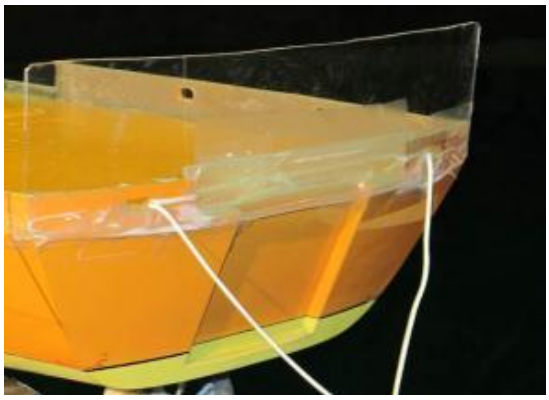

Figure 9. Model 5720 with backsplash shield on the stern shown.

Model Propulsion

The full-scale R/V Melville is fitted with two podded propulsor units (Figure 10). Each full scale unit contains a 5-bladed, right handed propeller and can be operated independently and can rotate 360 degrees. The propulsor slew rate is 2 rpm, or 12 deg/sec. During operations, when the standard autopilot is employed, the rate of turn of the ship is 60 deg/min.

For this model-scale test, existing propulsion units were modified and used for Model 5720. Modifications included the addition of a bottom strut on the inboard side of the unit, and a redesign of the propeller. A five bladed right handed propeller was constructed using the process of Selective Laser Sintering (SLS) for each unit (Propellers 5573 and 5574 in the NSWCCD propeller library). Propeller geometry was based on photographs of the R/V Melville propellers and designed to fit the existing propulsion units. The propulsion pods used on the model are shown in Figure 11. Figure 12 provides a side by side comparison of R/V Melville propeller and designed model scale propeller. The slew rate of the model propulsion units was scaled to the full scale slew rate (model scale slew rate = 57.55 deg/sec).

A comparison of the actual propulsion system to the model propulsion system is provided in Table 2. As previously stated, the primary objective of this test was to collect model ship motion data and the ability to provide the thrust needed to meet speed requirements was of primary concern. Therefore, the differences in overall pod dimensions were assumed to have a negligible effect on model ship motions.

For the model test, the pods were mechanically linked to steer at the same angle and rate and did not operate independently. A push rod was attached to a rotary actuator and potentiometer under the aft deck. The rotary actuator was powered with the 32 VDC instrument batteries and was controlled by an Advanced Motion Controls 25A8K motor controller. Feedback monitoring and control of the propulsion system was also provided by the on board computer (OBC) and signal conditioning unit. Each pod had a range of motion of ±45 degrees. This is representative of typical underway operating conditions.

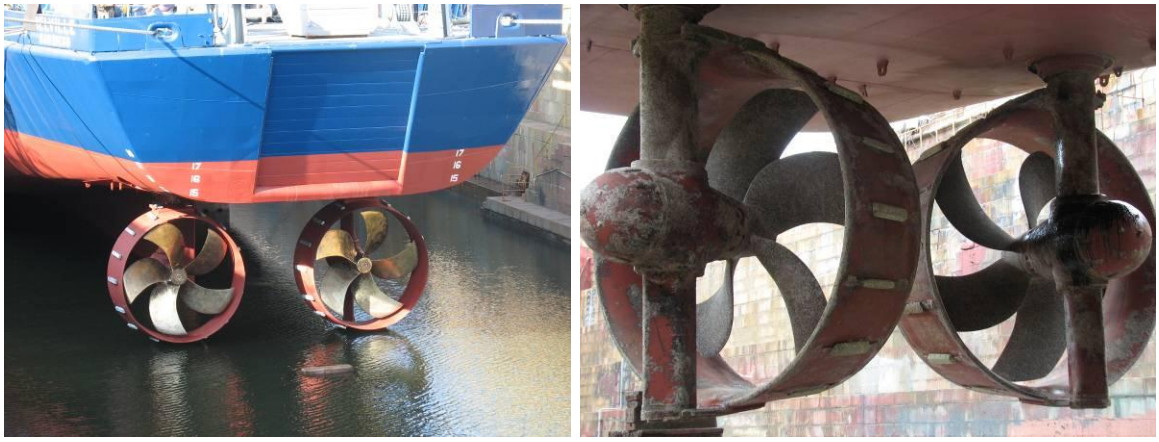

Figure 10. R/V Melville propulsion system.

Figure 11. Model 5720 propulsion pods.

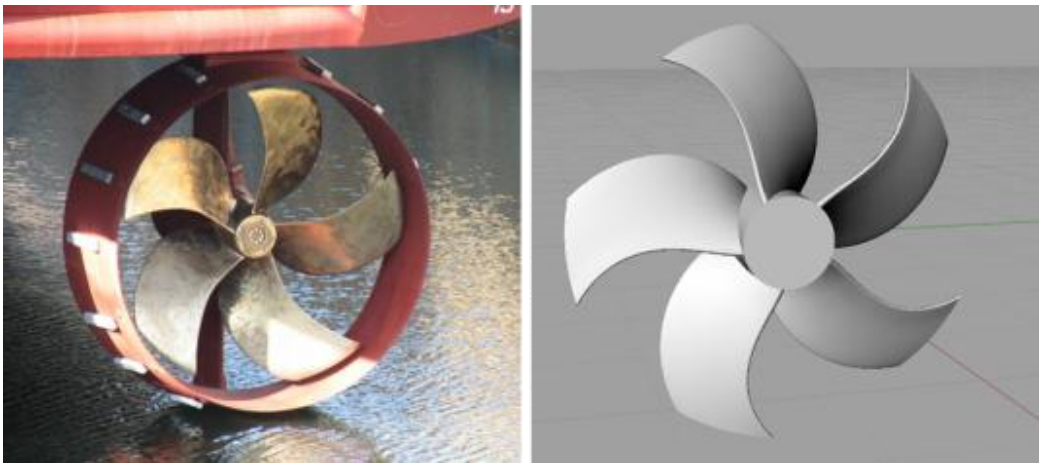

Figure 12. Side by side comparison of R/V Melville propeller and rendering of designed model propeller.

Table 2. Comparison of R/V Melville and Model 5720 propulsion system measurements. All measurements are in model scale dimensions.

	R/V Melville	Model 5720	Ratio (Model 5720/Melville)
No. of Blades	5	5	
propulsor stock (mm)	15.90	28.58	1.80
ducted prop diameter (mm)	119.27	108.00	0.91
duct diameter, LE (mm)	145.77	150.98	1.04
duct diameter, TE (mm)	130.31	135.56	1.04
ducted prop hub diameter (mm)	39.76	26.59	0.67
Slew rate (deg/sec)	57.55	57.55	1.00

Model Control

The model was manually controlled using two drivers. One driver controlled the steering angle of the pods using a steering wheel, while the other controlled the shaft speed using a throttle. Shaft speed was adjusted to match the carriage speed and the steering angle was varied to keep the model at a constant heading and within the perimeter of the carriage moonpool.

MASK Carriage Operations with a Tethered Model

The model was loosely restrained under the MASK carriage with tethers (nylon cord) for all test conditions (for example, see Figure 5). The tethers restrained the model during acceleration and deceleration phases of a carriage run, and served as a safety line for cases when the model heading was not maintained in line with the carriage, while at speed. In this configuration, a cable bundle, which spanned from the inside the model to the carriage, was used to link the carriage wave height sensors with the model and to provide communication between the model systems and the model data acquisition system. Data collection began once it was verified that the tether cords and cable bundle were not in tension and the model was running at the same speed and heading as the carriage. A digital read out of model speed and a visual check of the model location under the carriage and the tether ropes and cable bundle were used to determine if the model was unrestrained and at speed. The model was driven via a pair of joysticks from the carriage; a steering wheel to control the steering angle of the pods and a throttle for shaft speed adjustment, an autopilot was not used. Therefore, model speed was controlled by the driver as he/she maintained model speed to match the constant carriage speed.

Model Ballasting

For seakeeping experiments, the model is ballasted with the proper displacement, center of gravity, and roll, pitch, and yaw moment of inertia. For this experiment, only one load condition, the design payload, was tested. This load condition corresponded to Load Condition 1 in Revision B of Melville Trim and Stability Book (Glosten Associates, 2010). A summary of this condition is provided in Table 3. (Note: the gyradius of the R/V Melville was not available for this load condition; therefore, standard Naval Architecture estimates were used, as given in the table below).

The model was ballasted by NSWCCD to the specified load condition, in accordance with the procedure found in the Quality Management System (QMS) procedure 00-5500-094-16. The NSWCCD QMS is a collection of registered procedures. The QMS procedures referenced in this report were last updated in August 2011. For this experiment, it was assumed that the yaw moment of inertia (MOI) was equal to pitch MOI.

During model outfitting, the weight and location of each component was logged, so its contribution to the model's center of gravity and inertial characteristics could be determined. Once the fixed components were located in the model as required by mechanical and instrumentation needs, the model was weighed and initial ballast conditions were measured. This measurement was accomplished by performing an in-air center of gravity (CG) and gryradius measurement by attaching the model to the "A-Frame" inertial gear in a pendulum type fashion, as shown in Figure 13. The attachment

of the model to the pivot gear was accomplished with a channel mounted to two end plates, which bolted into the side of model (Figure 14) The initial longitudinal center of gravity (LCG) was determined by attaching the pivot gear at the LCG location, and then noting the amount and position of weight required to move the model to effectively zero trim. The vertical center of gravity (VCG) was determined by adding weights at known longitudinal locations and noting the change in trim. The VCG was determined by resolving the associated force diagram as the model CG swung under the pivot to offset the longitudinal trim weight. The inertial characteristics were determined by measuring the roll and pitch periods of the suspended model once the CG had been determined. The roll and pitch inertias were then calculated based upon pendulum theory and application of the parallel axis theorem. The locations of movable weights and components were calculated in spreadsheet fashion to satisfy required ballast conditions. This whole process was performed multiple times, adjusting ballast locations, until the measured ballast condition satisfied the desired ballast conditions. The results of the ballast effort is listed in Table 4. All ballast properties obtained were within 1% to 3% of the desired values.

An inclining test was performed, following QMS procedure 00-5500-094-16, as it relates to Model Dynamic Ballasting, to verify the load condition. To accomplish this, a plastic tab was constructed and attached to the model at its longitudinal center of gravity (LCG). An example of this rig is shown in Figure 15. This setup allows for the placement of brass weights previously manufactured for the inclining experiment. Various brass weights were added to generate adequate roll inclination data sets to both port and starboard rolls. The data set was analyzed to calculate a mean transverse meta-centric height for the data set. A Wyler inclinometer placed at the stern and on centerline was used to record roll angle. This instrument was needed because the Goodrich gyro which was already onboard had insufficient accuracy for this purpose. The inclining test was repeated at the end of the experiment to verify the addition of the chimney and backsplash shield did not alter the ballast condition. The results of the pre- and post-incline experiment are shown in Table 4.

Table 3. Summary of Load Condition 1: Design Payload, 100% Fuel.

Full Scale*			**Model Scale****	
Displacement (kN)	28674.0		Displacement (N)	2299.2
Draft at FP (m)	4.89		Draft at FP (m)	0.213
Draft at AP (m)	5.01		Draft at AP (m)	0.218
VCG (m above BL)	5.89		VCG (m above BL)	0.256
VCG w/ FSCorr (m above BL)	6.22		VCG w/ FSCorr (m above BL)	0.270
LCG (m aft FP)	36.94		LCG (m aft FP)	1.606
TCG (m stbd)	-0.03		TCG (m stbd)	-0.001
GMt (m)	1.42		GMt (m)	0.062
FSCorr (m)	0.33		FSCorr (m)	0.014
GM w/Fscorr (m)	1.09		GM w/Fscorr (m)	0.047
Roll gyradius	0.39B		Roll gyradius	0.39B
Pitch gyradius	0.25L		Pitch gyradius	0.25L
Yaw gyradius	0.25L		Yaw gyradius	0.25L

*salt water **fresh water

Figure 13. Model 5720 suspended from the A-frame.

Figure 14. Mounting apparatus for model attachment to the pivot gear.

Table 4. Achieved mass and inertial characteristics for Model 5720, as tested 3/2012.

		Target	Achieved	% Error	Target	Achieved	Error
Displacement	(kN)	28674.00	28547.48	-0.44%	2299.20	2289.06	-0.44%
LCG (aft FP)	(m)	36.94	36.94	–	1.606	1.606	–
TCG (stbd)	(m)	-0.03	-0.03	--	-0.001	-0.001	--
VCG (above BL)	(m)	5.89	6.07	3.03%	0.256	0.264	3.03%
k_{pitch}	(m)	19.350	19.265	-0.44%	0.841	0.838	-0.44%
	%	0.25Lpp	0.249Lpp		0.25Lpp	0.249Lpp	
k_{pitch}/L_{BP}	--	0.250	0.249	-0.44%	0.250	0.249	-0.44%
k_{roll}	(m)	5.460	5.290	-3.11%	0.237	0.230	-3.11%
	%	0.39B	0.378B		0.39B	0.378B	
$k_{roll}/Beam_{WL}$	--	0.390	0.378	-3.11%	0.390	0.378	-3.11%
k_{yaw}	(m)	19.350	19.265	-0.44%	0.841	0.838	-0.44%
	%	0.25Lpp	0.249Lpp		0.25Lpp	0.249Lpp	
k_{yaw}/L_{BP}	--	0.250	0.249	-0.44%	0.250	0.249	-0.44%
Roll Period (0 kts)	sec	–	–	–	–	–	–
GM_t w/Fscorr (pre)	(m)	1.090	1.086	-0.36%	0.047	0.047	-0.36%
GM_t w/Fscorr (post)	(m)	1.090	1.056	-3.10%	0.047	0.046	-3.10%

*seawater **freshwater

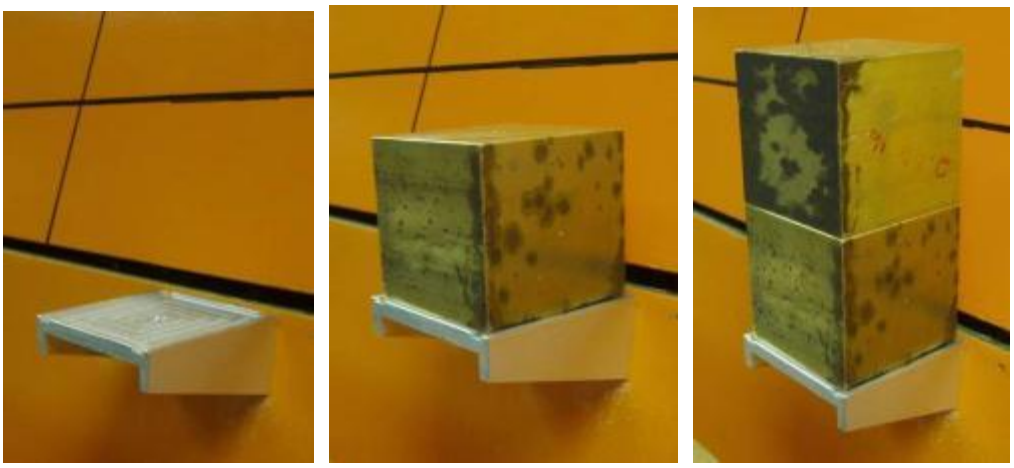

Figure 15. Example of an Inclining Test Rig.

INSTRUMENTATION

This experiment was conducted using carriage-based wave height sensors, model motion and control sensors, bridge mounted wave height sensors, and a GPS based tracking system.

All model motion and control sensors were housed in the model. One power source was used to power the instrument circuit and a separate source powered the propulsion circuit. All power was provided by batteries that resided within the model. All model data was collected at a sample rate of 24 Hz and filtered using a 6 Hz constant time delay 8 pole filter. The carriage-based wave height sensors were collected on the same system as the model sensor to ensure synchronization. These sensors were connected to the model via the tethered cable bundle.

The coordinate system used for the model measurements was right handed, with X positive forward, Y positive to port, and Z positive up. Rotations were positive using the right hand rule around the axes. The propulsion pod rotation polarity followed the same rotation designation; therefore, positive pod motions caused a negative yaw and yield a turn to starboard. Propeller shaft speed was always positive. Astern propulsion was indicated by negative throttle command. Accelerations were positive in the direction of positive displacement and reported at the location of the instrument. Heading type data measurements are all positive when increasing clockwise from their respective zero reference axis (model's bow or North), irrespective of their local vertical axis direction.

Table 5 is a table of the locations of all instruments housed in the model. The model and carriage measurement sensors are summarized in Table 6. Critical data channels were marked by a "Y." Backup channels for all critical sensors are also noted.

The tracking system (described in more detail below) was used to track the location of the model and the carriage in the MASK basin. Model tracker data was collected at 24 Hz. Carriage tracker data was collected at 40 Hz.

Wave height measurements were made from six fixed ultrasonic wave height probes mounted on the MASK bridge (Figure 2). The wave measurement channels are defined in Table 7. The data rate for these sensors was 48 Hz. For head, beam, and

following seas, the MASK bridge was set at the 0 degree position shown in Figure 2. For bow and quartering seas, the MASK bridge was rotated to a 45 degree position. Locations of the wave height sensors for each bridge setting are provided in the Coordinate System section of this report.

Table 5. Table of instrument locations.

Instrument Locations and Properties for Model 5720						
	Model Scale			**Full Scale**		
Instrument	**X, aft FP**	**Y, relative CL**	**Z, abv keel**	**X, aft FP**	**Y, relative CL**	**Z, abv keel**
	[m]	**[m]**	**[m]**	**[m]**	**[m]**	**[m]**
Accelerometer - Fwd	0.26	0.00	0.26	5.99	0.00	5.91
Accelerometer - CG	1.61	0.00	0.25	36.94	0.00	5.78
Accelerometer - Aft	3.28	0.00	0.25	75.37	0.00	5.71
KVH	0.41	0.00	0.24	9.41	0.00	5.44
Micro Strain	0.44	0.00	0.17	10.04	0.00	3.91
Voltage Monitor Box 1	1.02	0.02	0.17	23.45	0.53	3.86
Voltage Monitor Box 2	1.02	-0.02	0.17	23.45	-0.53	3.86
F-V Converter Signal	1.01	0.00	0.11	23.26	0.00	2.45
Computer and Filter	1.26	0.00	0.15	29.04	0.00	3.44
Power Distribution and Signal Interface	1.20	0.00	0.27	27.66	0.00	6.16
G5.0 PCE Wireless w/POE Module-1	1.65	0.20	0.25	37.92	4.67	5.79
Systron Donner	1.72	0.05	0.27	39.50	1.11	6.21
Gyro-Pitch-Roll	1.61	-0.14	0.26	36.98	-3.13	5.92
Ethernet Switch	1.73	0.08	0.20	39.77	1.78	4.59
Cisco Air-BR1310G-A-K9-R Power Box	1.73	-0.07	0.20	39.87	-1.61	4.71
Cisco Air-BR1310G-A-K9-R	2.03	-0.09	0.12	46.65	-2.08	2.74
Master Relay Box-1	1.97	0.10	0.13	45.22	2.22	2.89
Rudder Survo Amp Box-1	2.09	0.10	0.13	48.00	2.22	2.89
Battery Wooden Beam Assembly Port	2.00	0.20	0.14	45.94	4.60	3.32
Battery Wooden Beam Assembly Stbd	2.00	-0.20	0.14	45.94	-4.57	3.32
Battery Fwd Port (#3)	1.96	0.18	0.22	44.98	4.08	5.00
Battery Mid Port (#2)	2.03	0.18	0.22	46.74	4.08	5.00
Battery Aft Port (#1)	2.11	0.18	0.22	48.49	4.08	5.00
Battery Fwd Stbd (#4)	1.97	-0.18	0.22	45.28	-4.08	5.00
Battery Mid Stbd (#5)	2.03	-0.18	0.22	46.74	-4.08	5.00
Battery Aft Stbd (#6 - Tracker Battery)	2.11	-0.18	0.22	48.63	-4.08	5.00
Motor Servo Amp Box	2.45	0.12	0.22	56.38	2.75	5.13
BM250E	2.44	0.06	0.15	56.09	1.46	3.40
Reduction Gearbox	2.44	-0.14	0.19	56.09	-3.22	4.26
Rudder Steering Assembly	2.68	0.11	0.26	61.73	2.56	6.05
Paddle Wheel Signet Marine	1.65	-0.06	0.06	37.97	-1.32	1.35

Table 6. Model Data Channel list.

Channel Name	A/D Ch#	Critical Sensor	Backup Sensor	Units	Source	Manufacturer	Type Transducer	Model	Serial Number	BarCode
Shaft Speed	0	Y	None	RPM	Sensor	Encoder Products CO / Analog Devices / CDNSWC	ACCU Coder / F to V / Electronic Circuit	260-T-02-S-0200-ROC-1-S-XF-1-N / 451J / NA	NA	39595 / 39594
Steering Angle	1	Y	None	Deg	Sensor	Bourns	Rotary Potentiometer	6574S-1-103	NA	39596
KVH Sin	2	Y	None	volts	Sensor	KVH	Fluxgate Compass	C-100	NA	39449
KVH Cos	3	Y	None	volts	Sensor					
KVH Ref	4	Y	None	volts	Sensor					
Roll Angle	5	Y	Roll 3DM 3XI	Deg	Sensor	BF Goodrich	Vertical Gyro	VG34-0809-1	120	39357
Pitch Angle	6	Y	Pitch 3dw 3XI	Deg	Sensor					
Roll Rate S/D	7	Y	None	Deg/s	Sensor	BEI Systron Donner	Angular Rate Sensor	QRS14-100-103	45952	39597
Pitch Rate S/D	8	Y	None	Deg/s	Sensor	BEI Systron Donner	Angular Rate Sensor	QRS14-100-103	45955	39598
Yaw Rate S/D	9	Y	None	Deg/S	Sensor	BEI Systron Donner	Angular Rate Sensor	QRS14-50-103	45318	39599
Vert CG Accel	10	Y	Bow or Stern Vert Acc	g	Sensor	Columbia	Tri-Axial Mass Accelerometer	SA-307HPTX	1756	39466
Trans CG Accel	11	Y	Bow or Stern Trans Acc	g	Sensor					
Long CG Accel	12	Y	Bow or Stern LongAccel	g	Sensor					
Vert Bow Accel	13	N	NA	g	Sensor	Columbia	Triaxial Mass Accelerometer	SA-307TX	1629	39503
Trans Bow Accel	14	N	NA	g	Sensor					
Long Bow Accel	15	N	NA	g	Sensor					
Vert Stern Accel	16	N	NA	g	Sensor	Columbia	Triaxial Mass Accelerometer	SA-307TX	1690	39035
Trans Stern Accel	17	N	NA	g	Sensor					
Long Stern Accel	18	N	NA	g	Sensor					

Table 6 cont. Model data channels.

Channel Name	A/D Ch#	Critical Sensor	Backup Sensor	Units	Source	Manufacturer	Type Transducer	Model	Serial Number	BarCode
Speed Thru Water	19	N	NA	fps	Sensor	GF Signet	PaddleWheel Flow Meter	2536 Rotor-X	6.1E+10	39601
Carrg Speed	20	N	NA	KTS		Analog Devices/CDNSWC	F to V Electronic Circuit			
Wave Hght West	21	Y	NA	in	Sensor	Ultrasonic	Senix	TSPC30S1-232		
Wave Hght East	22	Y	NA	in	Sensor	Ultrasonic	Senix	TSPC30S1-232		
Wave Hght South	23	Y	NA	in	Sensor	Ultrasonic	Senix	TSPC30S1-232		
Wave Hght North	24	Y	NA	in	Sensor	Ultrasonic	Senix	TSPC30S1-232		
Electronics Batt	25	Y	NA	Volts	Sensor	CR Magnetics	Voltage Transducer	CR5310-50	807001499	39602
Propulsion Batt	26	Y	NA	Volts	Sensor	CR Magnetics	Voltage Transducer	CR5310-100	807001477	39603
Heading uStrain Ch3	27	Y	NA	DegM	Sensor	Microstrain	Gyro Orientation	3DM-GX1	P#3017-7019	39600
Roll uStrain Ch1	28	N	NA	Deg	Sensor					
Pitch uStrain Ch2	29	N	NA	Deg	Sensor					
KVH Calc Heading	NA	N	None	DegM	Calculated	KVH	Fluxgate Compass	C-100		39449
Bow Tracker Sensor Bottom	NA	N	None	in	Receiver	Nikon Metrology	Laser Detector	Mini Vector Bar	0102706-A 11050100	
Bow Tracker Sensor Top	NA	Y	None	in	Receiver	Nikon Metrology	Laser Detector	Mini Vector Bar	0102706-A 11050100	
Tracker G5 PCE - Wired Hub	NA	Y	None	NA	Bow & Aft Sensors	Nikon Metrology	Position Calculation Engine	G5		
Aft Tracker Sensor Bottom	NA	N	None	in	Receiver	Nikon Metrology	Laser Detector	Mini Vector Bar	0102706-A 11050101	
Aft Tracker Sensor Top	NA	Y	None	in	Receiver	Nikon Metrology	Laser Detector	Mini Vector Bar	0102706-A 11050101	
IGPS Digital Input						Nikon Metrology	Digital Input Module			

Table 7. Bridge Data Channel List.

Channel Name	A/D Ch#	Units	Source	Manufacturer	Type Transducer	Model	Serial Number	BarCode
Bridge Wave Hght 1	1	in	Sensor	Ultrasonic	Senix	TSPC30S1-232		NA
Bridge Wave Hght 3	2	in	Sensor	Ultrasonic	Senix	TSPC30S1-232		NA
Bridge Wave Hght 4	3	in	Sensor	Ultrasonic	Senix	TSPC30S1-232		NA
Bridge Wave Hght 5	4	in	Sensor	Ultrasonic	Senix	TSPC30S1-232		NA
Bridge Wave Hght 6	5	in	Sensor	Ultrasonic	Senix	TSPC30S1-232		NA
Bridge Wave Hght 8	6	in	Sensor	Ultrasonic	Senix	TSPC30S1-232		NA

Model Motion Sensors

Vertical Gyro

Rotational displacements (pitch and roll) were measured using Goodrich Model VG34 Vertical Gyroscopes. This miniature dual axis electro-mechanical spinning mass gyro provided the primary vertical rotation displacement outputs. The vertical gyro provided adequate response for the high roll and pitch motions. However, the transverse and longitudinal acceleration values of the Columbia CG accelerometer provided the best repeat measurement of roll and pitch attitude for calm water zeroes.

Microstrain Gyro Enhanced Orientation Sensor

The MicroStrain 3DM-3XI combined three axis of angular rate gyros, accelerometers, and magnetometers to provide various combinations of gyro stabilized Euler rotations. By using a combination of microprocessors and the analog output option, the 3DM-3XI provided heading, roll, and pitch. The heading was used as the backup heading to the KVH compass, and the roll and pitch were used as backup to the vertical gyro. The KVH compass, described in more detail in the model control section, was used to provide heading feedback to the helmsman during runs.

Rate Gyro

Body axis angular rates of rotation were measured onboard by three orthogonally mounted BEI (Systron Donner Inertial Division) solid-state GyroChip II rate gyros. The BEI device uses a vibrating quartz tuning fork sensing element in conjunction with a piezoelectric material to produce a voltage proportional to a rate of rotation. Model QRS14-00100-103 was installed along the roll and pitch axis of the model and is rated at 100 degrees per second maximum rate. One additional unit (Model QRS14-00050-103) was installed parallel to the yaw axis, and is rated at 50 deg/s.

Accelerometer

Accelerations at the bow, stern, and center of gravity were measured with Columbia tri-axial mass accelerometers. The three accelerometer locations bounded the habitable areas of the hull, and can be translated to additional locations in the hull using rigid body assumptions. All vertical axis channels installed in the hull are +/-2 g full range, while the transverse and longitudinal channels are rated at +/-1 g. The units can withstand shock loads up to 1000 g's and survive vibration environments up to 2000 Hz. Performance degrades near the unit's natural frequency of about 130 Hz.

Model Control Sensors

The model control was monitored via the shaft speed, steering angle, and model heading.

Shaft Speed

Propeller shaft speed was measured using an ACCU Coder Model 260-T-02-S-0200-R-OC-1-S-XF-1-N manufactured by Encoder Products Co. The resolution of the optical encoder for this model test was 120 pulses/revolution. The encoder was mounted to the open end of the port right angle gear box. Pulses from the encoder were converted to analog voltage by an onboard frequency-to-voltage (F-to-V) converter and associated electronics on an NSWCCD designed electronic box. For this test, a two channel F-to-V electronic box was used to support pulses from the Speed Through Water x-type paddlewheel flow sensor.

Steering Angle

Steering angle was measured by a Bourns potentiometer. The potentiometer was mounted to the shaft of a Globe motor that slews the pods according to a steering command signal generated from the helmsman. The Bourns potentiometer tracks the shaft position of the Globe motor. The pods were connected through rigid arms and linkages to the motor shaft.

Compass

A KVH compass (model C100) was used on the model to record magnetic heading. The sensor was gimbal mounted, automatically compensated for magnetic variation, and measured course to within +/- 0.5 degrees. The compass was used by the helmsman to monitor the heading during the runs. However, the primary heading channel was provided by the model tracker system.

Speed Through Water

Model speed through the water was measured with a GF Signet PaddleWheel Flow meter that was mounted to the underside of the model, near amidships, on the skeg. This instrument provides the speed of the flow past the hull. Output pulses from the flow sensor were converted to analog voltage by an onboard F-to-V converter and associated electronics on an NSWCCD designed electronic box. For this test, a two channel F-to-V electronic box was used to support pulses from two pulse-type sensors. A manufacturer calibration relating pulses to velocity was used for system checkout. However, the final pulse to model velocity calibration was determined during throttle setting/speed calibration procedures.

Speed Over Ground

A tracker system (described below) was used to provide a GPS based speed measurement of the model and the carriage. The carriage speed was also measured using a speed Rotopulse sensor with F-to-V converter. The carriage speed was calculated knowing the diameter of the pickup wheel, the number of encoder pulses per rotation, and the setting for the frequency to voltage converter, as verified by a calibrated signal generator.

Model Tracking System

The Nikon Metrology Indoor Global Positioning System (iGPS) system was used to track both the model and carriage location in the basin. This system consists of seven shore-based transmitters rigidly mounted at fixed locations around the basin (Figure 2), model and carriage mounted detectors (Figure 5), and associated electronics and software.

The shore transmitters act like fixed indoor satellites, to provide reference locations within the basin. The transmitters have rotating heads, which generated two infrared laser fanned beams and infrared LED strobes, which flashed once per revolution. The two fanned laser beams were tilted ±30° with respect to the spin axis of the transmitter. In addition, the transmitter's fanned laser beams provide an elevation coverage range of ±30° with respect to the horizontal plane. The head of each transmitter rotated at slightly different speeds, centered on an operating speed of approximately 40Hz. The model mounted detectors identified the transmitter reference based upon its rotation speed.

The elevation of each detector relative to a transmitter was determined by calculating the difference in time between the arrival of each transmitter's laser fan beam 1 and 2 at the detector. The azimuth of each detector relative to a transmitter was calculated by the time difference of the infrared LED pulse and the arrival the transmitter's laser fan beam 1. The distance of each detector relative to a transmitter required visibility and range information from two or more transmitters, which intersect at the detector. This intersection fixed the detector in space, providing an accurate distance measurement between each transmitter and detector.

Nikon Surveyor software was used to complete the iGPS system by collecting and outputting 6-DOF data from the model array of four rigidly mounted detectors. A "frame" was created in Surveyor by inputting the known locations of each detector with respect to the other detectors in the array and a desired frame origin. The frame origin is a single coordinate system in space, located with respect to the other detector points in the frame. For Model #5720, the frame coordinate system was virtually located at the CG. The data reports the CG's position and orientation in space with respect to the fixed transmitters in the MASK basin. The tracker system was only used to provide x and y location and relative wave heading data for the model. Surge, sway, and heave information was not available directly from the tracker data. Data for surge, sway, and heave can be recovered from the accelerometer data.

In addition to tracking model position, a third detector array (containing four detectors) was mounted at the west end of the MASK carriage, to allow tracking of the carriage within the basin. The ability to track model location and carriage location provided the ability to determine an instantaneous position of the model, relative to the carriage and four carriage wave probes, for each run.

Wave Environment Sensors

The wave environment was measured with both carriage and bridge mounted Senix ultrasonic wave height measurement sensors. Each sensor emitted ultrasonic pulses that bounce off of a target. The return pulse was then read with a piezoelectric element. Using the speed of sound and pulse return time, the sensor was able calculate the distance to the target.

Four Senix wave probes were mounted to the MASK carriage and moved with the carriage to measure the local wave-field. Figure 16 shows a schematic of the model under the MASK carriage and the location of the wave probes. As previously discussed, six additional stationary Senix probes were fixed to the MASK bridge (Figure 2), to capture the global wave-field. Depending on the target relative wave heading required for each condition, the MASK bridge was set at either a 0 degree (for head, beam, and following seas) or a 45 degree angle (for bow and quartering seas), relative to the north side/long bank of the basin. Details of locations of the both the carriage and bridge mounted wave height sensors relative to the MASK basin and model are provided in the Coordinate System section of this report.

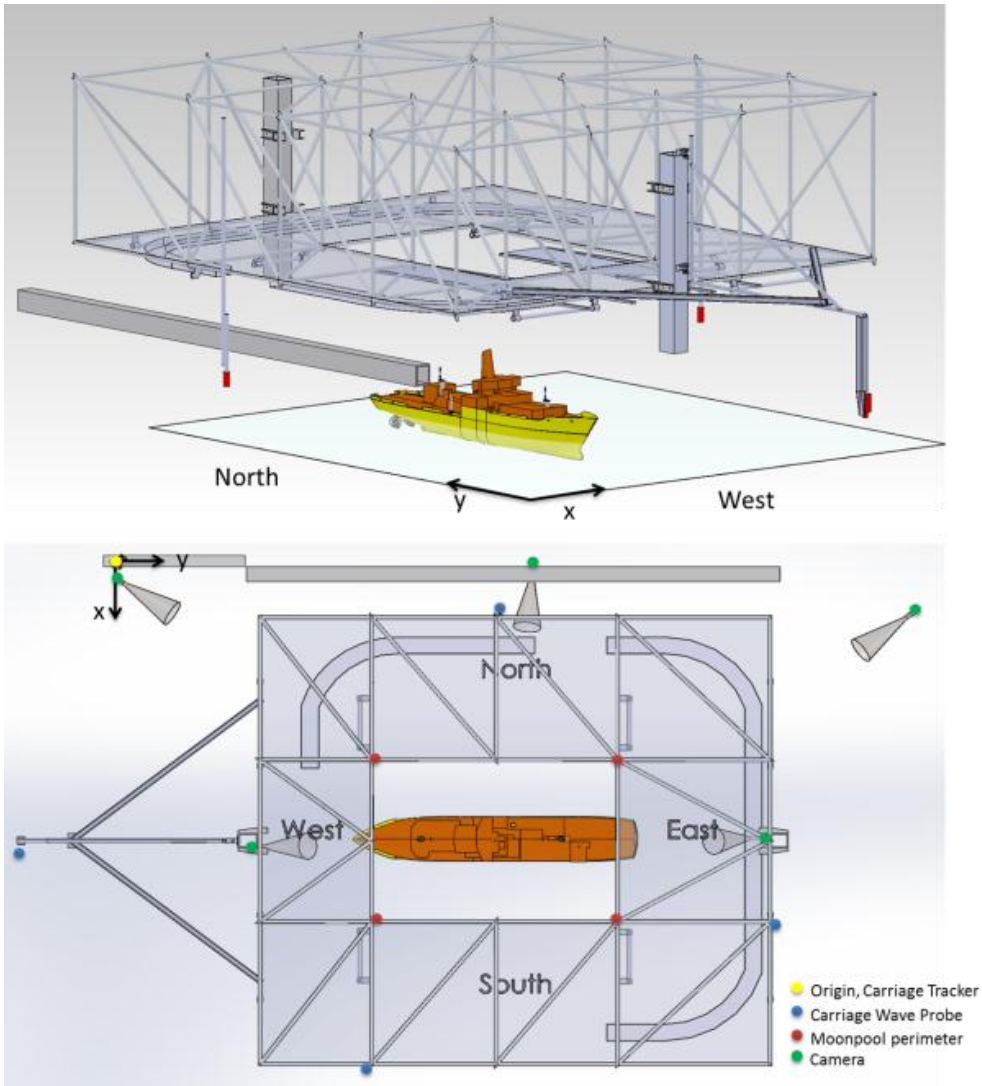

Figure 16. Schematic of model and carriage based wave probes for a head seas condition.

Data Acquisition

Three data acquisition systems were used to collect the required data. The model system was controlled by the model Onboard Computer (OBC) and collected the model and carriage data (carriage speed and carriage wave probes). The tracker system was located on the carriage and linked to model system via a switching box. The bridge system collected the bridge wave probes and communicated with the model system via a wireless network. All computers involved in data acquisition were time synchronized using an ESE-102 GPS master clock and time-sync program linking them to one network. Table 8 summaries the data collection software that was used for this experiment.

The OBC was used to control the model and collect data. Input to the OBC included signals from the motion sensing instruments, sensors collecting control and status of systems on the model, and instruments measuring model or environment data associated with the test. The OBC communicated in real time with the shore-based bridge wave computers over an 802.11b or Wi- Fi network from a wireless Workgroup Bridge on the model to an Access Point associated with an isolated local area network onshore. Prior to output over the wireless network, the OBC Ethernet stream was merged with the tracker data stream via a switching box.

The OBC data transmitted from the model was unpacked, collected, and stored in computers located on the carriage. A remote laptop computer, configured with a virtual driver control console, allowed for remote monitoring and control of the model. This computer monitored the same data stream as stored for data collection, but was restricted to presenting information on control systems to a LabView™ based driver control console displayed real-time on the computer's screen. A second carriage-based computer unpacked the data stream and stored the model and control information as collected data only.

Table 8.Summary of data collection software.

Control Software	
Current Version	Control-Melville-2012.exe Implementation Date 02/28/2012
	Revision from last version
	Rudder Range +- 50deg
Previous Version	_Model Control 46th-r2011-000 Implementation Date 8/15/2011
Model OBC	
Current Version	_Model - 46th-r2012-003.exe Implementation Date 02/28/2012
	Modified DAQ Read to include a short timeout to free up CPU to allow other processes (Specifically ESE Time Service) time to execute.
Previous Version	_Model - 46th-r2011-000 Implementation Date 8/15/2011
Collection Software	
Current Version	_Collection-DDG1000 46th wSS R08.llb Implementation date 02/28/2012
	Changed header on TME output file to match standards tme file set in Code 5500 Data Directory and File Structure r004.doc
Previous Version	_Collection-DDG1000 46th wSS R01 Implementation date 8/15/2011
Wave Bridge Software	
Current Version	BWP-20120227-02a.exe Implementation Date 02/27/2012
	Added a cpu clock time to the data stream.
Previous Version	_Wave Analysis r2011 Implementation Date 7/13/2011
Wave Collection Software	
Current Version	_MAIN - Wave Bridge Collection-r2012wMDLRun-001 Implementation Date 02/27/2012
	Breaksout new bridge CPU time channel.
Previous Version	_MAIN - Wave Bridge Collection-r2011wMDLRun-001 Implementation Date 8/15/2011
Tracker Software	
Current Version	Nikon Surveyor 1.4.24 Implementation 04/2011
Previous Version	Nikon Surveyor 1.4.24 Implementation 04/2011

Video

Video was recorded with four fixed carriage mounted cameras. The locations of these cameras are illustrated in Figure 16 and provided in Table 19. The east camera was used only in head, bow, and beam conditions to capture the model generated wave-field. In quartering and following conditions, the model was rotated 180 degrees and the west camera was used to capture the generated wave-field.

EXPERIMENTAL METHODS

To verify model and wave-field characteristics, several preliminary procedures were conducted in preparation for testing. These preliminary steps consisted of determining the regular and irregular wave settings, measuring roll decay characteristics of the model, and determining speed settings of the throttle control. Once the preliminary procedures were completed, seakeeping in regular and irregular waves was completed as described below.

Wave-maker Settings

Prior to testing the model, the wave-maker blower motor speed (RPM) and dome lip immersion settings required to generate the desired wave conditions were determined. A historical database of blower RPM settings for the various wave frequencies of interest was used. However, due to the many variables and non-linearities of the wave-making system, the blower RPM settings were verified prior to the test. Wave calibrations were performed following the Wave Generation Calibration procedure, 00-5500-114-03. During wave calibrations, the bridge was set at a 30 degree position to maximize the coverage of the ultrasonic wave probes. The wave frequency was set, and the initial blower RPM input was executed by the wave-maker operator. Wave elevation data was recorded from the six active bridge ultrasonic wave probes. A harmonic analysis was performed to determine the average wave-field statistics for a particular RPM setting. Statistical outliers were not included in the average. This process was performed for all of the prescribed wave conditions.

For regular wave operation of the wave-makers, a frequency generator input the prescribed sinusoidal drive signal to the wave-makers. The pneumatic blower motor speed (RPM) and pneumatic dome lips were altered as required to produce the wave conditions of interest. For irregular wave operation, uni-directional seas were generated, from either the long or short bank of wave-makers (Figure 2), depending on the desired wave heading.

Roll Decay

Calm water roll decay tests were performed at 0, 8, and 12 knots full scale. The tests were carried out with the model tethered to the carriage. For each measurement, the model was brought up to the desired speed on a straight course beneath the moving carriage. Once it was verified that the model matched the carriage speed and heading, the steering angle of the propulsion pods was kept constant. The model was excited to roll by quickly depressing either the port or starboard side, in line with the model CG, and then quickly releasing it, so only an impulse force excited the model to roll. The model was allowed to roll until the motion amplitude decayed to less than 1°. This process was repeated at least twice (once for each side, port and starboard) for each speed condition.

Speed Calibration

The speed calibration was the process whereby the throttle command voltage required to achieve a particular model speed was determined. In addition, this process was used to calibrate the paddlewheel, which measured the model speed through water. Speed calibrations were performed following the Ship and Model Speed Calibration procedure, 00-5500-114-02, with the model in free-running mode. The MASK bridge was moved to the south side of the basin. The model was driven in a clockwise fashion around the basin, such that it was driven in a straight line parallel to the longbank wave-makers, approximately 6 meters out from the wave-maker. A pre-measured distance of 30.5 meters along the north shore was used as a reference distance, along which the model was timed to determine the model velocity. This procedure was performed at multiple throttle command voltages, bounding the range of speeds to be tested. The throttle command voltages, paddle wheel voltage, propeller RPM, and measured stopwatch speed were noted along with battery voltage. The throttle command voltages, paddlewheel voltage, and propeller RPM were recorded and plotted versus measured speed. Once a suitable relationship curve was defined for the speed range, the speed calibration was complete.

Seakeeping in Regular Waves

Seakeeping tests in regular waves were conducted for two speeds: 8 and 12 knots (full scale), three headings: head, beam, and following seas; and three wave conditions: 1/60, 1/30 and 1/15 wave steepness. The 1/60 wave steepness was chosen to provide a nominally linear condition, while the 1/30 and 1/15 wave steepness were chosen to provide increasingly nonlinear conditions. Five wave frequencies, at each wave heading, were tested at the 1/60 steepness case to provide data to aid in the validation of motion RAOs. The 1/30 and 1/15 wave steepness runs were only carried out at the frequency corresponding to a λ/LWL ratio of 1. Table 9 provides details of each regular wave condition.

Regular wave runs were performed, as described in QMS procedure 00-5500-094-32. For all regular wave runs, the model was tethered to the carriage. The wave-maker was started and stopped for each regular wave run. After the first few of waves passed the model, the carriage was accelerated to the desired speed. Once the carriage was up to speed and the model was free (verifying that the safety lines were loose), data collection began. The model drivers adjusted model settings, as needed, to keep the model as close to the center opening of the moonpool as possible and on a steady course. This procedure was followed for all the regular wave conditions.

Repeat runs of the 1/60 steepness head and beam sea conditions were made following a new procedure designed to allow both transient and steady state motion to be collected. For these runs, data collection began with the model in calm water, before the wave-maker was started. Timing was adjusted so the carriage and model accelerated in calm water and reached a steady state before encountering the generated waves. Once the model was confirmed at speed, a switch was toggled, marking the location in the data file. The end result was a data file that contained both the transient and steady state motion for a complete run.

Table 9. Details of the regular wave conditions.

Full Scale								
			1/60		1/30		1/15	
λ/LWL	Period	Stationary Frequency	Height	λ	Height	λ	Height	λ
	(sec)	(Hz)	(m)	(m)	(m)	(m)	(m)	(m)
0.5	4.98	0.963	0.6	38.7				
1	7.04	0.681	1.3	77.4	2.6	77.4	5.2	77.4
1.5	8.63	0.556	1.9	116.1				
2	9.96	0.482	2.6	154.8				
2.5	11.13	0.431	3.2	193.5				

Model Scale								
			1/60		1/30		1/15	
λ/LWL	Period	Stationary Frequency	Height	λ	Height	λ	Height	λ
	(sec)	(Hz)	(m)	(m)	(m)	(m)	(m)	(m)
0.5	1.04	0.963	0.3	1.7				
1	1.47	0.681	0.7	3.4	1.3	3.4	2.7	3.4
1.5	1.80	0.556	1.0	5.0				
2	2.08	0.482	1.3	6.7				
2.5	2.32	0.431	1.7	8.4				

Seakeeping in Irregular Waves

Seakeeping in uni-directional irregular waves was performed in Sea States (SS) 3, 4, and 5, at 5 headings, and for three ship speeds. A Bretschneider (BS) spectrum was used to model each sea state (SS). The standard used by the U.S. Navy to define fully developed Sea States is NATO STANAG 4194 (1983). Table 10 provides details for each irregular wave condition. The heading conditions tested were head (180 deg), bow (225 deg), beam (90 deg), stern (45 deg), and following (0 deg) seas. The speeds were 8, and 12 knots (full scale).

All wave runs were performed, as described in QMS procedure 00-5500-094-32, as it relates to irregular wave test conditions. The run time per condition was determined in order to enable the derived statistics to be reported at the 95% confidence level, which provided a good estimate of significant single amplitude (SSA) values (Pierce, 1985). A series of realizations were needed to accumulate sufficient exposure time. Table 11 summarizes the irregular wave run and run times needed for each irregular wave condition. The wave-maker was operated continuously for approximately 35-40 minutes at a time, in order to avoid significant wave reflections and repeating effects. During this time, consecutive runs were made and the time between runs was dependent on the time it takes to back up the carriage and model to the starting

point. After 35-40 minutes, wave-maker operation were ceased and a wait time of approximately 20 minutes was used to ensure the basin had settled and that the effects of the previous run had diminished enough to be considered negligible.

Table 10. Summary of the irregular wave conditions.

ANNUAL SEA STATE OCCURRENCES IN NORTH ATLANTIC						
Full Scale				Model Scale		
SS	Mean Hs (m)	Most Probable Tp (s)		SS	Hs (m)	Most Probable Tp (s)
3	0.9	7.5		3	0.038	1.6
4	1.9	8.8		4	0.082	1.8
5	3.2	9.7		5	0.141	2.0

Table 11. Summary of Irregular Wave Seakeeping runs and required run time.

Irregular Waves: Seakeeping Runs					
Speeds (kts)	Speeds (kts)	Heading	Sea State	95% Run Time (min)	95% Run Time (min)
Full Scale	Model Scale			Model Scale	Full Scale
0	0	0 (Following)	3	4	19
8	1.67	0 (Following)	3	7	34
8	1.67	45 (Quartering)	3	7	34
8	1.67	90 (Beam)	3	4	19
8	1.67	225 (Bow)	3	2	10
8	1.67	180 (Head)	3	2	10
12	2.5	0 (Following)	3	7	34
12	2.5	45 (Quartering)	3	7	34
12	2.5	90 (Beam)	3	4	19
12	2.5	225 (Bow)	3	2	10
12	2.5	180 (Head)	3	2	10
0	0	0 (Following)	4	4	19
8	1.67	0 (Following)	4	7	34
8	1.67	45 (Quartering)	4	7	34
8	1.67	90 (Beam)	4	4	19
8	1.67	225 (Bow)	4	3	14
8	1.67	180 (Head)	4	3	14
12	2.5	0 (Following)	4	7	34
12	2.5	45 (Quartering)	4	7	34
12	2.5	90 (Beam)	4	4	19
12	2.5	225 (Bow)	4	3	14
12	2.5	180 (Head)	4	2	10
0	0	0 (Following)	5	5	24
8	1.67	0 (Following)	5	7	34
8	1.67	45 (Quartering)	5	7	34
8	1.67	90 (Beam)	5	5	24
8	1.67	225 (Bow)	5	3	14
8	1.67	180 (Head)	5	3	14
12	2.5	0 (Following)	5	7	34
12	2.5	45 (Quartering)	5	7	34
12	2.5	90 (Beam)	5	5	24
12	2.5	225 (Bow)	5	3	14
12	2.5	180 (Head)	5	3	14

MEASUREMENT UNCERTAINTY ANALYSIS

This section provides the results of the uncertainty analysis applied to the model instrumentation and wave height sensors. Additional details about the theory and calibration procedures applied to each instrument can be found in Appendix A.

Model Instrumentation Summary

The calibration constants, statistics, and uncertainty estimates for the model instrumentation are listed in Table 12, and a summary of the recommended uncertainty estimates is shown in Table 13. Table 14 contains the constants for the voltage monitors. In Table 12 and Table 14, the pre-test measurements and calibration constants for the test are highlighted in yellow while the post-test measurements are highlighted in light green. The calibration constants used for the test are indicated in bold red font.

One of the features of this test series was the repeat calibrations for pre- and post-test. The slope and intercept data is a measure of the reproducibility of the data, as defined by the ISO GUM (JCGM, 2008). A statistical hypothesis test was applied to both the slope and the intercept. In the T-test column of Table 12, a Pass indicated that the more recent value was statistically the same as the previous one at the 95 % confidence level. A Fail meant that this statistical test did not pass, and the slopes were different. For the slope, the *t*-test from Kleinbaum (1988)

$$t = (b_1 - b_2) / S_{b1-b2} \tag{1}$$

where *b1* and *b2* are the slopes of the two calibrations and $S_{b1\text{-}b2}$ is the standard deviation of the slope difference. The variance of the slope difference is

$$S^2_{b1-b2} = S^2_p [1/S_{xx1} + 1/S_{xx2}] \tag{2}$$

where the pooled estimate is

$$S^2_p = [(n_1 - 2)See^2_1 + (n_2 - 2)See^2_2] / [n_1 + n_2 - 4] \tag{3}$$

and *n* is the number of points in each calibration, *See* is the standard error of estimate, and

$$S_{xx} = \sum_{i=1}^{n} (x_i - < x >)^2 \tag{4}$$

where <*x*> is the average of *x*. The number of degrees-of-freedom for the Student-*t* comparison in Equation (3) is [$n_1 + n_2 - 4$].

For the t-test of the intercept, the slopes were assumed to be the same. The *t*-test in this case is as follows (Armitage, 1971)

$$t = d / S_d \tag{5}$$

where *d* is the difference in intercepts, given by

$$d = < y_1 > - < y_2 > - b(< x_1 > - < x_2 >) \tag{6}$$

and the pooled slope, *b*, for the two calibrations is

$$b = (b_1 S_{xx1} + b_2 S_{xx2}) / (S_{xx1} + S_{xx2}) \tag{7}$$

The variance of *d* is given by

$$S_d^2 = S_c^2\left[1/n_1 + 1/n_2 + \left(< x_1 > - < x_2 >\right)^2 / \left(S_{xx1} + S_{xx2}\right)\right] \quad (8)$$

and the residual mean square about the lines is

$$S_c^2 = \left[S_{yy1} + S_{yy2} + \left(b_1 S_{xx1} + b_2 S_{xx2}\right)^2 / \left(S_{xx1} + S_{xx2}\right)\right] / \left[n_1 + n_2 - 3\right] \quad (9)$$

The number of degrees of freedom for the Student-*t* comparison in this case is [$n_1 + n_2 - 3$].

In addition to the hypothesis test, the data from the newer calibration was corrected with the slope and intercept from the previous calibration, and the residual was computed. The maximum difference in this calculation is shown in Table 12 and Table 14, as *Max Diff*. If the calibration failed the hypothesis test, then *Max Diff* should be compared to the estimated uncertainty in the U95 column. The U95 column is the combined uncertainty of the calibration including the Type A from the individual calibration points, Type B from the calibration uncertainty of the reference, and the uncertainty from the curve fit. The maximum uncertainty in the calibration range was included in the combined uncertainty estimate. If the magnitude of Max Diff is larger than U95, consideration was given to assigning the magnitude of Max Diff as a better estimate of the uncertainty. The recommended uncertainty estimates from calibration from this process are summarized in Table 13.

Additional statistics given in Table 12 and Table 14 include the correlation coefficient and the standard error of estimate (*See*). The correlation coefficient is a measure of the linearity. For perfectly correlated data, the correlation coefficient is 1.0. The *See* is a measure of the standard deviation and is in the same physical units as the instrument. For perfectly correlated data, *See* will be zero. It is also a measure of the uncertainty. Typically, 3**See* is near the estimated uncertainty in the 95 % prediction limit from calibration theory. The next to the last column of the table, *Spec.*, is the manufacturer's specification on instrument accuracy. The column with the heading *CH* is the channel number on the data acquisition card.

In general, the most critical items in Table 12 for the angular measurements are the slopes. The intercepts for the accelerometers, vertical gyroscope, and MicroStrain may be corrected on the basis of zero measurements in calm water at zero model speed, if required. The intercept for the steering angle was corrected after installation with the rudder mechanically at zero degrees.

Wave Height

Wave height for this test series was measured with Senix model TSPC-30S1-232 ToughSonic Distance Sensors. The manufacturer's specification on accuracy is ±0.1 % full-scale or ±0.76 mm (±0.030 in.) for a 762 mm (30 inches) traverse distance. The probes consisted of six probes on the MASK bridge and four probes on the MASK carriage.

The probes were calibrated in-situ by movement of the probes vertically relative to a calm water surface. The bridge probe location was determined by pin locations at 127 mm (5 inches) over a 762 mm (30 inches) that were machined on a milling machine. The uncertainty in the probe location is assumed to be ±0.13 mm (±0.005 in.). The pin locations for the carriage were at 101.6-mm (4-inch) increments over a distance of 812.8 mm (32 inches).

An example of the calibration curve for a bridge probe is presented in Figure A13. The error bars in these figures include the combined uncertainty from the Type A and the position

uncertainty from the Type B estimate. The Type B had a negligible contribution. A nominal noise level of 3 mV rms has a value of 0.26 mm (0.010 inches) rms. With an averaging time of 91.5 s or 4390 samples, the resultant Type A uncertainty is ±7.9 μm (±0.00031 in.). As the figure indicates, the dominant uncertainty was from the curve fit. The bridge probe data were acquired on the MASK Wave Computer at a sample rate of 48 Hz with a low-pass filter setting of 12 Hz.

The carriage probe data were acquired with the model computer at a sample rate of 24 Hz and low-pass filter setting of 12 Hz. The nominal noise level for the model computer was 7 mV rms or 0.61 mm (0.024 inches) rms. The average collection time was 64.4 s or 1550 samples.

Summaries of the calibration results are presented in Table 15 for the bridge probes and Table 16 for the carriage probes. The results are presented in a format similar to that of the model instrumentation in Table 12. In this case, a post-test calibration was not available for a check on reproducibility. The range of uncertainty in wave height for all bridge probes from the Table 15 is ±0.59 to ±2.9 mm (±0.023 to ±0.12 inches), and for the carriage probes ±0.51 to ±0.96 mm (±0.020 to ±0.038 inches). The uncertainty in wave height is typically much larger than the uncertainty in the probe calibration (ITTC 2008c).

Correction for Zeroes

Because the devices for the measurement of pitch, roll, and acceleration may have an offset when they are installed in the model, the data acquired during the test was corrected with measurements in calm water at zero speed. The files from the runs at this condition are referred to as zeroes, and the correction is given by

$$x = x_{\mathrm{m}} - x_0 \tag{10}$$

where x_{m} is the measured value at model speed and x_0 is the zero value from zero speed and calm water. Since this measurement is made with the same instrument, the two measurements are correlated. Consequently, the Type B uncertainty from calibration does not contribute to the uncertainty in the corrected measurement. The only contributors to the combined uncertainty are then from the Type A from the two measurements, and the combined and expanded uncertainty is as follows:

$$U_{\mathrm{c}} = \sqrt{U_{\mathrm{Am}}^2 + U_{\mathrm{A0}}^2} \tag{11}$$

This uncertainty estimate applies to the average value of x, which may not be interest in some cases, such as the average wave height or roll angle where the average value would be zero, in theory.

Table 12. Calibration summary of Model 5720 instrumentation

Manufac.	Model #	Serial #	Function	Cal Date	Units	CH	Slope	T-test	Intercept	T-test	Correl.	Std Error (See)	Max Diff	U95	Spec.	
Columbia	SA-307TX	1755	CG Vert	17-Apr-12	g	10	0.25336	Pass	0.0071	Pass	0.9999355	0.00370	0.0059	0.0121	0.0020	
Columbia	SA-307TX	1755	CG Vert	12-Jan-12	g	10	**0.25357**		**0.0064**		0.9999663	0.00268		0.0094	0.0020	
Columbia	SA-307TX	1755	CG Trans	18-Apr-12	g	12	0.12675	Pass	0.0028	Pass	0.9999997	0.00042	0.0013	0.0014	0.0010	
Columbia	SA-307TX	1755	CG Trans	12-Jan-12	g	12	**0.12670**		**0.0028**		0.9999993	0.00071		0.0039	0.0010	
Columbia	SA-307TX	1755	CG Long	18-Apr-12	g	13	0.12691	Fail	0.0016	Fail	0.9999998	0.00039	0.0077	0.0013	0.0010	
Columbia	SA-307TX	1755	CG Long	12-Jan-12	g	13	**0.12759**		**0.0000**		0.9999989	0.00089		0.0042	0.0010	
Columbia	SA-307TX	1644	Bow Vert	12-Apr-12	g	14	0.25208	Pass	0.0014	Fail	0.9999747	0.00232	0.0048	0.0076	0.0020	
Columbia	SA-307TX	1644	Bow Vert	12-Jan-12	g	14	**0.25249**		**0.0007**		0.9999938	0.00114		0.0051	0.0020	
Columbia	SA-307TX	1644	Bow Trans	12-Apr-12	g	15	0.12633	Pass	0.0047	Pass	0.9999986	0.00096	0.0020	0.0029	0.0010	
Columbia	SA-307TX	1644	Bow Trans	12-Jan-12	g	15	**0.12636**		**0.0048**		0.9999987	0.00091		0.0042	0.0010	
Columbia	SA-307TX	1644	Bow Long	12-Apr-12	g	16	0.12600	Pass	0.0033	Fail	0.9999996	0.00051	0.0040	0.0016	0.0010	
Columbia	SA-307TX	1644	Bow Long	12-Jan-12	g	16	**0.12593**		**0.0010**		0.9999989	0.00084		0.0041	0.0010	
Columbia	SA-307TX	1643	Stern Vert	12-Apr-12	g	17	0.25180	Pass	0.0069	Fail	0.9999921	0.00258	0.0136	0.0086	0.0020	
Columbia	SA-307TX	1643	Stern Vert	12-Jan-12	g	17	**0.25278**		**0.0036**		0.9998994	0.00462		0.0155	0.0020	
Columbia	SA-307TX	1643	Stern Trans	12-Apr-12	g	18	0.12596	Pass	0.0040	Fail	0.9999992	0.00075	-0.0023	0.0023	0.0010	
Columbia	SA-307TX	1643	Stern Trans	12-Jan-12	g	18	**0.12587**		**0.0046**		0.9999987	0.00093		0.0042	0.0010	
Columbia	SA-307TX	1643	Stern Trans	18-Feb-09	g	17	0.12759		0.0054		0.999996	0.00180		0.0058	0.0010	(2)
Columbia	SA-307TX	1643	Stern Long	12-Apr-12	g	19	0.12614	Fail	0.0053	Fail	0.9999996	0.00055	0.0034	0.0017	0.0010	
Columbia	SA-307TX	1643	Stern Long	12-Jan-12	g	19	**0.12606**		**0.0033**		0.9999994	0.00061		0.0038	0.0010	
Rosemount	VG34-0803-3	20126	Roll	19-Apr-12	deg	6	-5.9897	Pass	0.762	Fail	-0.999891	0.524	1.559	1.595	1.0	
Rosemount	VG34-0803-3	20126	Roll	10-Jan-12	deg	6	**-6.0123**		**0.084**		-0.999955	0.336		1.038	1.0	
Rosemount	VG34-0803-3	20126	Pitch	19-Apr-12	deg	7	4.0477	Fail	-0.143	Pass	0.999761	0.464	1.135	1.431	1.0	
Rosemount	VG34-0803-3	20126	Pitch	11-Jan-12	deg	7	**3.9891**		**0.006**		0.999803	0.421		1.312	1.0	
Bourns	6574S-1-103		Rudder Angle	11-Apr-12	deg	2	11.630	Pass	-0.006	Fail	0.9999982	0.037	3.80	0.232		
Bourns	6574S-1-103		Rudder Angle	16-Mar-12	deg	2	**11.672**		**-3.671**		0.9997504	0.648		2.390		(4)
Bourns	6574S-1-103		Rudder Angle	25-Jan-12	deg	2	**11.624**		**-0.957**		0.9999960	0.071		0.302		
Bourns	6574S-1-103		Rudder Angle	23-Feb-09	deg	2	11.603		-0.288		0.999985	0.099		0.377		(2)
Analog Devices	AD451J		Shaft Speed	10-Apr-12	deg	1	301.9329	Pass	6.426	Fail	0.9999999	0.208	1.48	0.725		
Analog Devices	AD451J		Shaft Speed	13-Mar-12	rpm	1	**301.9168**		**5.299**		1.0000000	0.212		0.780		(5)
Analog Devices	AD451J		Shaft Speed	18-Jan-12	rpm	1	**116.6864**		**-0.334**		1.0000000	0.072		0.234		
Analog Devices	AD451J		Velocity	10-Apr-12	m/s		1.3174	Pass	0.156	Fail	0.9999991	0.00083	0.0070	0.0045		
Signet	2536	1050070	Velocity	29-Feb-12	m/s	20	**1.3183**		**0.151**		0.9816940	0.042		0.173		
Analog Devices	AD451J		Velocity	23-Jan-12	m/s	20	**1.3183**		**0.151**		0.9999988	0.00096		0.0045		
Analog Devices	AD451J		Velocity	5-Aug-11	m/s	22	1.7709		0.128		1.0000000	0.00027		0.0023		(3)
Systron Donner	QRS14-100-103	39523	Roll Rate	12-Apr-10	deg/s	8	**-20.038**	Fail	**-0.515**	Fail	-1.000000	0.011	0.087	0.0492	1.0	(2)
Systron Donner	QRS14-100-103	39523	Roll Rate	9-Mar-09	deg/s	8	-20.028		-0.488		-1.000000	0.022		0.0741	1.0	(2)
Systron Donner	QRS14-100-103	39722	Pitch Rate	12-Apr-10	deg/s	9	**20.021**	Fail	**0.469**	Fail	1.000000	0.016	0.104	0.0611	1.0	(2)
Systron Donner	QRS14-100-103	39722	Pitch Rate	9-Mar-09	deg/s	9	20.035		0.492		1.000000	0.015		0.0574	1.0	(2)
Systron Donner	QRS14-50-103	39526	Yaw Rate	12-Apr-10	deg/s	10	**-10.015**	Fail	**-0.316**	Pass	-1.000000	0.020	0.050	0.0734	1.0	(2)
Systron Donner	QRS14-50-103	39526	Yaw Rate	9-Mar-09	deg/s	10	-10.006		-0.314		-1.000000	0.009		0.0353	1.0	(2)
Microstrain	3DM-GX1		Roll	12-Apr-12	deg	29	72.5474	Pass	-176.555	Fail	0.999982	0.210	1.30	0.642	0.50	
Microstrain	3DM-GX1	3017-7019	Roll	12-Jan-12	deg	29	**72.7086**		**-177.955**		0.999965	0.299		0.930	0.50	
MicroStrain	3DM-GX1		Roll	18-Apr-07		25	72.643		-177.185		0.999989	0.164		0.595	0.50	(2)
Microstrain	3DM-GX1		Pitch	12-Apr-12	deg	30	-72.8073	Pass	177.477	Fail	-0.999975	0.151	-1.41	0.470	0.50	
Microstrain	3DM-GX1	3017-7019	Pitch	12-Jan-12	deg	30	**-72.9740**		**178.983**		-0.999943	0.227		0.727	0.50	
MicroStrain	3DM-GX1		Pitch	18-Apr-07		26	-72.859		177.340		-0.999987	0.109		0.399	0.50	(2)

Notes:

(1) Signs for slope and intercept are in model coordinates.

(2) Calibration data from DTMB Model 5647 with System C

(3) Calibration data from DTMB Model 5702 with System E

(4) Bourns potentiometer replaced during test

(5) Gain changed for shaft speed

Pre-test calibration data.

Post-test calibration data

Table 13. Summary of Uncertainty in Model 5720 Instrument Calibration.

Manufac.	Model #	Serial #	Function	Units	CH	Low Range	High Range	U95	U95 (% fs)
Analog Devices	AD451J		Shaft Speed	rpm	1	0.0	1162	1.48	0.13
Bourns	6574S-1-103	Old	Rudder Angle	deg	2	-45	45	0.302	0.67
Bourns	6574S-1-103	New	Rudder Angle	deg	2	-35	35	0.232	0.66
Rosemount	VG34-0803-3	20126	Roll	deg	6	-60	60	1.59	2.7
Rosemount	VG34-0803-3	20126	Pitch	deg	7	-35	35	1.43	4.1
Systron Donner	QRS14-100-10	39523	Roll Rate	deg/s	8	-100	100	0.0870	0.087
Systron Donner	QRS14-100-10	39722	Pitch Rate	deg/s	9	-100	100	0.104	0.10
Systron Donner	QRS14-50-103	39526	Yaw Rate	deg/s	10	50	50	0.0734	0.15
Columbia	SA-307TX	1755	CG Vert	g	11	-1.0	0.0	0.0121	1.2
Columbia	SA-307TX	1755	CG Trans	g	12	-1.0	1.0	0.00393	0.39
Columbia	SA-307TX	1755	CG Long	g	13	-1.0	1.0	0.00415	0.42
Columbia	SA-307TX	1644	Bow Vert	g	14	-1.0	0.0	0.00763	0.76
Columbia	SA-307TX	1644	Bow Trans	g	15	-1.0	1.0	0.00419	0.42
Columbia	SA-307TX	1644	Bow Long	g	16	-1.0	1.0	0.00409	0.41
Columbia	SA-307TX	1643	Stern Vert	g	17	-1.0	0.0	0.0155	1.5
Columbia	SA-307TX	1643	Stern Trans	g	18	-1.0	1.0	0.00423	0.42
Columbia	SA-307TX	1643	Stern Long	g	19	-1.0	1.0	0.00382	0.38
Signet	2536	1050070	Velocity	m/s	20	0.69	1.40	0.173	12.4
Microstrain	3DM-GX1		Roll	deg	29	-60	60	1.30	2.2
Microstrain	3DM-GX1		Pitch	deg	30	-35	35	1.41	4.0

Table 14. Calibration Summary of Model 5720 Voltage Monitors.

Manufac.	Model #	Serial #	Function	Cal Date	Units	CH	Slope	T-test	Intercept	T-test	Correl.	Std Error	Max Diff	U95	Spec.
CR Magnetics	CR5310-100		Prop Battery	11-Apr-12	V	27	20.0709	Fail	0.444	Fail	0.9999998	0.01036	0.256	0.0485	0.50
CR Magnetics	CR5310-100	6020581437	Prop Battery	25-Jan-12	V	27	**20.0873**		**0.192**		0.9999998	0.01083		0.0468	0.50
CR Magnetics	CR5310-100		Prop Battery	11-Feb-09	V	19	20.0571		0.513		0.9999998	0.01073		0.0412	0.50
CR Magnetics	CR5310-50		Elec Battery	12-Apr-12	V	26	10.0570	Pass	0.183	Fail	0.9999993	0.01273	0.0788	0.0552	0.25
CR Magnetics	CR5310-50	5101590587	Elec Battery	25-Jan-12	V	26	**10.0666**		**0.112**		0.9999983	0.02033		0.0860	0.25
CR Magnetics	CR5310-50		Elec Battery	9-Feb-09	V	18	10.0422		0.256		0.9999999	0.00495		0.0234	0.25

Table 15. Calibration Summary of MASK Bridge Probe Wave Height Transducers.

Manufac.	Model #	Serial #	Location	Cal Date	Units	CH	Slope	Intercept	Correl	Std Error	U95	U95 (% fs)	Spec.
Senix	TSPC-30S1-232	4141996	BP1	19-Jul-11	mm	1	-87.5011	444.907	-0.9999995	0.277	1.288	0.338	0.76
Senix	TSPC-30S1-232	4120477	BP3	19-Jul-11	mm	2	-87.4592	407.823	-0.9999999	0.126	0.595	0.156	0.76
Senix	TSPC-30S1-232	4141999	BP4	19-Jul-11	mm	3	-87.4300	451.466	-0.9999975	0.629	2.906	0.763	0.76
Senix	TSPC-30S1-232	4141998	BP5	19-Jul-11	mm	4	-87.3995	424.791	-0.9999988	0.428	1.982	0.520	0.76
Senix	TSPC-30S1-232	4141997	BP6	19-Jul-11	mm	5	-87.4682	429.668	-0.9999995	0.292	1.355	0.356	0.76
Senix	TSPC-30S1-232	4141995	BP8	19-Jul-11	mm	6	-87.4932	454.498	-0.9999998	0.182	0.843	0.221	0.76

Table 16. Calibration Summary of MASK Carriage Probe Wave Height Transducers.

Manufac.	Model #	Serial #	Location	Cal Date	Units	CH	Slope	Intercept	Correl	Std Error	U95	U95 (% fs)	Spec.
Senix	TSPC-30S1-232	4143268	CP East	1-Mar-12	mm	22	-87.2979	438.312	-0.9999996	0.236	0.955	0.235	0.76
Senix	TSPC-30S1-232	4143324	CP West	1-Mar-12	mm	23	-87.2289	432.892	-0.9999997	0.200	0.811	0.200	0.76
Senix	TSPC-30S1-232	4143267	CP South	1-Mar-12	mm	24	-87.2009	437.694	-0.9999999	0.123	0.509	0.125	0.76
Senix	TSPC-30S1-232	4143325	CP North	1-Mar-12	mm	25	-87.2293	432.521	-0.9999999	0.133	0.548	0.135	0.76

DATA INTERPRETATION

The objective of this model test was to provide a controlled data set of measured model ship motion and wave environment data, supporting the development and testing of proposed ESMF technologies. The deliverables include the measurement data files. This section details the data files that were obtained and the supporting information needed to understand and interpret the data sets. The following section, Experimental Results and Data Analysis, presents some example results and analysis. A data CD, which accompanies this report, includes the data and analysis presented in these two sections. Details of the contents of the data CD are provided in Appendix B.

Data Files

Data collection was performed using three independent systems: model, tracker, and the bridge wave height probes. The model system collected all model data and the carriage wave height probe data. These files have a *.tmq* file extension. The tracker provided x and y location data of the model and carriage as well is model heading information. These files have a *.ttq* extension. The bridge wave height probes collected wave height data for the six stationary wave probes suspended from the MASK bridge. These files have a *.twq* extension.

All data are presented in full scale and metric units. All speeds are presented in knots. Any redundant data channels were removed from the data files. Redundant channels were defined as additional sensors that were provided as back-up channels to the primary sensor. Anomalies in the data were identified and removed. Anomalies were identified through review of the electronic log (E-Log), written logs, data time histories, and video files. The majority of anomalies identified were control changes or "rope tugs" during a run. The anomalies were logged by run and systematically removed. The header statistics for all runs with data cuts were re-calculated to reflect the removal of data. Each run with any data cuts is denoted by an "a" after the Run Number in the filename. The data cuts were consistently applied to all of the data files, model, tracker, and bridge waves, to remove the same time slice of data from each file.

Model and Carriage Data (.tmq Files)*

The *.tmq* files contain the data recorded by the model acquisition system: model motions, rates, accelerations, shaft speed, steering angle, and data from the carriage mounted wave height sensors. All model data are reported in the ship coordinate system, as defined in the Instrumentation section. In addition, a Count Time channel is provided. This channel begins at t=0 seconds and propagates at the model sample rate (24 Hz model scale). The Time MDL channel is obsolete.

Each *.tmq* file contains the run number, date, time, etc., and edited data in full scale engineering units, with the addition of the *.tmq* creation time and date. For regular waves, there was only one run per condition. To satisfy the irregular wave run time requirements multiple runs define each irregular wave condition. The *.tmq* for each individual file is provided on the data CD. To determine the statistics per irregular wave condition, all *.tmq* file runs that comprised an irregular wave condition were assembled into a concatenated *.tmq* file and statistics were calculated from the concatenated data for each channel. The concatenated files are not provided, but a summary of the calculated statistics is provided. An example of a *.tmq* file is shown in Appendix C.

Tracker Data (.TTQ Files)

The tracker system was used to provide x and y model location and relative wave heading data. Surge, sway, and heave data were not directly available from the tracker data. Data for these three degrees-of-freedom can be recovered from the accelerometer data if desired.

A *.ttq* file is provided for each run. Each file contains the relative wave heading of the model, the x and y location of the model in both global and local coordinates, the average model speed calculated for the entire run, and the x and y location of each carriage wave height probe in the global coordinate system. The global and local coordinate systems are defined in the Coordinate System section. In addition, a Relative Time channel is provided. This channel begins at t=0 seconds and propagates at the tracker sample rate (24 Hz model scale). The time at t=0 seconds corresponds to t=0 seconds in the model (*.tmq*) files. A cross correlation analysis on model roll and model pitch data measured by the model and tracking system was used to verify this time consistency. An example of a *.ttq* file is shown in Appendix C.

The global x and y time history of the carriage location provided by the carriage tracker was used to determine the x and y time history of model in the local coordinate system. This data was also used to calculate the x and y time histories of each carriage wave height sensor in the global coordinate system.

Bridge Wave Data (.TWQ Files)

The bridge system was used to collect data from the bridge wave height sensors. A *.twq* file is provided for each run and contains a time history for each of the six wave sensors. Similar to the model and tracker data, a Relative Time channel is also provided that begins at t=0 seconds and propagates at the bridge data sample rate (48 Hz model scale). The data point at t=0 seconds was intended to correspond with the model and tracker data at t=0 seconds. However, this was not able to be independently verified. All three data acquisition systems were synchronized to a GPS time clock to ensure synchronization and the GPS time data was recorded in each data set. Upon completion of testing, it was discovered that while the bridge system was synchronized with the GPS system at the start of each day, the source of the time channel intended to synchronize the data files was not the common GPS computer time, as previously understood. Instead it was a timestamp from the bridge DAQ card. Therefore, while the independent data acquisition systems were synchronized using the GPS time clock, there was no way to independently verify the data acquisition began at the same time on the bridge wave collection system as the other systems.

To quantify the uncertainty in the synchronization of the bridge system with the model and tracker system, a comparison between the duration of each model and wave file was made on a per run basis. Figure 17 shows a histogram of the difference in file duration and Table 17 lists the run numbers associated with each bin. Bin spacing is set at 0.1 seconds. A positive time difference indicates the model file (*.tmq*) was longer than the wave file (*.twq*). Conversely, a negative time difference indicated that the wave file was longer than the model file. All but four files fell within a ±1.5 second range, these files are noted in Table 17. Based on this analysis, the bridge wave height data is provided, with the understanding there is a maximum uncertainty of ±1.5 seconds in the start time of the file, relative to the model and tracker data. An example of a *.twq* file is shown in Appendix C.

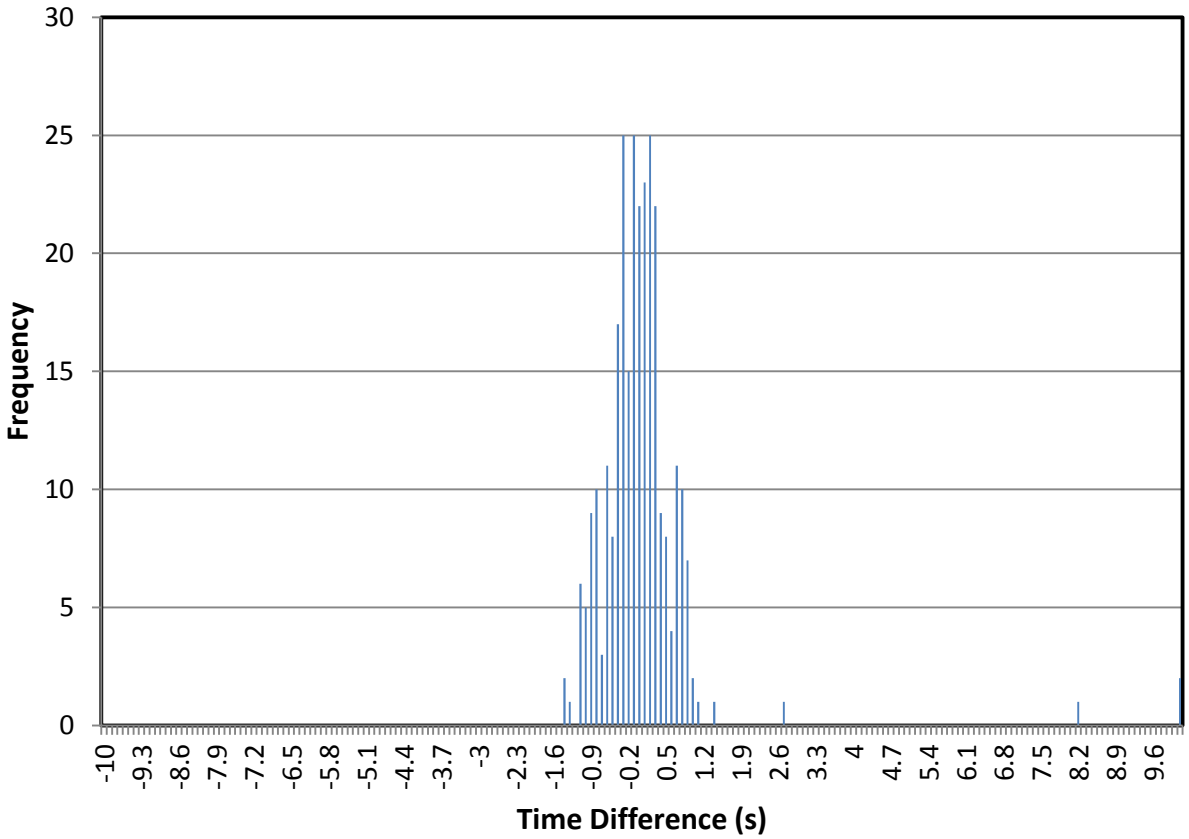

Figure 17. Histogram of model and wave data file duration difference

Table 17. Table of histogram bin data.

Bin	Run Number
-10.0:	
-9.9:	
.	
.	
.	
-1.4:	759, 811
-1.3:	714
-1.2:	
-1.1:	508, 604, 636, 652, 676, 829
-1.0:	391, 619, 784, 786, 824
-0.9:	257, 304, 385, 502, 512, 747, 754, 778, 860
-0.8:	529, 637, 662, 686, 689, 710, 814, 819, 856, 861
-0.7:	530, 679, 684
-0.6:	339, 351, 352, 514, 607, 611, 638, 773, 777, 832, 855
-0.5:	300, 513, 601, 614, 627, 690, 838, 839
-0.4:	372, 457, 492, 503, 526, 646, 654, 664, 704, 709, 737, 768, 769, 787, 803, 810
-0.3:	305, 336, 379, 464, 465, 467, 482, 486, 597, 600, 625, 634, 641, 647, 655, 673, 678, 681, 708, 720, 746, 761, 783, 817, 828
-0.2:	252, 256, 354, 362, 506, 510, 538, 624, 633, 698, 702, 712, 734, 812, 825, 834
-0.1:	262, 301, 355, 375, 459, 493, 531, 532, 534, 596, 603, 617, 649, 665, 666, 670, 722, 730, 741, 752, 758, 774, 822, 833
0.0:	340, 368, 371, 453, 466, 487, 507, 528, 595, 612, 660, 669, 674, 692, 703, 735, 736, 765, 780, 788, 837, 853
0.1:	341, 347, 489, 500, 509, 511, 535, 592, 618, 620, 648, 650, 683, 691, 728, 731, 738, 740, 755, 809, 813, 854
0.2:	309, 334, 491, 494, 504, 525, 536, 594, 613, 639, 680, 705, 716, 717, 721, 723, 742, 753, 767, 823, 826, 840, 857, 897
0.3:	254, 306, 332, 357, 455, 483, 495, 501, 598, 610, 626, 635, 668, 677, 770, 804, 815, 818, 820, 827, 836, 850
0.4:	490, 527, 653, 715, 733, 750, 751, 785, 805, 831
0.5:	329, 346, 516, 628, 682, 687, 729, 851
0.6:	622, 718, 764, 859
0.7:	308, 345, 359, 499, 599, 609, 623, 643, 688, 701, 763
0.8:	316, 373, 376, 533, 621, 661, 663, 685, 766, 852
0.9:	318, 458, 497, 498, 651, 667, 675, 779
1.0:	672, 830
1.1:	358
1.2:	
1.3:	
1.4:	806
.	
2.7:	748
.	
8.2:	909
.	
9.9:	
10.0:	
.	
20.35:	448
.	
39.02:	895

Coordinate Systems

The tracking system provided data relative to the defined coordinate system. For this experiment, the origin for the tracking system was set at the northwest corner of the MASK basin, as shown in Figure 18. This origin defines the global coordinate system. The tracking system outputs the x and y location of the model CG and carriage relative to this origin.

As shown in Figure 18, waves were generated from either the north/long bank (for beam seas) or the West/short bank (for all other wave headings). The MASK bridge was set in either a 0 degree or 45 degree position, depending on desired wave heading. Figure 19 provides a plot of the bridge wave height sensor locations in the global system for each bridge setting. Table 18 provides the tabled data. When the bridge was set at the 0 degree position, the orientation of the global and local coordinate system coincide. When the bridge was set at the 45 degree position, the local coordinate system was rotated by 45 degrees relative to the global coordinate system. The relative orientation was taken into account during the calculation of the model and carriage wave height sensor locations, in local and global coordinates respectively.

The origin of the local coordinate system is defined at the location of the carriage tracker javelin used to track carriage location. This detector was set at the northwest corner of the carriage, as shown in Figure 20. The distances of the carriage wave height sensors, moonpool perimeter, and cameras relative to the carriage tracker are provided in Table 19. Figure 21 provides a plot of the carriage wave height sensors, moonpool perimeter, and cameras in the local coordinate frame.

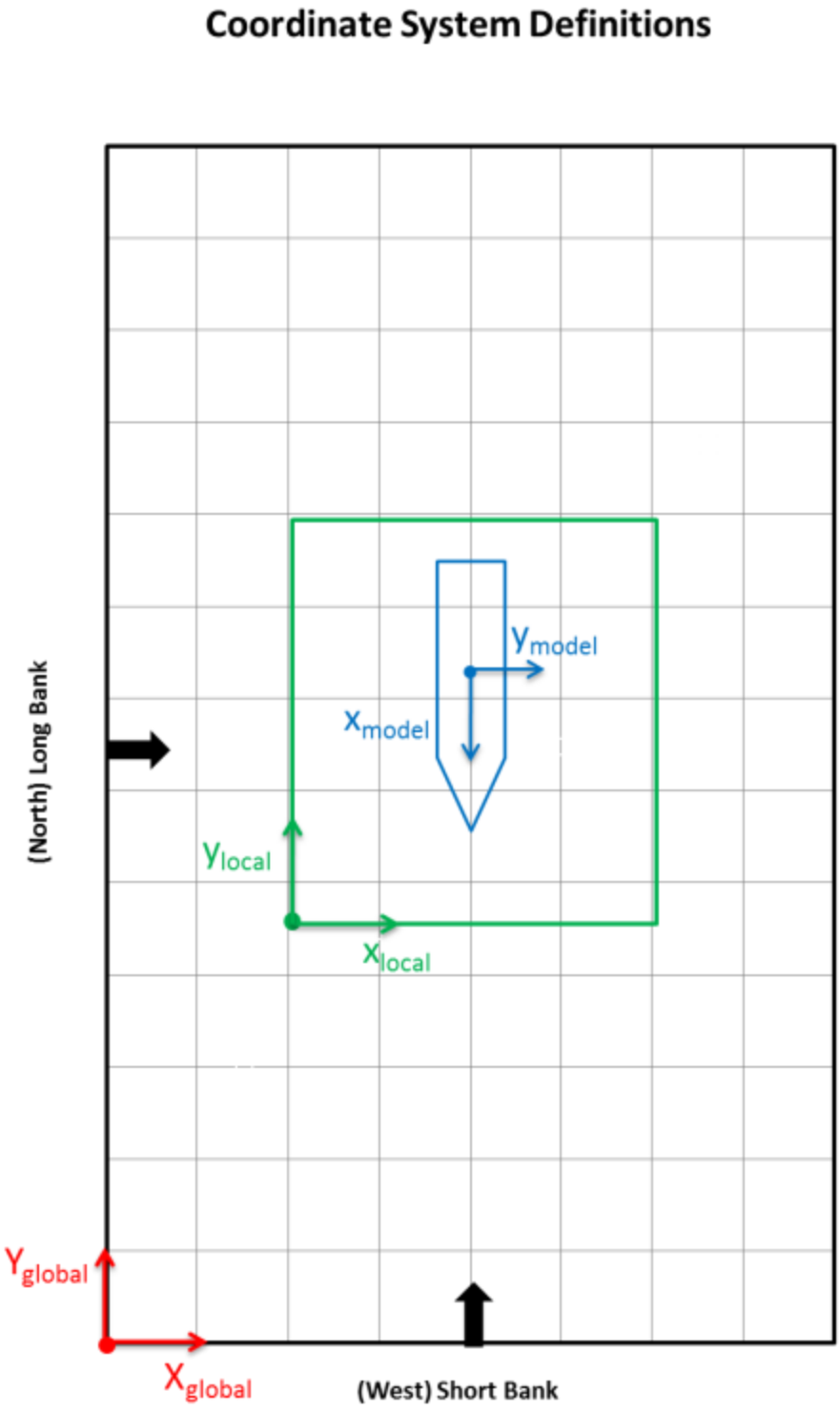

Figure 18. MASK basin coordinate system definition.

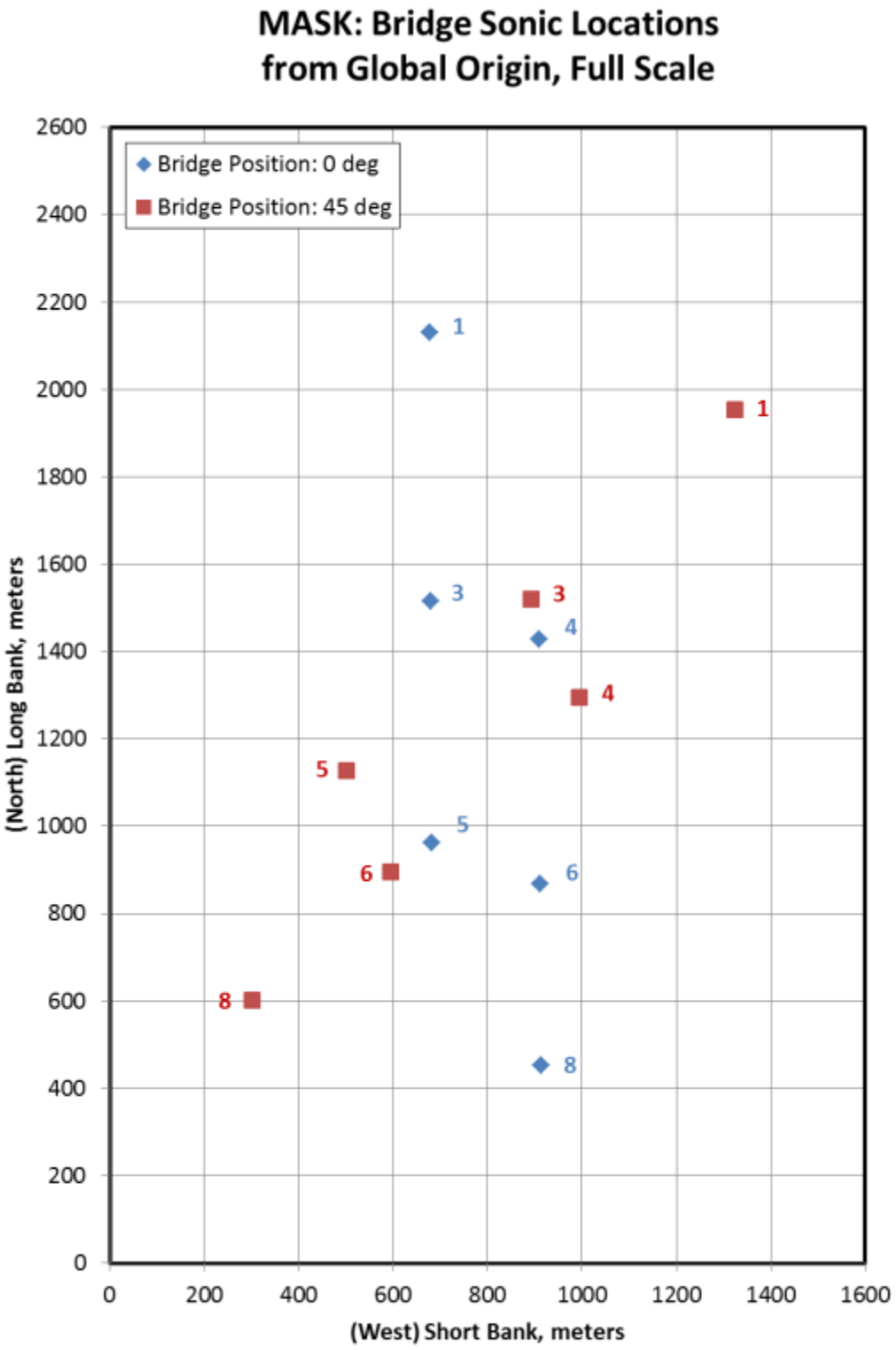

Figure 19. Location of bridge wave height sensors in the global coordinate system for two bridge settings: 0 and 45 degrees. The (0,0) point coincides with the origin of the global coordinate system. All locations given in full scale units.

Table 18. Location of bridge wave height probes measured relative to the global/MASK origin.

Bridge Position: 0 deg		
	X	Y
	meters	meters
Wave Ht 1	677.31	2129.89
Wave Ht 3	680.74	1514.50
Wave Ht 4	910.17	1428.32
Wave Ht 5	681.57	960.86
Wave Ht 6	912.15	868.47
Wave Ht 8	913.12	452.73

Bridge Position: 45 deg		
	X	Y
	meters	meters
Wave Ht 1	1324.94	1952.73
Wave Ht 3	892.98	1518.82
Wave Ht 4	993.76	1294.94
Wave Ht 5	500.83	1128.24
Wave Ht 6	595.89	896.31
Wave Ht 8	302.30	602.45

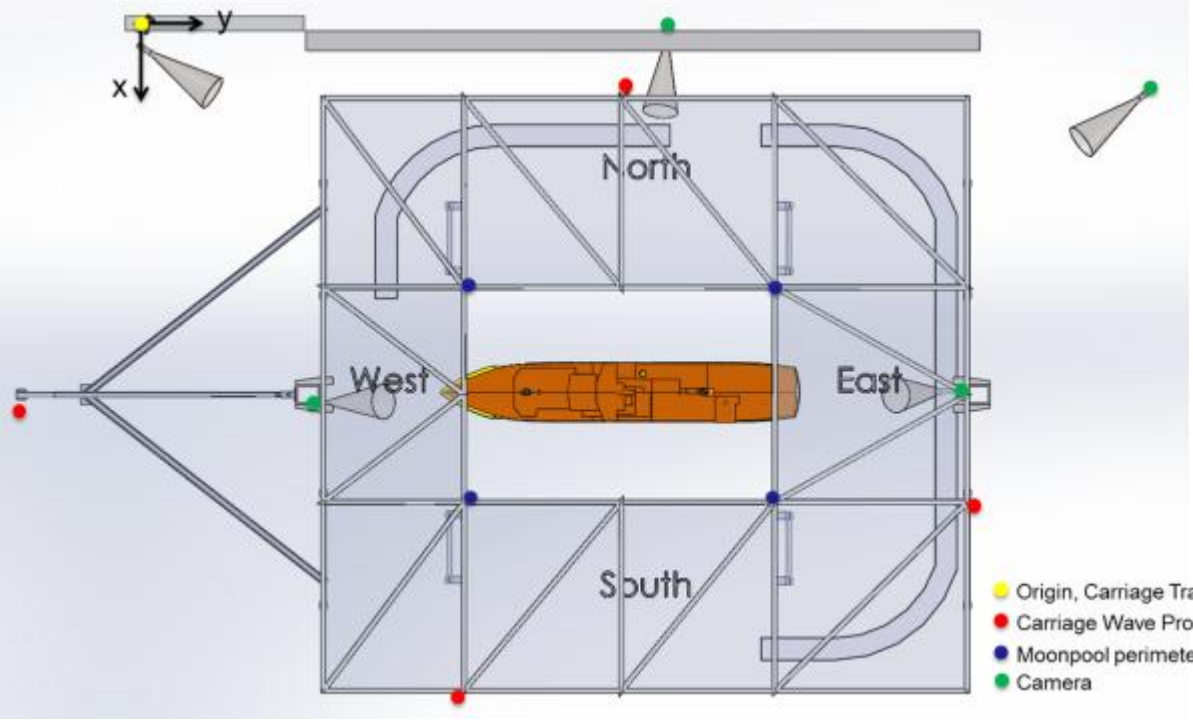

Figure 20. Top view of the local coordinate system.

Table 19. Carriage wave height sensors and camera locations in the carriage/local coordinate system.

Local Coordinate System

Javelin Mount (Carriage Origin)		
	x, meters	**y, meters**
	0.00	0.00
Carriage Sonics		
East	118.03	212.70
South	162.99	91.17
West	94.25	-12.53
North	19.06	130.64
Moonpool		
SE Corner	113.19	169.07
SW Corner	113.16	97.07
NW Corner	65.27	97.14
NE Corner	65.02	168.09
Camera Locations		
Camera W Lens	91.07	64.81
Camera W Aft	91.18	59.60
Camera NW Lens	9.32	23.37
Camera NW Aft	5.72	17.84
Camera N Lens	7.30	143.92
Camera N Aft	0.80	144.55
Camera NE Lens	20.17	254.51
Camera NE Aft	16.28	259.69
Camera E Lens	88.46	208.20
Camera E Aft	88.11	212.48

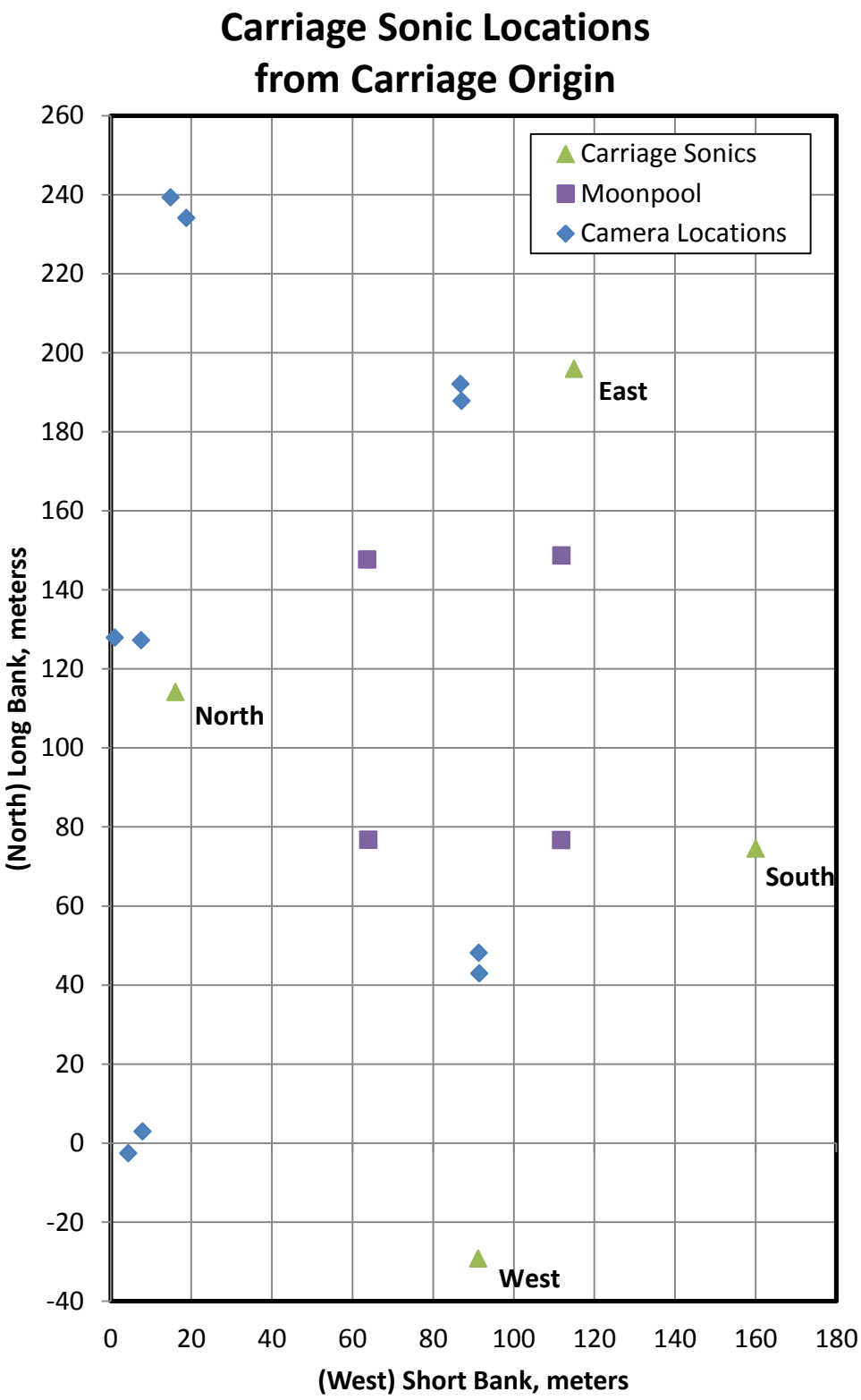

Figure 21. Plot of carriage wave height sensors, moonpool perimeter, and camera locations in the carriage/local coordinate system. The (0,0) point coincides with the origin of the local coordinate system. All locations given in full scale units.

Relative Wave Heading

All heading information is provided as relative wave heading, μ, as defined in Figure 22. In the figure, X and Y are the axes of the global coordinate system. Ship heading data, ψ, was taken from the tracker data. The primary wave heading, β, was dependent on the bank from which the waves were generated. When waves were generated by the short bank, β = 90 and for waves generated from the long bank β = 0.

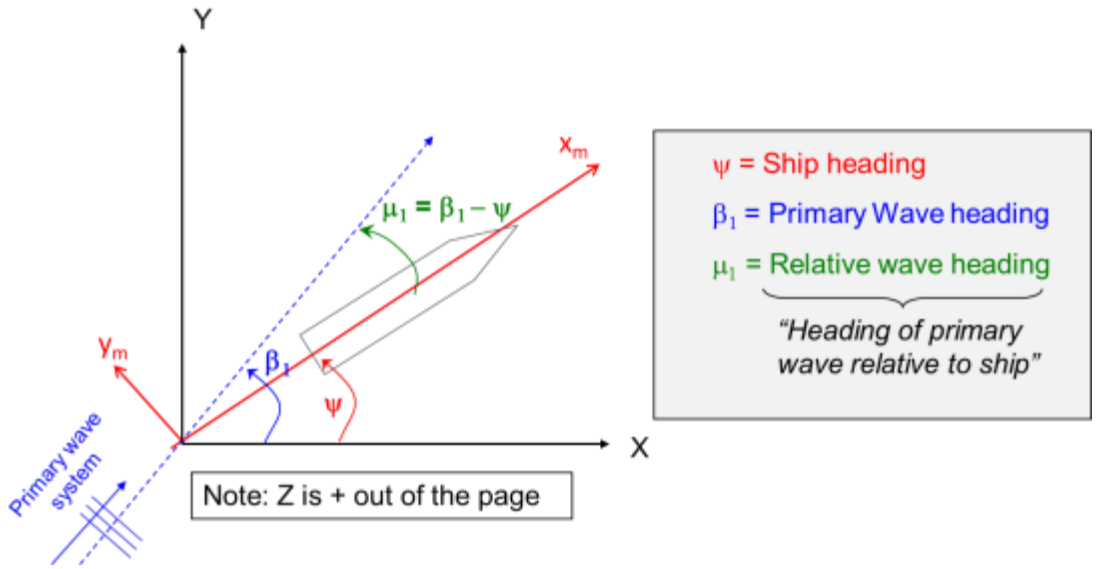

Figure 22. Definition of relative wave heading, μ.

EXPERIMENTAL RESULTS AND DATA ANALYSIS

This section presents the results of the wave-maker calibration, roll decay experiment, and some preliminary analysis on the seakeeping in regular and irregular waves data. The roll decay results and seakeeping results are provided as part of the data CD included with this report.

Wave-maker Settings

The pneumatic wave-makers, while not perfect, can yield consistent results assuming the hydraulic drive cylinders of the pneumatic wave-maker valves have been tuned, and the blower RPM, the lip settings of the domes, and the signal frequency are documented. If the hydraulic cylinders are tuned to provide a consistent movement based upon the drive signal input to the amplifier, then all other variables of the wave-making system, barring environmental factors, can be repeated consistently. Atmospheric changes, in terms of the air density input to the blower system, can create variations in wave output, but this variation is a small factor in the overall wave-maker output.

Wave-maker calibrations were performed in December 2011 and January 2012. The waves were monitored as the test proceeded, and any variability was minimized with small adjustments to blower RPM. Table 20 and Table 21 summarize the results of the wave condition settings for regular and irregular waves respectively.

Table 20. Wave condition settings for regular wave seakeeping.

m5720 Melville: Regular Wave Settings									
Wave Slope (Target), λ	Wave Slope (actual), λ	λ/LWL	Frequency Target	Frequency Acutal	H (Target)	H (Actual)	BRPM	Bank	Lips
			Hz	Hz	inches	inches	Actual		
1/60	63.35	0.5	0.963	1.0684	1.1	1.07	300	Short	UP
1/60	59.414	1	0.681	0.681	2.21	2.24	340	Short	UP
1/60	59.674	1.5	0.556	0.555	3.31	3.35	520	Short	DOWN
1/60	60.31	2	0.482	0.482	4.42	4.40	625	Short	DOWN
1/60	59.883	2.5	0.431	0.432	5.52	5.55	510	Short	DOWN
1/60	59.539	0.5	0.963	0.963	1.1	1.13	320	Long	UP
1/60	62.014	1	0.681	0.680	2.21	2.16	320	Long	UP
1/60	59.854	1.5	0.556	0.555	3.31	3.35	530	Long	DOWN
1/60	59.522	2	0.482	0.481	4.42	4.51	700	Long	DOWN
1/60	60.535	2.5	0.431	0.429	5.52	5.54	535	Long	DOWN
1/30	29.874	1	0.681	0.68	4.42	4.47	575	Short	UP
1/30	30.938	1	0.681	0.68	4.42	585	4.32	Long	UP
1/15	15.12	1	0.681	0.681	8.83	8.89	1000	Short	UP
1/15	15.222	1	0.681	0.681	8.83	8.74	1060	Long	UP

Table 21. Wave condition settings for irregular wave seakeeping.

m5720 Melville - Irregular Waves													
Condition	Hs (Target)	Hs (Actual)	Tm (Target)	BRPM	Bank	Lips	Gen File	PSD File	TFN File	High Pass	Factor	Signal	Generation Variables
	inches	inches	sec							Cutoff Freq		Sign DA	
BS-SS3	1.51	1.541	1.564	410	Short	UP	MVBSSS3SB	BR015156	*.TSC	0.350	7.740	14.00	SMSN, RndmOff, Flow=0.3,Fhigh=2.62
BS-SS3	1.51	1.464	1.564	410	Long	UP	MVBSSS3LB	BR015156	*.TL1	0.350	7.675	14.00	SMSN, RndmOff, Flow=0.3,Fhigh=2.62
BS-SS4	3.22	3.144	1.825	640	Short	UP	MVBSSS4SB	BR032184	*.TSA	0.280	4.170	14.01	SMSN, Rndm Off, Fhigh=2.5 Flow=0.25
BS-SS4	3.22	3.069	1.825	670	Long	UP	MVBSSS4LB	BR032184	*.TLA	0.280	3.65	14.00	SMSN, Rndm Off, Fhigh=2.5 Flow=0.25
BS-SS5	5.56	5.529	2.023	1090	Short	DOWN	MVBSSS5SB	BR059205	*.TS9	0.304	2.912	14.00	SMSN, RndmOff, Fhigh=2.00 Flow=0.20
BS-SS5	5.56	5.424	2.023	1220	Long	DOWN	MVBSSS5LB	BR059205	BR056202.TL3	0.304	2.784	14.00	SMSN, RndmOff, Fhigh=2.00 Flow=0.20

Roll Decay

Roll decay experiments were performed at speeds: 0, 8, and 12 knots full scale. The roll decay coefficient, *N*, is defined by the equation :

$$N = \frac{1}{2\pi} \cdot \ln \frac{\varphi_1}{\varphi_2} \tag{12}$$

where φ_1 and φ_2 are successive amplitudes in the roll decay time history. Figure 23 provides an example of a roll decay time history of the successive peaks and troughs that were identified. The presented data uses the envelope analysis method, where roll amplitudes are measured from peak to trough, or trough to peak. The envelope method avoids the effects of an inaccurate mean or "zero" roll value reference. Figure 24 provides a plot of *N* vs. Mean Roll Amplitude for each speed. There is some scatter observed at the small angles (< 2 degrees) in the 12 knot case. Overall, there is good correlation among the three speeds.

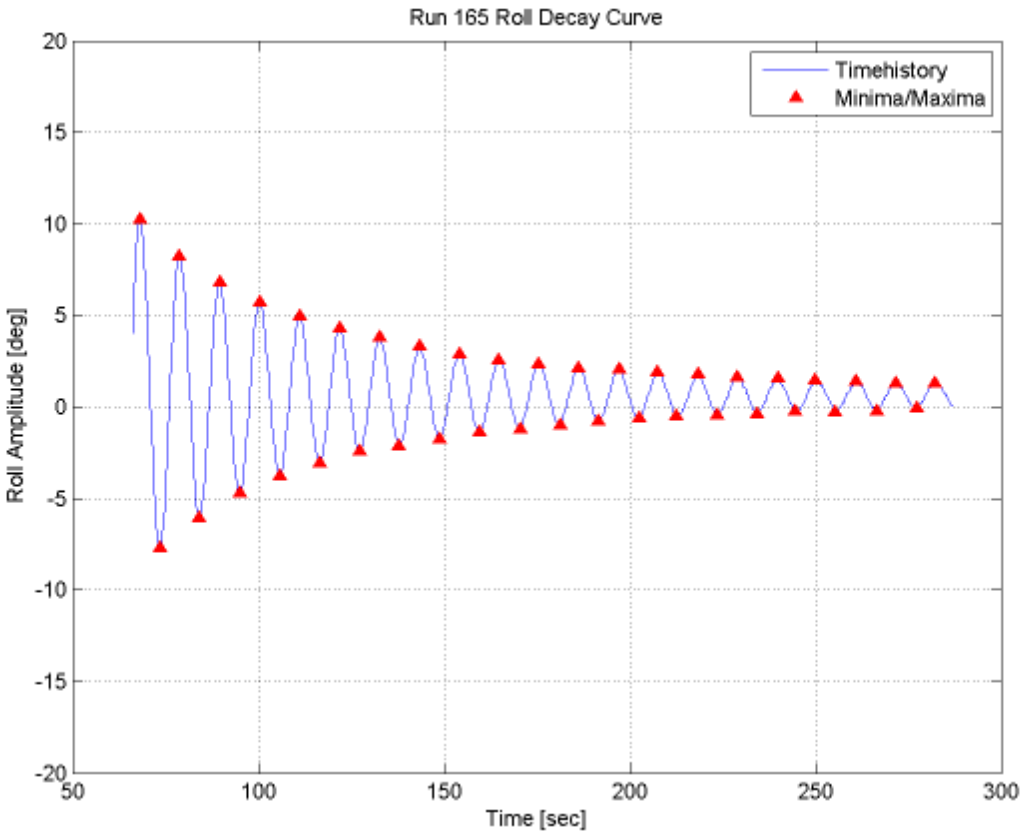

Figure 23. Example of roll decay time history.

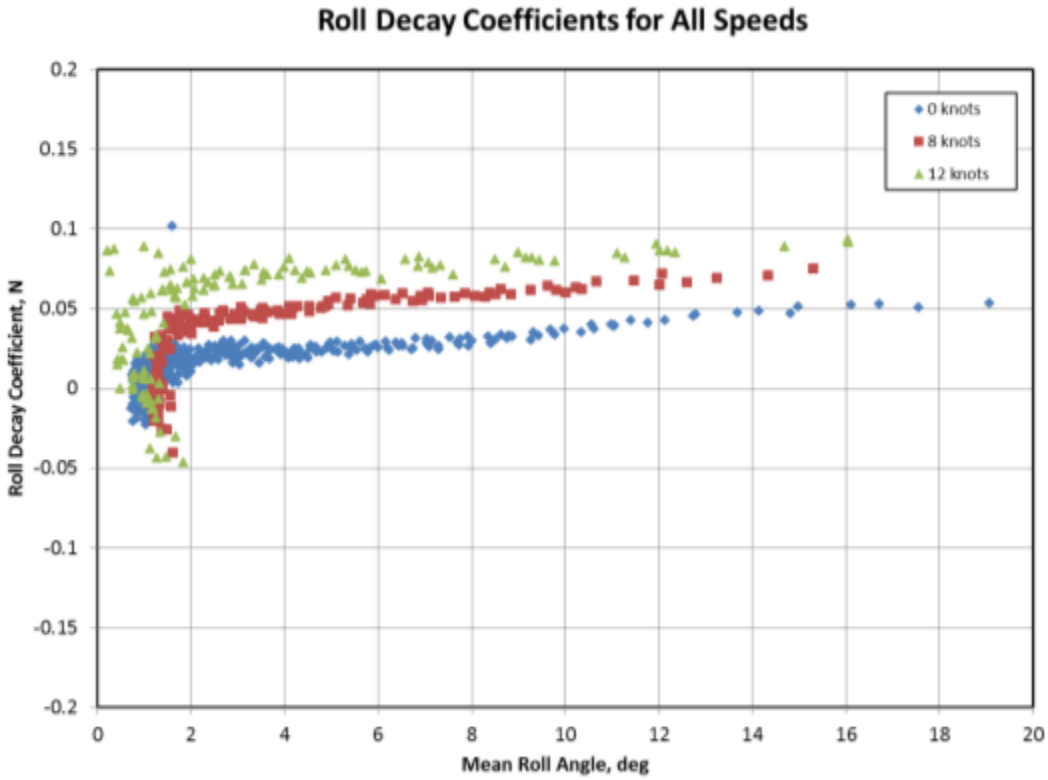

Figure 24. Roll decay coefficients for 0 (blue), 8 (red), and 12 (green) knots full scale.

Seakeeping in Regular Waves

The purpose of the regular wave runs was to produce a simplified set of model scale data to aid in the development, testing, and validation of predicted ship motions. The 1/60 wave steepness was chosen to provide a nominally linear condition while the 1/30 and 1/15 wave steepness were chosen to provide increasingly nonlinear conditions.

Five wave frequencies, at each wave heading, were tested at the 1/60 steepness case to provide data to aid in the validation of motion RAOs. The 1/30 and 1/15 wave steepness runs were only planned for at the frequency corresponding to a λ/LWL ratio of 1. The 12 knot, 1/30 wave steepness, head seas condition was unachievable, as the RPM needed to overcome the added wave resistance was outside of the range of the model motor controller. For similar reasons, the majority of the 1/15 conditions were also unachievable. A limited data set for the 8 knot, 1/15 wave steepness, beam seas condition was obtained. Table 22 summaries the achieved planned and achieved regular wave conditions.

Table 22. Summary of planned and achieved regular wave conditions.

Regular Waves						
1/60						
Wave Frequency	**Head**		**Beam**		**Following**	
(Hz)	**8 kts**	**12 kts**	**8 kts**	**12 kts**	**8 kts**	**12 kts**
0.963	xx	xx	xx	xx	x	x
0.681	xx	xx	xx	xx	x	x
0.556	xx	xx	xx	xx	x	x
0.482	xx	xx	xx	xx	x	x
0.431	xx	xx	xx	xx	x	x
1/30						
Wave Frequency	**Head**		**Beam**		**Following**	
(Hz)	**8 kts**	**12 kts**	**8 kts**	**12 kts**	**8 kts**	**12 kts**
0.963						
0.681	x		x	x	x	x
0.556						
0.482						
0.431						
1/15						
Wave Frequency	**Head**		**Beam**		**Following**	
(Hz)	**8 kts**	**12 kts**	**8 kts**	**12 kts**	**8 kts**	**12 kts**
0.963						
0.681			x			
0.556						
0.482						
0.431						

x standard collect only		fully achieved condition
xx standard and transient collection		unachieved condition
		unplanned condition

Standard Runs vs. Transient Runs

Both standard run and transient runs were completed for the 1/60 steepness head and beam conditions. The standard run followed QMS procedures, providing only steady state data, while the transient method, as previously described, provided both transient and steady state motions. Figure 25 provides example plots for a transient run. Data collection began with the model sitting at its starting point, in calm water (approx. 0-175 seconds in Figure 25). Timing was adjusted so the carriage and model accelerated in calm water (approx. 175-225 seconds in Figure 25) and reached a steady state before then encountering the generated waves. Once the model was confirmed at speed and the tether ropes were loose, a switch was toggled, marking the location in the data file (at approx. 225 seconds in Figure 25). The CMD Word channel in the model data file was used to mark this location, and is shown in Figure 25.

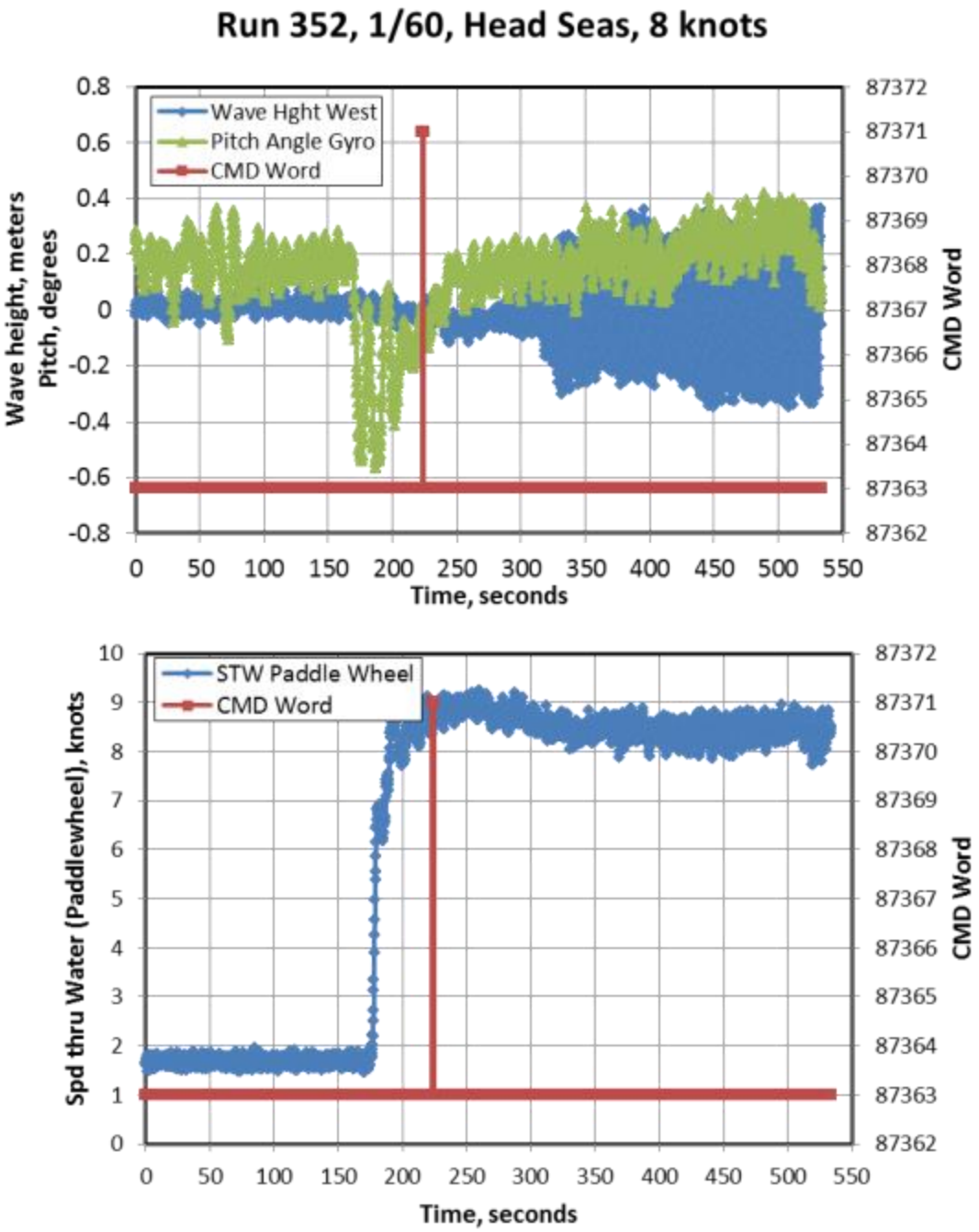

Figure 25. Example data from a regular waves transient run.

Statistical Analysis

For all regular wave runs, all model data channels were analyzed on a per run basis using standard time-series statistical parameters: min, max, mean, standard deviation, significant single amplitude (SSA), and significant double amplitude (SDA). Significant amplitudes were estimated based on Rayleigh distribution factors (significant single amplitude is assumed to be the average highest 1/3 amplitudes, which equals two times the standard deviation). These statistics are found in the individual model files (*.tmq* files). These statistics are also summarized

in statistical summary provided on the data CD that accompanies this report. For the transient runs the statistics are provided for the steady state portion of the run only.

Response Amplitude Operators (RAOs)

Pitch and roll Response Amplitude Operators (RAOs) were computed for all of the 1/60 wave steepness steady state runs (Table 22). Fourier analysis was performed on the roll, pitch, and carriage wave height sensor data. The RAOs are presented as the ratio of the 1st harmonic Fourier coefficient of the desired motion to the Fourier coefficient of the wave height. The wave height data used for analysis was dependent on the relative wave heading of the condition. The west carriage wave height sensor was used for head seas and the north sensor was used for beam and following seas. These probes were chosen because there were verified to be outside of the radiated waves of the model. Figure 26 and Figure 27 provide plots of the roll and pitch RAOs respectively for all headings and speeds. Table 23 provides the tabled results.

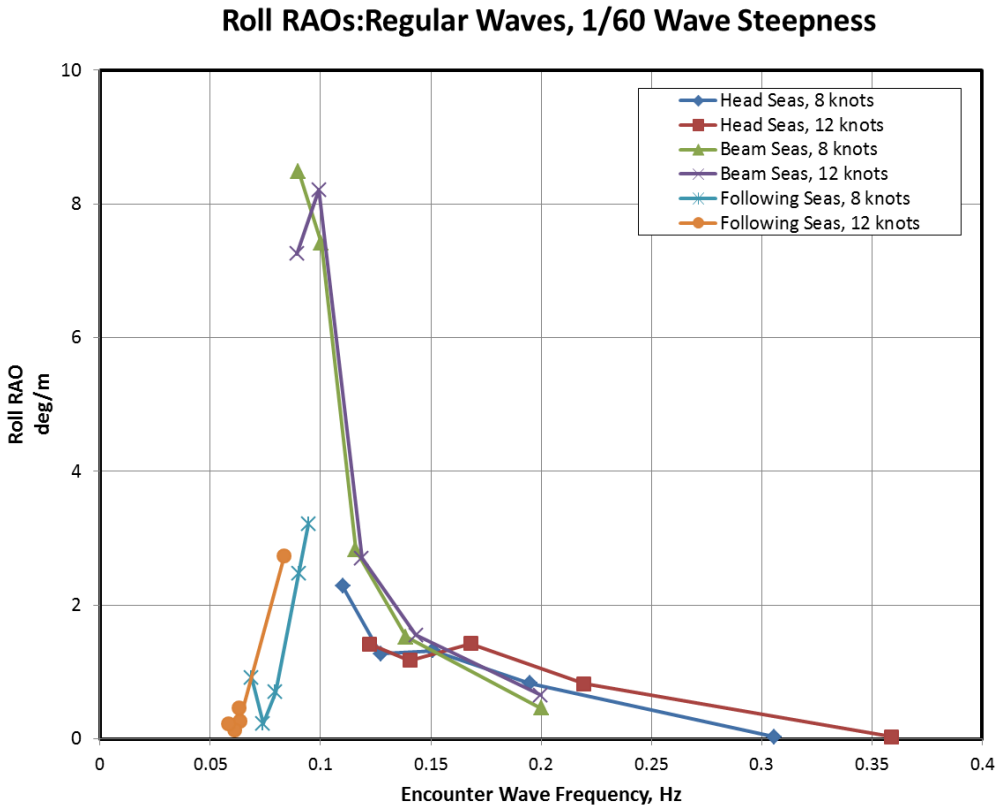

Figure 26. Regular wave roll RAOs for all headings and speeds, 1/60 wave steepness

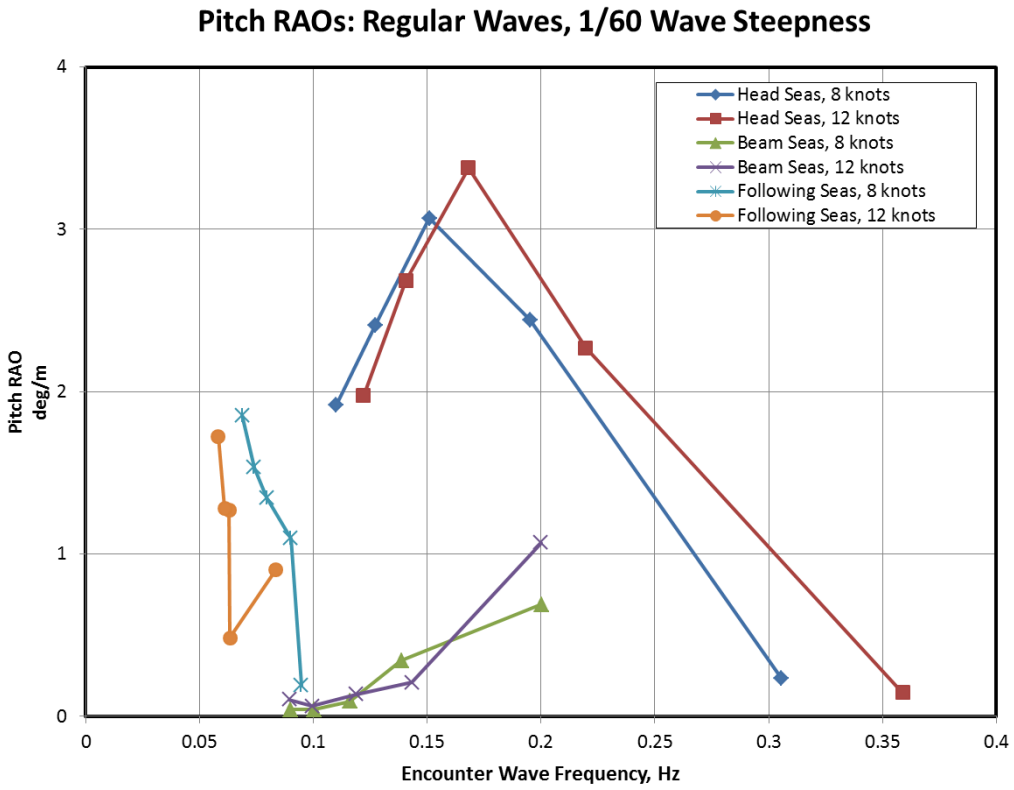

Figure 27. Regular wave pitch RAOs for all headings and speeds, 1/60 wave steepness.

Table 23. Summary of regular wave roll and pitch RAOs.

Run #	Speed, kts	Wave Slope	Frequency	Heading	rao-roll	rao-pitch	EncTp	FSCOEF-roll	FSCOEF-pitch	FSCOEF-wave
895	8	1/60	0.963	Head	0.02926	0.23305	3.27144	8.80E-03	7.01E-02	3.01E-01
300	8	1/60	0.681	Head	0.8284	2.44335	5.12492	4.96E-01	1.46E+00	5.98E-01
897	8	1/60	0.556	Head	1.31613	3.06818	6.62285	1.14E+00	2.65E+00	8.65E-01
256	8	1/60	0.482	Head	1.27317	2.40764	7.85914	1.51E+00	2.86E+00	1.19E+00
252	8	1/60	0.431	Head	2.28224	1.91962	9.08885	3.18E+00	2.68E+00	1.40E+00
304	12	1/60	0.963	Head	0.03086	0.14696	2.78624	9.06E-03	4.31E-02	2.94E-01
301	12	1/60	0.681	Head	0.82487	2.26856	4.55476	4.22E-01	1.16E+00	5.11E-01
262	12	1/60	0.556	Head	1.42593	3.37971	5.95153	1.27E+00	3.01E+00	8.92E-01
257	12	1/60	0.482	Head	1.17663	2.68173	7.11517	1.39E+00	3.17E+00	1.18E+00
254	12	1/60	0.431	Head	1.41829	1.9746	8.19469	2.02E+00	2.81E+00	1.42E+00
305	8	1/60	0.963	Beam	0.46346	0.68745	4.99785	1.63E-01	2.41E-01	3.51E-01
308	8	1/60	0.681	Beam	1.52157	0.34208	7.21309	9.16E-01	2.06E-01	6.02E-01
318	8	1/60	0.556	Beam	2.82833	0.09037	8.62645	2.98E+00	9.53E-02	1.05E+00
329	8	1/60	0.482	Beam	7.41064	0.04078	9.97612	9.26E+00	5.09E-02	1.25E+00
332	8	1/60	0.431	Beam	8.48725	0.04074	11.11294	1.40E+01	6.73E-02	1.65E+00
306	12	1/60	0.963	Beam	0.65423	1.06828	5.00265	2.43E-01	3.98E-01	3.72E-01
309	12	1/60	0.681	Beam	1.54929	0.20784	6.97484	9.76E-01	1.31E-01	6.30E-01
316	12	1/60	0.556	Beam	2.69751	0.13472	8.42072	2.80E+00	1.40E-01	1.04E+00
371	12	1/60	0.482	Beam	8.21069	0.0609	10.06068	9.89E+00	7.34E-02	1.20E+00
334	12	1/60	0.431	Beam	7.25509	0.10161	11.18537	1.16E+01	1.62E-01	1.60E+00
448	8	1/60	0.963	Following	3.20868	0.18872	10.57045	1.05E+00	6.20E-02	3.29E-01
455	8	1/60	0.681	Following	2.466	1.09553	11.09334	1.52E+00	6.75E-01	6.16E-01
458	8	1/60	0.556	Following	0.69535	1.34692	12.56925	6.94E-01	1.34E+00	9.99E-01
464	8	1/60	0.482	Following	0.22716	1.53306	13.53194	3.15E-01	2.13E+00	1.39E+00
466	8	1/60	0.431	Following	0.91159	1.85452	14.5456	1.42E+00	2.89E+00	1.56E+00
453	12	1/60	0.963	Following	2.73637	0.90396	11.96784	4.49E-02	1.48E-02	1.64E-02
457	12	1/60	0.681	Following	0.26229	0.48353	15.77207	1.96E-01	3.61E-01	7.46E-01
459	12	1/60	0.556	Following	0.47014	1.2688	15.87499	3.88E-01	1.05E+00	8.25E-01
465	12	1/60	0.482	Following	0.13969	1.2781	16.35371	1.93E-01	1.77E+00	1.38E+00
467	12	1/60	0.431	Following	0.23168	1.72229	17.20668	3.30E-01	2.45E+00	1.42E+00

Seakeeping in Irregular Waves

The purpose of the irregular wave runs was to simulate a realistic ocean environment, producing a set of model scale data to aid in the development, testing, and validation of predicted ship motion platforms. Seakeeping in irregular waves was performed in three sea states, two speeds, and five headings, as shown in Table 24.

Table 24. Summary of achieved irregular wave seakeeping conditions.

Irregular Waves										
Heading	**Head**		**Bow**		**Beam**		**Quartering**		**Following**	
Speed	**8 kts**	**12 kts**	**8 kts**	**12 kts**	**8 kts**	**12 kts**	**8 kts**	**12 kts**	**8 kts**	**12 kts**
BS-SS3	x	x	x	x	x	x	x	x	x	x
BS-SS4	x	x	x	x	x	x	x	x	x	x
BS-SS5	x	x	x	x	x	x	x	x	x	x

Statistical Analysis

For all irregular wave runs, all model data channels were analyzed on a per run basis using standard time-series statistical parameters: minimum, maximum, mean, standard deviation, significant single amplitude (SSA), and significant double amplitude (SDA). Significant amplitudes were estimated based on Rayleigh distribution factors (significant single amplitude is assumed to be the average highest 1/3 amplitudes, which equals two times the standard deviation). These statistics are found in the individual model files (*.tmq* files).

In addition, individual runs were concatenated to create a complete condition file. Runs were assembled based on the irregular wave run time requirement per conditions. From these assembled data sets, minimum statistics (maximum, minimum, mean, standard deviation, single significant amplitude) were calculated for all model data channels. These statistics are summarized in a statistical summary file provided in the data CD that accompanies this report. Table 25 is an excerpt of the full statistical summary for the irregular wave conditions. The calculated statistics are presented for roll and pitch.

Table 25. Excerpt of irregular wave seakeeping conditions statistical summary.

Run Numbers	Condition	Heading	Speed	Carriage Spd, Tracker	Model Spd, Tracker	Run Time, Actual	Roll Angle Gyro, deg						Pitch Angle Gyro					
			knots	knots	knots	sec	Max	Min	Mean	Stdev	SSA	SDA	Max	Min	Mean	Stdev	SSA	SDA
698, 701-702, 710	BS-SS3	Head	8	7.92	7.98	1075.87	1.39	-0.22	0.56	0.22	0.44	0.88	1.57	-1.31	0.14	0.46	0.92	1.84
746-748, 750	BS-SS3	Bow	8	7.94	7.95	1231.34	1.88	-0.05	0.85	0.31	0.63	1.26	1.97	-1.52	0.15	0.50	1.00	2.01
809-813	BS-SS3	Beam	8	7.92	7.97	1582.64	2.77	-1.32	0.71	0.53	1.06	2.13	0.66	-0.55	0.16	0.16	0.33	0.65
603-604, 607, 609-613	BS-SS3	Quarter	8	7.93	7.96	2319.20	4.67	-4.14	0.56	1.17	2.34	4.68	1.48	-0.97	0.17	0.32	0.64	1.29
486-487, 489-494	BS-SS3	Follow	8	7.94	7.97	2391.74	2.61	-2.44	0.26	0.67	1.35	2.70	1.42	-1.08	0.20	0.32	0.63	1.26
703-705, 707-709	BS-SS3	Head	12	11.88	11.99	1108.45	1.35	-0.45	0.41	0.25	0.49	0.98	1.88	-1.47	0.18	0.44	0.89	1.78
751-755	BS-SS3	Bow	12	11.91	12.01	956.58	1.76	-0.44	0.67	0.31	0.62	1.24	2.22	-1.61	0.22	0.49	0.98	1.96
803-806, 814-815, 817-820	BS-SS3	Beam	12	11.89	12.70	1752.09	2.22	-1.18	0.63	0.56	1.11	2.22	0.85	-0.44	0.26	0.17	0.34	0.69
614, 617-628	BS-SS3	Quarter	12	11.88	11.94	2456.29	3.81	-2.22	0.43	0.79	1.59	3.17	1.28	-0.93	0.26	0.31	0.62	1.24
495, 497-504, 506-508	BS-SS3	Follow	12	11.91	11.96	2256.46	1.38	-1.25	0.13	0.37	0.73	1.47	1.04	-0.83	0.21	0.27	0.53	1.07
720-723	BS-SS4	Head	8	7.94	7.93	1209.16	2.49	-1.60	0.58	0.57	1.14	2.28	3.87	-3.86	0.12	1.04	2.07	4.14
758-759, 761, 763	BS-SS4	Bow	8	7.94	7.86	1140.62	2.92	-2.19	0.86	0.71	1.42	2.84	4.48	-3.49	0.09	1.09	2.18	4.35
822-826	BS-SS4	Beam	8	7.93	7.95	1517.66	6.07	-4.61	0.70	1.87	3.75	7.49	0.84	-0.68	0.14	0.23	0.47	0.93
633-639, 641	BS-SS4	Quarter	8	7.94	7.97	2422.12	9.62	-9.65	0.34	2.74	5.48	10.96	2.73	-2.54	0.13	0.70	1.40	2.80
509-514, 516	BS-SS4	Follow	8	7.95	8.00	2130.57	4.35	-3.81	0.20	1.28	2.57	5.14	2.29	-1.82	0.15	0.69	1.39	2.77
712, 714-719	BS-SS4	Head	12	11.89	11.91	1190.58	2.55	-1.32	0.41	0.52	1.05	2.09	3.27	-3.17	0.18	1.07	2.15	4.30
764-770	BS-SS4	Bow	12	11.90	11.87	1287.09	3.44	-1.84	0.76	0.64	1.28	2.56	3.99	-3.31	0.12	1.06	2.12	4.25
827-834	BS-SS4	Beam	12	11.85	11.90	1459.14	5.32	-4.47	0.41	1.59	3.18	6.37	1.01	-0.68	0.22	0.24	0.48	0.96
643, 646-655	BS-SS4	Quarter	12	11.91	12.00	2045.64	5.57	-4.40	0.19	1.53	3.06	6.13	2.32	-1.98	0.19	0.63	1.25	2.51
525-536, 538	BS-SS4	Follow	12	11.90	11.91	2441.30	2.43	-1.35	0.17	0.44	0.87	1.74	2.01	-1.62	0.21	0.54	1.09	2.18
728-731, 733, 741	BS-SS5	Head	8	7.93	7.92	1787.46	3.85	-4.01	0.30	1.05	2.10	4.20	6.38	-5.92	0.11	1.85	3.71	7.42
773-774, 777-779	BS-SS5	Bow	8	7.94	7.81	1263.89	4.93	-3.25	0.71	1.36	2.72	5.45	6.03	-5.42	0.01	1.69	3.39	6.78
836-840	BS-SS5	Beam	8	7.93	7.92	1517.06	13.45	-12.70	0.63	4.06	8.11	16.23	1.19	-1.03	0.12	0.31	0.63	1.25
660-668	BS-SS5	Quarter	8	7.94	7.96	2471.47	14.27	-16.47	-0.06	4.72	9.44	18.87	3.84	-3.58	0.14	1.15	2.30	4.59
592, 594-601	BS-SS5	Follow	8	7.92	7.84	2564.39	5.40	-3.79	0.44	1.45	2.90	5.80	5.07	-3.72	0.15	1.37	2.73	5.47
734-738, 740, 742	BS-SS5	Head	12	11.90	11.79	1232.74	2.55	-3.19	0.22	0.85	1.70	3.40	5.72	-5.28	0.17	1.84	3.68	7.36
780, 783-788	BS-SS5	Bow	12	11.90	11.85	967.17	4.52	-2.75	0.79	1.03	2.06	4.12	5.13	-5.73	0.15	1.71	3.41	6.83
850-857, 859-861	BS-SS5	Beam	12	11.90	13.73	2043.84	10.50	-10.24	0.40	3.76	7.52	15.03	1.27	-1.39	0.18	0.33	0.65	1.31
669-670, 672-681	BS-SS5	Quarter	12	11.91	11.94	2220.09	10.20	-11.79	-0.29	3.17	6.33	12.67	3.88	-3.23	0.23	1.19	2.38	4.75
682-692	BS-SS5	Follow	12	11.91	11.94	2096.20	2.05	-1.13	0.36	0.45	0.89	1.79	2.81	-2.70	0.24	0.95	1.91	3.81

Achieved Wave Spectra

Spectral analysis was performed on the bridge wave height data to determine the achieved wave spectra for each irregular wave condition. The power density spectrum for each wave probe was calculated using the concatenated time history data. During the concatenation process, no adjustments were made to the wave elevation data to correct or smooth for discontinuities that occur at the intersection point of the individual files. For each probe, the wave elevation time history was divided into overlapping sections with the length of each section and the amount of overlap controlled by the user. Each section of data was windowed using a Hanning window function, given by:

$$w_i = 0.5\left(1 - \cos\left(\frac{2\pi i}{N}\right)\right) \tag{13}$$

where w_i is the value of the window function at index value i and N is the number of points in a section of data. A discrete fast Fourier transform (FFT) was performed on each section of windowed data using the build-in FFT function in MatLab. For each index, the magnitude squared of the discrete Fourier transform was averaged using all the sections of data providing the discrete power density spectrum for each wave height probe. The power density spectrum was normalized so that the total power per unit time was consistent with that of the wave elevation time history. This was done to ensure the power density spectrum was not influenced by the collection length of a particular set of runs.

For each probe, the significant wave height was calculated as four times the square root of the area under the discrete power spectrum curve. This area was determined using a trapezoid rule integration scheme. The modal period for each probe was calculated by identifying the frequency value with the largest energy content and inverting to a period value. An average significant wave height and modal period was also determined for each condition. This was accomplished by calculating an averaged discrete power spectrum from the discrete power density spectrums from each probe. The average significant wave height and average modal period were then calculated using the same approach that was applied for individual probe results but now using the averaged discrete power spectrum.

Figure 28 is an example of the output of the wave spectra analysis. The data CD that accompanies this report provides the spectrum analysis results for each irregular wave condition. Due to limitations of the wave-maker, which make it difficult to produce energy at the high frequencies, it is typical that the achieved spectra has less energy at the higher frequencies than the target frequencies.

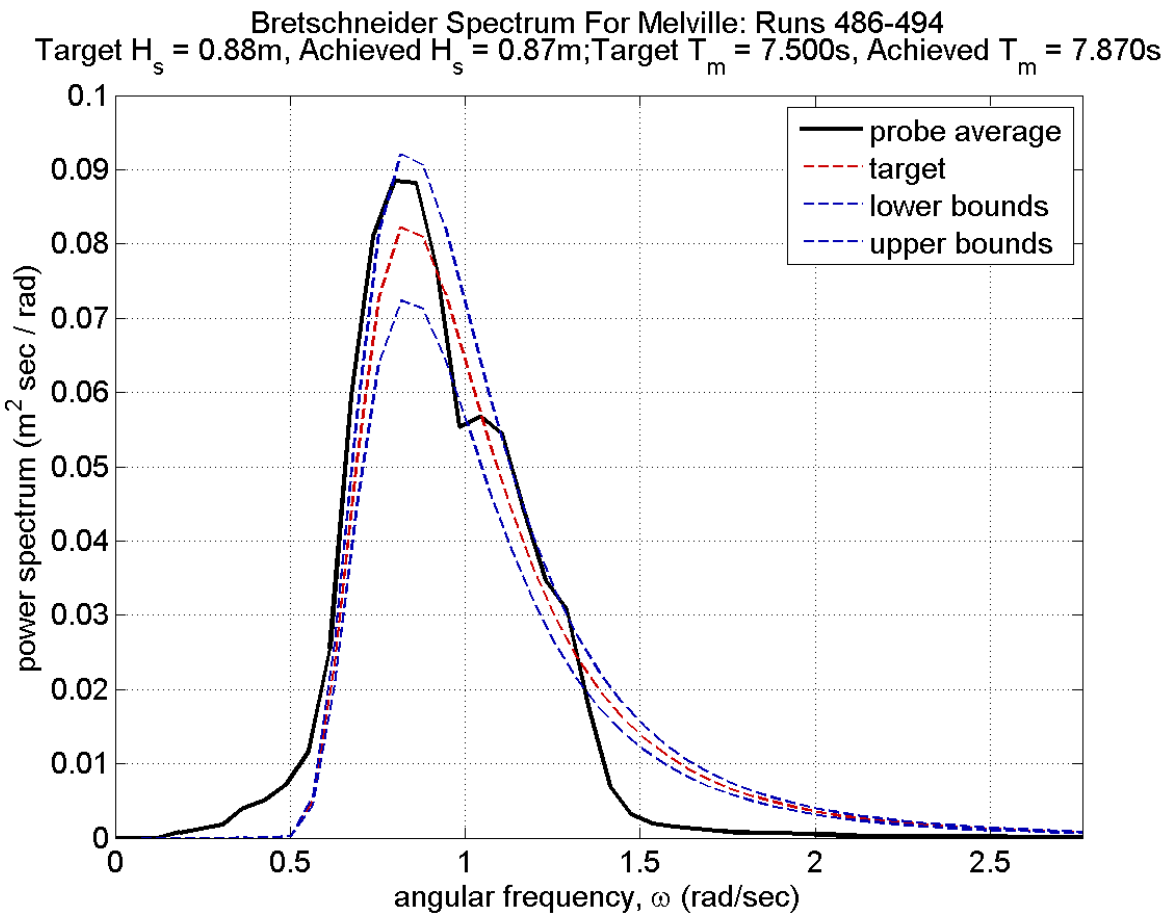

Figure 28. Example of achieved versus target wave spectra. Condition: BS-SS3, 8 knots, following seas.

Table 26. Summary of achieved significant wave height (H_s) and modal period (T_m) for each irregular wave condition.

Run Numbers	Condition	Heading	Target Speed	Hs (Target)	Ave Hs	BP 3 Hs	BP 4 Hs	BP 5 Hs	BP 6 Hs	BP 8 Hs	Tm (Target)	Ave Tm	BP 3 Tm	BP 4 Tm	BP 5 Tm	BP 6 Tm	BP 8 Tm
#	---	---	(knots)	(m)	(m)	(m)	(m)	(m)	(m)	(m)	(sec)	(sec)	(sec)	(sec)	(sec)	(sec)	(sec)
698;701;702;710	BS-SS3	Head (180 deg)	8.0	0.88	0.93	0.93	1.04	0.90	0.91	0.92	7.50	6.82	6.02	7.31	6.82	6.82	6.82
746;747;748;750	BS-SS3	Bow (225 deg)	8.0	0.88	0.93	0.93	1.02	1.00	0.98	0.80	7.50	7.31	7.87	7.87	7.31	7.31	7.31
809;810;811;812;813	BS-SS3	Beam (90 deg)	8.0	0.88	0.91	0.83	0.89	0.96	0.92	1.00	7.50	7.87	7.31	7.87	7.87	7.87	7.87
603;604;607;609;610;611;612;613	BS-SS3	Quartering (45 deg)	8.0	0.88	0.90	0.94	0.99	0.92	0.93	0.79	7.50	6.82	7.31	6.82	6.82	6.82	6.82
486;487;489;490;491;492;493;494	BS-SS3	Following (0 deg)	8.0	0.88	0.87	0.78	0.91	0.85	0.92	0.95	7.50	7.87	8.53	7.87	7.87	8.53	6.82
703;704;705;707;708;709	BS-SS3	Head (180 deg)	12.0	0.88	0.94	1.00	1.09	0.87	0.86	0.91	7.50	6.82	7.31	7.87	6.82	6.82	6.82
751;752;753;754;755	BS-SS3	Bow (225 deg)	12.0	0.88	0.91	0.94	0.97	0.98	0.93	0.79	7.50	7.87	7.87	6.82	7.31	7.87	6.82
803;804;805;806;814;815;817;818;819;820	BS-SS3	Bow (225 deg)	12.0	0.88	0.92	0.83	0.92	0.97	0.94	1.01	7.50	7.31	6.82	7.31	7.31	7.87	7.31
614;617;618;619;620;621;622;623;624;625;626;627;628;629	BS-SS3	Quartering (45 deg)	12.0	0.88	0.88	0.92	0.93	0.95	0.89	0.77	7.50	7.31	7.87	7.87	7.31	7.31	7.31
495;497;498;499;500;501;502;503;504;505;506;507;508	BS-SS3	Following (0 deg)	12.0	0.88	0.85	0.88	0.84	0.85	0.86	0.90	7.50	7.87	5.39	7.87	5.68	9.30	7.31
720;721;722;723	BS-SS4	Head (180 deg)	8.0	1.88	2.00	2.01	2.14	1.87	2.04	2.00	8.80	8.53	10.23	9.30	8.53	10.23	8.53
758;759;760;761;763	BS-SS4	Bow (225 deg)	8.0	1.88	1.95	2.09	2.01	2.06	2.00	1.60	8.80	9.30	9.30	9.30	9.30	10.23	7.31
822;823;824;825;826	BS-SS4	Beam (90 deg)	8.0	1.88	1.93	1.76	1.84	2.00	1.94	2.11	8.80	7.87	9.30	7.87	9.30	7.87	7.87
633;634;635;636;637;638;639;641	BS-SS4	Quartering (45 deg)	8.0	1.88	1.98	2.07	2.05	2.18	2.00	1.59	8.80	8.53	8.53	9.30	8.53	9.30	8.53
509;510;511;512;513;514;516	BS-SS4	Following (0 deg)	8.0	1.88	1.73	1.64	1.79	1.62	1.84	1.81	8.80	8.53	10.23	8.53	7.87	8.53	8.53
712;714;715;716;717;718;719	BS-SS4	Head (180 deg)	12.0	1.88	1.99	2.03	2.22	1.86	1.93	1.94	8.80	8.53	10.23	8.53	8.53	8.53	8.53
764;765;766;767;768;769;770	BS-SS4	Bow (225 deg)	12.0	1.88	1.95	2.07	2.01	2.03	2.02	1.61	8.80	8.53	8.53	7.87	7.87	9.30	7.87
827;828;829;830;831;832;833;834	BS-SS4	Beam (90 deg)	12.0	1.88	1.90	1.70	1.79	1.99	1.94	2.10	8.80	7.87	7.87	7.87	8.53	7.87	7.87
643;646;647;648;649;650;651;652;653;654;655	BS-SS4	Quartering (45 deg)	12.0	1.88	1.93	2.01	2.00	2.11	1.95	1.58	8.80	8.53	8.53	8.53	8.53	8.53	7.31
525;526;527;528;529;530;531;532;533;534;535;536;538	BS-SS4	Following (0 deg)	12.0	1.88	1.89	1.73	2.02	1.68	2.08	1.93	8.80	8.53	10.23	8.53	7.87	8.53	7.87
728;729;730;731;741	BS-SS5	Head (180 deg)	8.0	3.25	3.15	3.21	3.31	2.97	3.26	3.01	9.70	9.30	10.23	9.30	8.53	10.23	8.53
773;774;777;778;779	BS-SS5	Bow (225 deg)	8.0	3.25	3.12	3.21	3.21	3.49	3.23	2.36	9.70	10.23	10.23	10.23	10.23	10.23	9.30
836;837;838;839;840	BS-SS5	Beam (90 deg)	8.0	3.25	3.37	3.32	3.46	3.29	3.31	3.51	9.70	10.23	10.23	10.23	10.23	10.23	10.23
660;661;662;663;664;665;666;667;668	BS-SS5	Quartering (45 deg)	8.0	3.25	3.05	3.26	3.08	3.41	3.12	2.29	9.70	10.23	8.53	10.23	10.23	10.23	9.30
592;594;595;596;597;598;599;600;601	BS-SS5	Following (0 deg)	8.0	3.25	3.32	3.46	3.50	3.16	3.34	3.14	9.70	9.30	10.23	9.30	9.30	10.23	9.30
734;735;736;737;738;740;742	BS-SS5	Head (180 deg)	12.0	3.25	3.18	3.25	3.11	3.02	3.35	3.20	9.70	10.23	10.23	9.30	10.23	10.23	10.23
780;783;784;786;787;788	BS-SS5	Bow (225 deg)	12.0	3.25	3.06	3.27	3.19	3.36	3.14	2.27	9.70	9.30	8.53	9.30	9.30	9.30	9.30
850;851;852;853;854;855;856;857;859;860;861	BS-SS5	Beam (90 deg)	12.0	3.25	3.43	3.36	3.50	3.32	3.43	3.55	9.70	9.30	9.30	10.23	9.30	10.23	9.30
669;670;672;673;674;675;676;677;678;679;680;681	BS-SS5	Quartering (45 deg)	12.0	3.25	3.06	3.32	3.14	3.33	3.11	2.29	9.70	9.30	9.30	9.30	10.23	10.23	9.30
682;683;684;685;686;687;688;689;690;691;692	BS-SS5	Following (0 deg)	12.0	3.25	3.15	3.23	3.18	2.99	3.26	3.09	9.70	10.23	10.23	9.30	10.23	10.23	10.23

Response Amplitude Operators (RAOs)

Pitch and roll Response Amplitude Operators (RAOs) were computed for each irregular wave condition. Spectral analysis was performed on the roll, pitch, and carriage wave height data to compute the spectral densities of each signal. The ratio of motion to wave data was calculated by dividing the spectral density of the desired motion by the spectral density of the wave data. The RAO for each encounter frequency is equal to the square root of the spectral density ratios. The wave height data used for analysis was dependent of the relative wave heading of the condition. The west carriage wave height sensor was used for head and bow seas, the north sensor was used for beam and following seas, and the south sensor was used for quartering seas. These probes were chosen because there were verified to be outside of the radiated waves of the model Figure 29 and Figure 30 provide plots of the roll and pitch RAOs respectively for all headings in SS3, and a model speed of 8 knots. Appendix D provides plots for all irregular wave conditions.

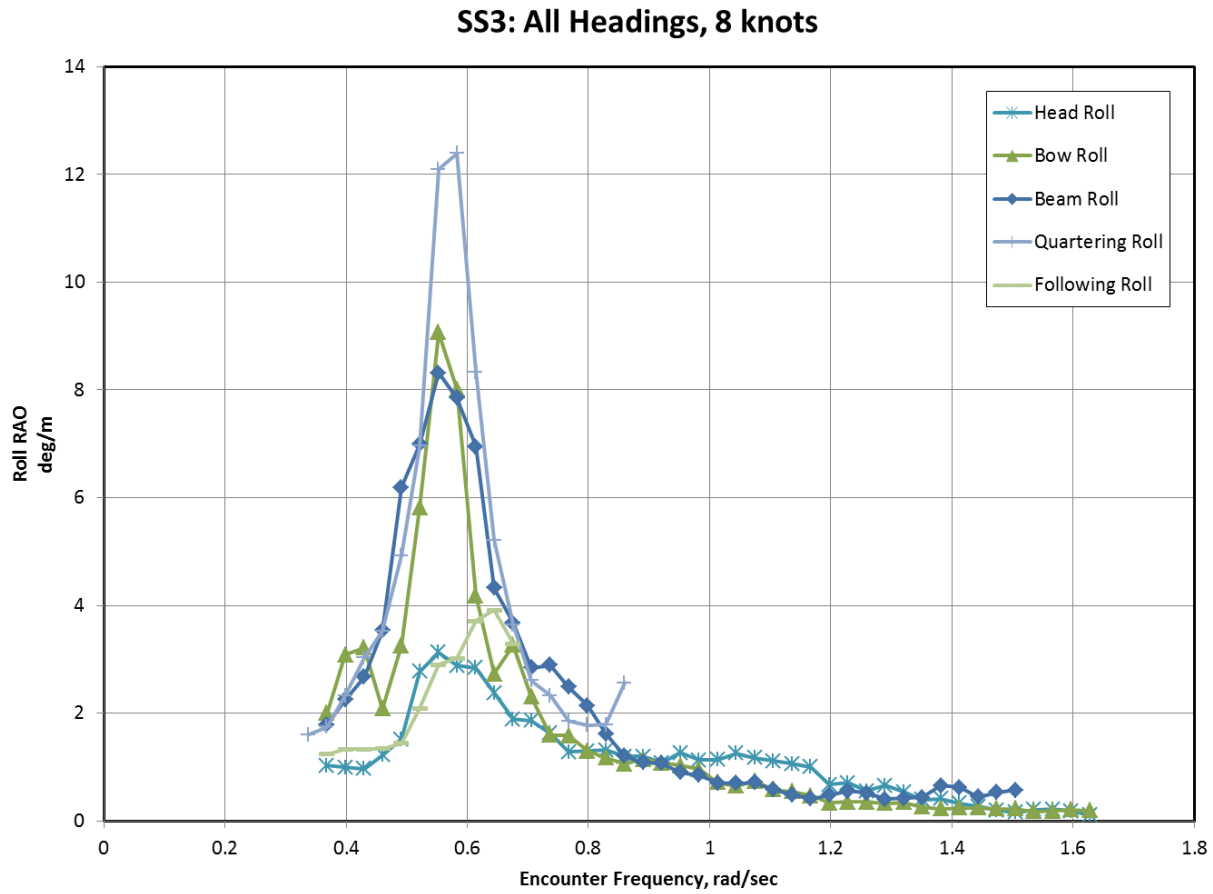

Figure 29. Roll RAOs for SS3, all headings, 8 knots.

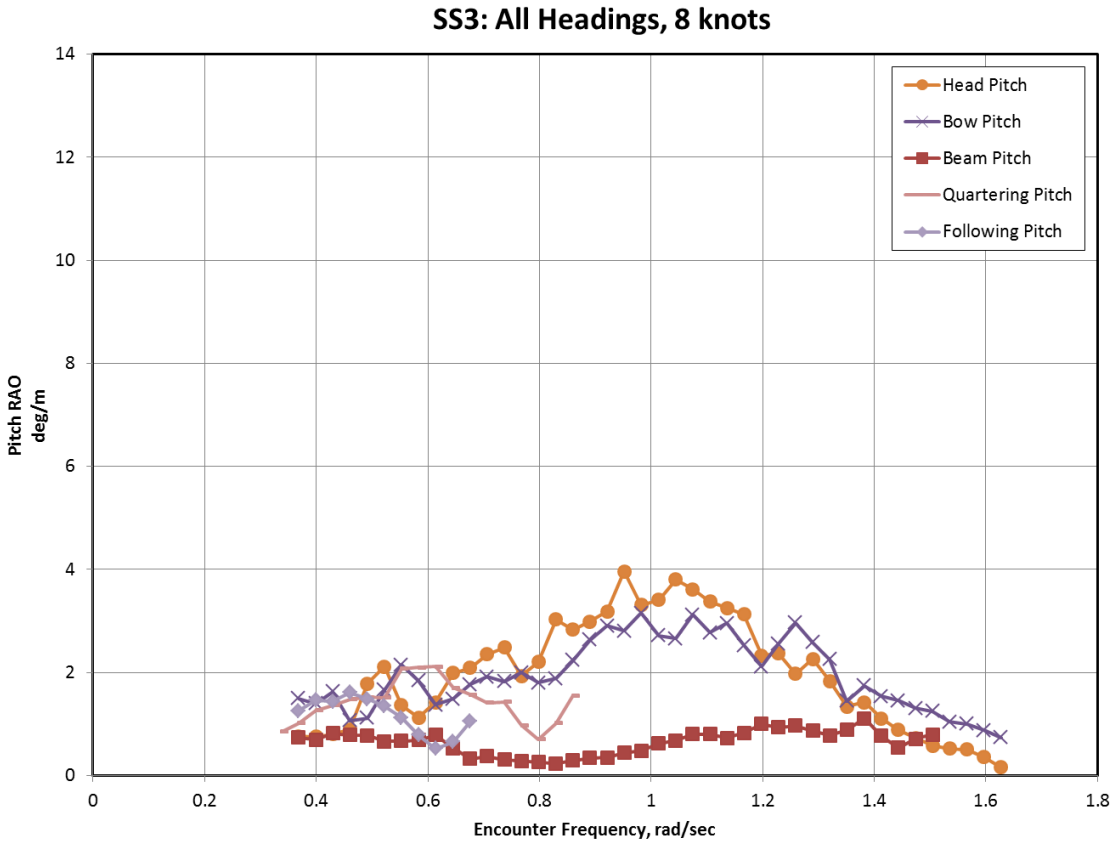

Figure 30. Pitch RAOs for SS3, all headings, 8 knots.

Statistical Uncertainty

Statistical uncertainty differs from measurement uncertainty and is determined from a finite number of experimental records, while probabilistic concepts, such as variance, are defined for an infinite data set. As a result, the calculation of such quantities on any real-world data set is only an estimate of the actual quantity. The estimate is a random number, and as with any random number, has its own distribution, mean value, and variance. The assessment of statistical uncertainty is a means of determining the variations in the data. It is typically performed using the boundaries of the confidence interval, where the true value is contained with a given confidence probability, such as 95%, which is used for most engineering applications.

A statistical uncertainty analysis was performed for each irregular wave condition. An estimate of the variance in the model roll and pitch data and individual bridge probe wave height sensors was determined on a per run and per condition basis. Details of the theory and application of this analysis can be found in Appendix E. Figure 31 shows an plot of the estimate of variance in pitch and roll for the irregular wave condition: SS3 in beam seas at 8 knots. An estimate of the variance and the 95% confidence interval were determined for each run, as shown by the blue dots and red lines in Figure 31. In addition, the mean for the condition (an ensemble of all of the runs) and its confidence interval were determined. The same process was applied to each bridge wave height probe for each irregular wave condition. The complete results of this analysis can be found on the data CD that accompanies this report.

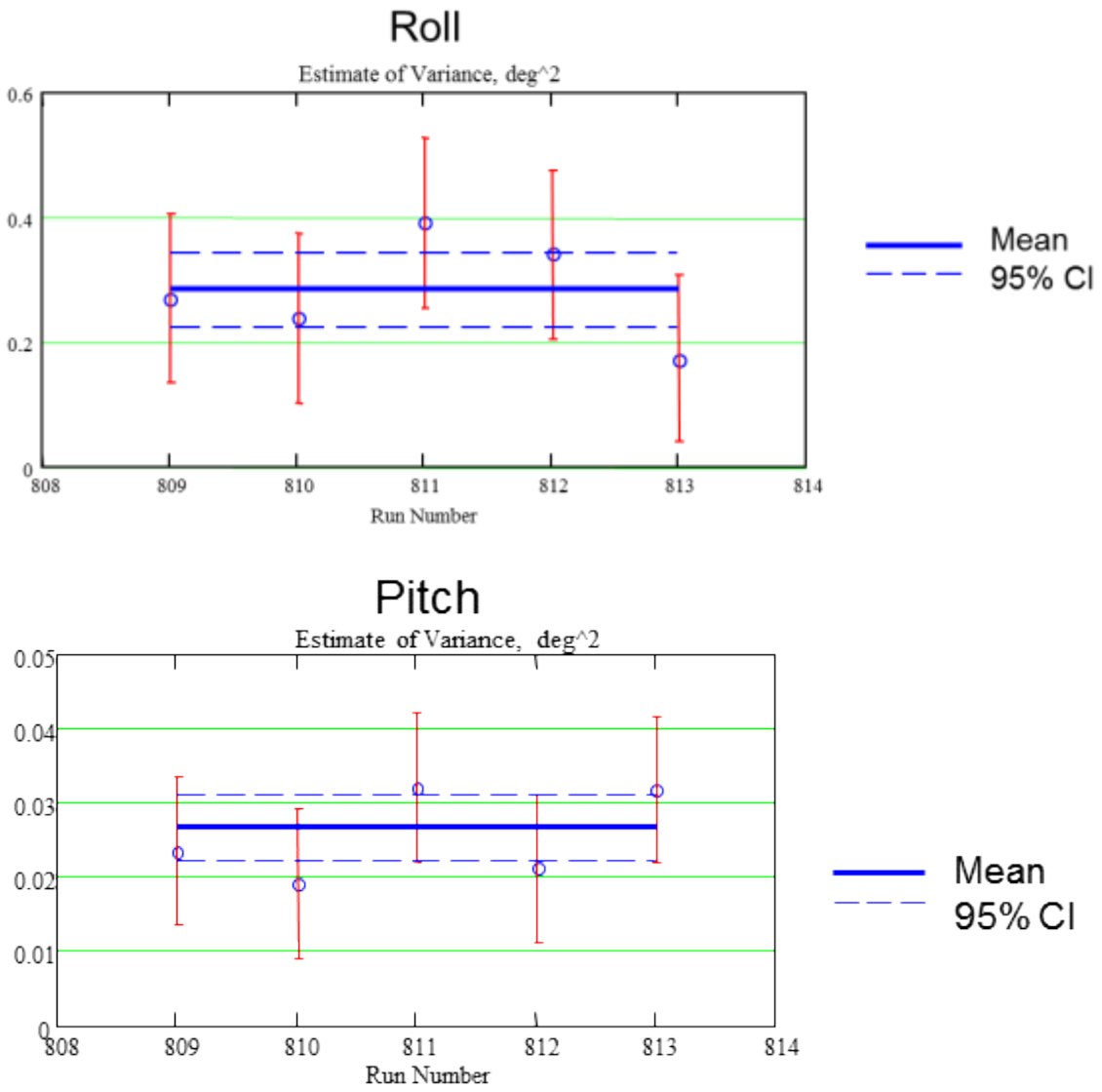

Figure 31. Example of statistical uncertainty analysis results. SS3, Beam Seas, 8 knots, estimate of the variance for roll and pitch.

SUMMARY

An experimental assessment of the roll decay characteristics and seakeeping performance of a 1/23rd scale model of R/V Melville, Model 5720 was completed during a three week test period in March 2012. Some conditions for seakeeping runs in the higher wave steepness conditions, 1/30 and 1/15, were unable to be obtained in head seas due to an RPM limit set by the motor controller. All uni-directional irregular wave conditions were completed as planned.

A comprehensive data set of time synchronized model motions, wave environment, and model location relative to the wave environment was presented. A data CD, which accompanies this report, includes the data sets outlined in the Data Interpretation section of this report and the results and analysis that were presented.

This page intentionally left blank

APPENDIX A: MEASUREMENT UNCERTAINTY THEORY AND DETAILS

Theory

Uncertainty analysis presented in this report is based upon the ISO Guide to the Uncertainty in Measurement (GUM) (JCGM, 2008) and the uncertainty analysis procedure from the International Towing Tank Conference (ITTC) (ITTC, 2008a). The analysis consists of two methods of evaluation: Type A and Type B. For this report, all uncertainties are defined at the 95% confidence limit (U95). The Type A standard uncertainty is computed from the time series data acquired during the test or from repeat observations and is defined in Equation (A-1) for the mean value:

$$u_A = u/\sqrt{n} \tag{A-1}$$

where the standard deviation of *x*, *u*, is

$$u^2 = \left[1/(n-1)\right]\sum_{i=1}^{n}\left(x_i - < x >\right)^2 \tag{A-2}$$

and the mean of x is

$$< x >= (1/n)\sum_{i=1}^{n} x_i \tag{A-3}$$

where *n* is the number of samples, or observations.

The Type A expanded uncertainty is defined as follows:

$$U_A = k u_A \tag{A-4}$$

where *k* is the coverage factor. At the 95% confidence level, *k* equals 2. For small sample sizes, the coverage factor may be replaced by the inverse Student *t* at the 95% confidence level, t_{95}.

The Type B method (JCGM, 2008) for standard uncertainty is evaluation by means other than statistical as defined by Equation (A-1). Per the ISO GUM (JCGM, 2008), these include the following:

- Previous measurement data
- Experience or general knowledge
- Manufacturer's specifications
- Calibration data or other certificates
- Uncertainties assigned to the reference data from handbooks.

For this report, the Type B uncertainty is determined primarily from calibration of the instruments with traceability to the National Institute of Standards and Technology (NIST), which is the National Metrology Institute (NMI) for the USA. NIST traceability is required per the procedure of the Seakeeping Division (Park and Dipper, 2011). For most electronic instruments, the uncertainty in the reference standards is small in comparison to the uncertainty in the electronic transducers. For conversion of the voltages from the analog to digital (A-to-D) converter, or data acquisition card (DAC), in the data acquisition system to engineering units or

physical units, the slopes and intercepts from regression analysis of the calibration data are applied to the data. The uncertainty in calibration is described in an ITTC procedure (2008b), Seakeeping Division procedure (Park and Dipper, 2011)0, and the details are described by calibration theory from Scheffe (1973) and Carroll, et al (1988).

Scheffe (1973) developed a statistical theory of calibration. A simplified method with detailed examples is provided by Carroll, et al. (1988). The prediction limit in this case is given by

$$f(x) - See(c_1 + c_2 s_{xx}) \le y \le f(x) + See(c_1 + c_2 s_{xx}) \tag{A-5}$$

where $c_1 = t_{N-2}$, $c_2 = \sqrt{2F_{2,\,N-2}}$ and t is the inverse Student-t probability density function (pdf) and F is the inverse Fisher pdf.

From Equation (A-5), the uncertainty in x for a linear equation in physical units is determined from Scheffe (1973)

$$x_h = < x > + \left[bD - (-1)^h \left(See * c_2 \right) \left(C / N + D^2 s_{xx} \right)^{1/2} \right] / C \tag{A-6a}$$

$$C = b^2 - (c_2 See)^2 / s_{xx} \tag{A-6b}$$

$$D = b(x - < x >) - (-1)^h See * c_1 \tag{A-6c}$$

where $h = 1$ and 2 are the upper and lower bounds, respectively.

The inverse Student-t and Fisher pdfs may be found in tables in standard statistical references and mathematical handbooks, such as Ross (2004). These functions are also available in Microsoft Excel. Other statistical functions such as the slope (a), intercept (b), average ($<x>$) and standard error of estimate (See), effectively the standard deviation of the curve fit, are available in Excel.

For those quantities not measured directly such as Froude number and non-dimensional wavelength and height, the uncertainties are propagated to obtain the combined expanded uncertainty from the following equation, given in JCGM, 2008 and ITTC, 2008a.

$$U_c^2 = \sum_{i=1}^{N} \left[\left(\partial f / \partial x_i \right) U\left(x_i \right) \right]^2 \tag{A-7}$$

where the derivative is known as the sensitivity coefficient. This equation is applicable to uncorrelated or statistically independent measurement quantities.

For this test series, the instruments were calibrated twice: January 2012 (pre-test calibration), and April 2012 (post-test calibration). Since multi-calibrations were performed, data will be shown which compares the more recent calibration to the older one, with the older calibration values of slope and intercept as the reference.

Accelerations

Tilt Table

Accelerations were measured at three model locations: the bow, stern, and center of gravity (CG). Acceleration is referenced to local acceleration of gravity, *g*, by a tilt table. For the pre-test calibration, the reference angle was measured with an Applied Geomechanics Pro 3600 with a measurement uncertainty of ±0.20°. For the post-test calibration, the accelerometers were calibration by a second tilt table with a resolution of 10 minutes of arc. The second table was calibrated with the Wyler Clino 2000 multi-purpose inclination-measuring instrument, which has a resolution of 5 s and an uncertainty of ±30 s (±0.0083°), and the angles checked with an Applied Geomechanics Pro 3600. Consequently, the error bars for the pre-test and post-test calibrations have different sizes.

Acceleration Calibration by Inclination

***Longitudinal Acceleration*.** For longitudinal acceleration, an accelerometer is calibrated by tilting it about the y-axis in pitch. The acceleration is then

$$\mathrm{du/dt} = \dot{\mathrm{u}} = \mathrm{g}\sin\alpha \quad du/dt = \dot{u} = -g\sin\theta \tag{A-8a}$$

$$(du/dt)/g = \dot{u}/g = -\sin\theta \quad (\mathrm{du/dt})/\mathrm{g} = \dot{\mathrm{u}}/\mathrm{g} = \sin\alpha \tag{A-8b}$$

The longitudinal acceleration is positive for pitch bow up, or a negative pitch angle. From Equation (A-8), a negative pitch angle produces a negative value of the sine function; consequently the acceleration is positive. Pitch down or positive pitch angle produces a negative acceleration.

Vertical Acceleration. Vertical acceleration may be calibrated in either pitch or roll. Acceleration is always negative for either positive or negative roll angles. The vertical acceleration is given by

$$dw/dt = \dot{w} = g(\cos\varphi - 1) \tag{A-9a}$$

$$(dw/dt)/g = \dot{w}/g = \cos\varphi - 1 \tag{A-9b}$$

The vertical acceleration is referenced to local gravity so that under static conditions the vertical acceleration is zero. Calibration results for vertical acceleration in this document are reported for tilt in roll.

The sensor arrangement for the vertical component is also sensitive to pitch; consequently, the vertical component should also be calibrated in pitch so that the vertical acceleration can be corrected for deviations of the sensor in pitch and roll. The equations for the pitch calibration are then

$$dw/dt = \dot{w} = g(\cos\theta - 1) \tag{A-10a}$$

$$(dw/dt)/g = \dot{w}/g = \cos\theta - 1 \tag{A-10b}$$

Transverse Acceleration. For transverse acceleration, an accelerometer is calibrated by tilting it about the *x*-axis in roll. The acceleration is then

$$\mathrm{dv/dt} = \dot{\mathrm{v}} = \mathrm{g}\sin\varphi \quad dv/dt = \dot{v} = g\sin\varphi \tag{A-11a}$$

$$(dv/dt)/g = \dot{v}/g = \sin\varphi \quad (\mathrm{dv/dt})/\mathrm{g} = \dot{\mathrm{v}}/\mathrm{g} = \sin\varphi \tag{A-11b}$$

The transverse acceleration is negative for roll to port (left) or a negative roll angle. Roll to starboard (right) produces a positive acceleration. The acceleration is opposite that in a static calibration as previously discussed.

Uncertainty in Acceleration

Since the accelerometers are calibrated by inclination, the uncertainty in acceleration must be computed from the law of propagation of uncertainty from Equation (A-7). The uncertainty in acceleration from the uncertainty in angle of inclination is then as follows.

From Equation (A-8), the standard uncertainty in longitudinal acceleration is

$$\mathrm{u}_{\dot{\mathrm{u}}}/\mathrm{g} = (\cos\alpha)\mathrm{u}_{\alpha}\, u_{\dot{u}}/g = (\cos\theta)u_{\theta} \tag{A-12}$$

For transverse acceleration from Equation (A-11)

$$\mathrm{u}_{\dot{\mathrm{v}}}/\mathrm{g} = (\cos\varphi)\mathrm{u}_{\varphi}\, u_{\dot{v}}/g = (\cos\varphi)u_{\varphi} \tag{A-13}$$

For vertical acceleration in roll from Equation (A-9)

$$\mathrm{u}_{\dot{\mathrm{w}}}/\mathrm{g} = |\sin\alpha|\mathrm{u}_{\alpha}\, u_{\dot{w}}/g = |\sin\varphi|u_{\varphi} \tag{A-14}$$

The expanded uncertainty at the 95% confidence limit in local *g* from the uncertainty in tilt angle for transverse and vertical accelerations is shown in Figure A1. As indicated in Equations (A-12) and (A-13), the result is the same for transverse and longitudinal accelerations. From this figure, the uncertainty in g from calibration with the digital protractor can be large in comparison to the manufacturer's specification of 0.1 %, or 1 mg (0.001 g) for a 1 g range transducer. However, calibration with the calibrated settings of the tilt table with a measured uncertainty of ±0.05° yields an uncertainty much smaller. The uncertainty in reference angle for the Columbia accelerometers is better than ±0.05°.

Columbia Triaxial Accelerometer

Example plots of the residuals in the calibration of acceleration at the CG with the Columbia Triaxial Accelerometer SN 1755 are shown in Figure A2, where the residuals are the differences between the data and the straight line fit from linear regression analysis. The dashed lines are the calibration uncertainties at the 95% prediction limit from statistical calibration theory while the error bars are the uncertainty in the measurement during calibration. This convention is applied to the plots in this section. In this calibration, the error bars are from a combination of the Type A uncertainty calculated during acquisition of the data and the Type B from the calibration uncertainty of the reference angle of ±0.20° for the pre-test calibration with an un-calibrated tilt table and ±0.050° for the post-test calibration with a calibrated tilt table. In a residual plot, the error bars are readily apparent but would be smaller than the symbols in a conventional linear plot.

For the CG accelerometer in Figure A2, the vertical and transverse components of acceleration pass both the slope and intercept hypothesis test in the post-test calibration, but the longitudinal component fails for the slope and intercept hypothesis test. Additionally, the maximum difference between the pre-test and post-test results for the vertical and longitudinal components is within the uncertainty estimates. Passing a hypothesis test means that the two

results in the comparison are identical statistically. Additional details of the hypothesis test for slope and intercept are described in more detail in a subsequent section. The slope is the critical parameter as the intercept is corrected from the zeroes collected during the model test under calm water conditions and zero model speed.

For the longitudinal acceleration, the difference between the pre-test and post-test calibration results has a maximum of 0.0077 g in comparison to the pre-test calibration maximum uncertainty of ±0.0042 g. Most of the difference between the two calibrations is in the slope. Consequently, the difference of 0.0077 g should be applied as the uncertainty estimate.

For the transverse acceleration, the calibration point at +1 g (+90°) in the post-test calibration was an outlier and was excluded from the curve fit in Figure A2b. In this case, removal of this point is not significant since the data are in very good agreement as indicated in the figure and by the hypothesis test.

Local Acceleration of Gravity

Local gravity in absolute units from Moose (1986) is 9.80100 ±0.00004 m/s^2 at the MASK. This value was computed from the National Oceanic and Atmospheric Administration (NOAA) National Geodetic Survey (NGS) of the U. S. Department of Commerce, with a latitude of 38° 58' 25" and longitude of 77° 11' 20". Actual local g should be applied in all calculations involving *g*, such as Froude number; however, the difference will likely be small in comparison to other uncertainties in the measurements.

Pitch and Roll Angle

For this test series, roll and pitch angles were measured with two transducers: Goodrich/Rosemount Aerospace VG34-0803-1 vertical gyroscope, and MicroStrain 3DM-GX1 gyro enhanced orientation sensor, which were calibrated with the same equipment as the Columbia accelerometers. Example results for pitch and roll for the Rosemount are shown as residual plots in Figure A3, while the results for the MicroStrain are presented in Figure A4.

Rosemount/Goodrich

Calibrating the Rosemount and leveling of the tilt table with the Pro 3600 should be adequate, since the Rosemount vertical gyroscope is nominally a ±1° device, per the manufacturer's specification. For roll, the post-test calibration passes a hypothesis test in slope and fails for the intercept. Pitch passes the intercept test but fails the slope test. Most of the difference for roll is in the intercept, and the largest difference of 1.6° should be applied as the uncertainty. As Figure A3 indicates, the post-test calibration is in very good agreement with the pre-test calibration for pitch, and the differences in angle are within the pre-test uncertainty estimate. The uncertainty estimates for pitch and roll exceed the manufacturer's specification.

MicroStrain

By comparison to the Rosemount, the performance of the MicroStrain is slightly better in the pre-test calibration as indicated by a lower data scatter and uncertainty in the residual plot in Figure A4, but the results were not reproducible in the post-test calibration. Pitch and roll both past the hypothesis test for slope but fail in intercept. The differences between the pre-test and post-test calibrations are quite large with a maximum difference of 1.3° for roll and 1.4° in pitch. In this case, the maximum differences should be applied as the uncertainty estimate.

Additionally, these differences are significantly larger than the manufacturer's specification of ±0.5°.

The MicroStrain has noise level that would result in lower quality data, as computed from the signal-to-noise ratio (SNR), than the Rosemount. The nominal noise level during calibration is 5 mV rms. For the roll angle, the noise level in physical units from the slope is 0.030° rms for the Rosemount and 0.36° for the MicroStrain. The noise level for the MicroStrain in roll is about 12 times larger than that from the Rosemount. A contributing factor is the calibration range. For the Rosemount, the voltage range is ±9.9 V over a roll angle range of ±60° while the range of the MicroStrain is +1.63 to +3.28 V or a voltage range of 1.61 V. For the future, the electronic circuit for the MicroStrain should be designed with a gain that uses more of the ±10 V range of the A-to-D converter.

Pod Steering Angle

The steering angle was measured via a Bourns 6574S-1-103 potentiometer and calibrated with the Pro 3600 Digital Protractor. During the test, the potentiometer failed and was replaced. The replacement potentiometer was calibrated in place with polar graph paper. The slope during post calibration was in agreement with the in-situ calibration via the hypothesis test. The lower uncertainty of ±0.23° obtained during the post-test calibration should be applied as the uncertainty estimate. The uncertainty estimate is similar to the original potentiometer of ±0.30°. The post-test calibration results are presented in Figure A5. As the figure indicates, the uncertainty is dominated by the uncertainty in the Pro 3600. The slope is the critical value since the actual zero reading must be determined when the transducer is connected to the rudder linkages.

Shaft Speed and Signet Paddlewheel Flow Sensor

Both the propeller shaft speed and Signet 2536 paddle wheel flow sensor are digital devices. The digital data are then amplified and sent to a frequency to voltage (F-to-V) converter, Analog Devices AD451J. The amplifier and F-to-V converter are then calibrated with a simulated input from square wave generator with a frequency counter for the measured frequency. The propeller shaft speed is sensed with an optical encoder, which produces 120 pulses per revolution. The simulated shaft speed in rpm (revolutions per minute), ω, from the frequency, f, in Hz is given by:

$$\omega = f/(60p) \tag{A-15}$$

where p is the number of pulses per revolution. The simulation factor for the water speed sensor is determined through calibration of the model speed with a stopwatch.

Shaft Speed

During the test, the gain was changed on the F-to-V converter for the model propeller shaft speed. Consequently, two sets of calibration exist. The calibration results for the shaft speed for the higher gain are presented in Figure A6. As this figure indicates, the F-to-V converter results are not reproducible and have a very high drift. At the time of calibration, the F-to-V converter is very linear and has a low uncertainty. For the March 2011 data, the maximum uncertainty was ±0.78 rpm. Most of the uncertainty in the error bars is from the Type A uncertainty as computed from the standard deviation of the voltage with a nominal value of ±0.26 rpm. The slopes for the

pre-test and post-test calibrations are the same but the intercepts are quite different. The maximum difference is 1.5 rpm; consequently, the uncertainty in shaft speed should be specified as ±1.5 rpm.

By comparison, the uncertainty in the initial calibration prior to the gain change had a maximum value of ±0.23 rpm. The Type A uncertainty in the initial calibration was nominally ±0.10 rpm. The nominal standard deviation for both gain settings was nominally 5 to 6 mV.

Speed through Water (STW)

Model speed was calibrated from the time over a 30.48 m (100 ft) distance. At the same time, speed was measured with the Nikon Metrology (formerly ArcSecond) Indoor Global Positioning System (iGPS) or laser tracker. The iGPS results were applied as the reference velocity and compared to the stopwatch results. The stopwatch calibration results for the Signet 2536 paddlewheel sensor are shown in Figure A7a. The speed range of the calibration was 0.69 to 1.40 m/s (2.3 to 4.6 ft/s). The maximum speed with the uncertainty estimate was 1.40 ±0.17 m/s or 4.58 ±0.57 ft/s (±12 %) where the uncertainty in the iGPS is assumed small in comparison to the curve fit.

For the stopwatch measurement, the velocity is given by

$$V = L / t \tag{A-16}$$

where L is the length and t is the time. The uncertainty in the speed by stopwatch is

$$U_V = \sqrt{(U_L / t)^2 + (L U_t / t^2)^2} \tag{A-17}$$

From NIST Handbook 44 (2012), the tolerance for a 30.48 m (100 ft) tape measure is 6.35 mm (¼ inch) or ±0.25 % relative uncertainty in speed. For a stopwatch over the time interval of the stopwatch measurement for model speed, the uncertainty is dominated by the reaction time of the stopwatch operator. From Gust, et al (2009)., the estimated reaction time is 0.48 s. Consequently, most of the uncertainty in speed is from the stopwatch by direct measurement. At the maximum calibration speed, the time was 22.14 s, or the contribution to the uncertainty in speed was ±2.2 % in comparison to ±0.25 % from distance and ±12 % from the curve fit.

From this calibration, the simulation factor for the function generator is 0.030611 m/s/Hz (0.10043 ft/s/Hz) with an offset correction of 0.1469 m/s (0.4821 ft/s). This calibration result was then applied to the pre-test and post-test calibration of the f-v converter with a function generator as presented in Figure A7b. The error bars in Figure A7 are primarily from the Type A method.

The post-test calibration slope passes the hypothesis test but fails the intercept test. The drift in this case is primarily in the intercept. The difference is nearly constant with a maximum value of 0.0070 m/s (0.023 ft/s). The maximum uncertainty in the pre-test calibration was ±0.0045 m/s (±0.015 ft/s). The uncertainty in the actual speed over water calibration is significantly larger with a value of ±0.17 m/s (±0.57 ft/s) in comparison to the difference of 0.0070 m/s (±0.023 ft/s). In this case, the drift is negligible in comparison to the direct SOW calibration.

As Figure A7b indicates, one outlier each was removed from the curve fit for the pre-test and post-test calibrations. Both outliers occurred at a 24 Hz input in both cases. In this case, the outliers are systematically reproducible and should not have been removed from the curve fit. With the inclusion of the outlier in the pre-test calibration, the maximum uncertainty in the curve

fit is slightly higher with a value of ±0.0061 m/s (±0.020 ft/s) in comparison to ±0.0045 m/s (±0.015 ft/s) with the outlier removed. Removal is a moot point, since the difference in the pre- and post-test calibrations is 0.0070 m/s (0.023 ft/s) and the uncertainty from the stopwatch calibration is ±0.17 m/s (±0.57 ft/s).

Model Speed from Shaft Speed

During the stopwatch calibration of model speed, both the output from the Signet paddlewheel sensor and propeller shaft speed were collected. The stopwatch calibration result from propeller shaft speed is shown in Figure A8. In this case, the maximum model speed as determined from shaft speed was 1.380 ±0.028 m/s or 4.529 ±0.092 ft/s (±2.0 %) at 1080.8 rpm. At the maximum model speed, the difference between the pre-test and post-test calibration of the f-v converter for the shaft speed was 1.5 rpm, which results in speed difference of 0.0018 m/s (0.0060 ft/s) or 0.13 %. Consequently, the speed difference due to the drift of the shaft speed is about 15 times smaller than the uncertainty in the stopwatch measurement. In this case, the contribution of drift of the shaft speed F-to-V converter to the uncertainty can be neglected. Furthermore, the uncertainty in model speed is smaller from propeller shaft speed than that from the Signet paddle wheel sensor, ±2.0 % versus ±12 % at the maximum model speed for the test.

MASK Carriage Speed

Carriage speed for the MASK is measured from the rotational rate and diameter of a metal wheel. The pulse output of the optical encoder for the wheel is fed to an F-to-V converter. The F-to-V converter is calibrated with a simulated input from a frequency generator. The carriage velocity is related to the input frequency by

$$V = \pi D f / p \tag{A-18}$$

where D is the diameter of the wheel, f is the frequency input, and p is the number of pulses/revolution of the optical encoder. From Equations (A-7) and (A-18), the uncertainty in the carriage speed is as follows:

$$U_V = (\pi / p)\sqrt{(DU_f)^2 + (fU_D)^2} \tag{A-19}$$

For the MASK carriage wheel, D = 177.39 mm (6.984 inches) and p = 500 pulses/rev. No recent data exists on the carriage wheel measurement. However, from measurements from Carriage #1 (Park et al, 2010), that wheel was measured with laser technology as 506.725 mm (19.94979 inches) with an average standard deviation from two sets of measurements in the diameter of 0.105 mm (0.00415 inches) or a relative uncertainty for a single measurement in diameter of ±0.042 % at the 95 % confidence level. With assumption that the uncertainty contribution from the frequency measurement is small in comparison to the variation in diameter, the relative uncertainty in the MASK carriage speed is estimated to be ±0.042 %.

The results for the calibration of the F-to-V converter are presented in Figure A9. For reference, the error bars in the figure were for an assumed arbitrary uncertainty in diameter of 0.025 mm (0.001 inches) or a relative uncertainty in speed of ±0.014 %, which is a factor of three smaller than the previous estimate of ±0.042 %. As the figure indicates, the uncertainty in the calibration of the F-V converter is much smaller than the error bars over the range of the model speed calibration in Figure A7a. Thus, the uncertainty in diameter is the significant contribution to the uncertainty in MASK carriage speed. Since the model operator must adjust the propeller shaft speed for the model to track the carriage, the more accurate measure of the

model speed will be from the model speed as computed from shaft speed or from the iGPS. For the MASK carriage, the model has four independent measurements of model speed: MASK carriage, Signet paddle wheel sensor, model shaft speed, and iGPS.

Rate Sensors

For this test series, pitch, roll, and yaw rates were measured with the Systron-Donner Gyrochip II. Two different models of this sensor were employed. In yaw, the model number was QRS14-00050-103 with a nominal gain of 10°/s/V and maximum rate of 50°/s, while for pitch and roll the model number was QRS14-00100-103 with a nominal gain of 20°/s/V and maximum rate of 100°/s. The nominal uncertainty for long-term stability over one year is 1.0°/s.

These sensors were calibrated in this test series with an Ideal Aerosmith model 1291BR, SN 23657, single-axis positioning and rate table system. The uncertainty per manufacturer's specification is ±0.01 % plus an uncertainty from the resolution of ±0.000125°/s.

Pre-test calibrations were not performed for this test. Post-test calibration data from April 2010 were applied from the previous test as the pre-test values for this test. The results are compared to a calibration from March 2009. The calibration results are presented in Figure A10. As the figure indicates the results are reasonably good and smaller than the manufacturer's specification.

Only the yaw rate passes the hypothesis test in intercept. All other items fail the hypothesis test. However, yaw rate from March 2009 is within the uncertainty of the April 2010 calibration. Much of the data for pitch and roll from March 2009 was within the uncertainty of the April 2010 calibration. For the most part, the pitch and roll data have an uncertainty of nominally ±0.10 deg/s from the difference between the two calibrations. Although these differences are larger than the calibration uncertainty, the differences are within the manufacturer's specification of long term stability of 1.0°/s for one year.

Battery Voltage Monitors

Battery voltage monitors were installed in the model for monitoring the propulsion and electronics batteries. A CR Magnetics CR5310-100 monitored the propulsion battery, while a CR5310-50 monitored the electronics battery output voltage. The calibration results are shown in Figure A11 and Figure A12 for propulsion and electronics, respectively. As the figures indicate, the post-test calibrations results were not within the uncertainty of the pre-test calibration. The maximum difference for propulsion was 0.26 V in comparison to the maximum pre-test calibration uncertainty of ±0.047 V, while the difference for the electronics was 0.079 V in comparison to an uncertainty of ±0.086 V. These results are well within the manufacturer's specification of 0.50 and 0.25 V, respectively. Since the CR Magnetics devices serve a monitoring function, the uncertainty is less important than the other instruments.

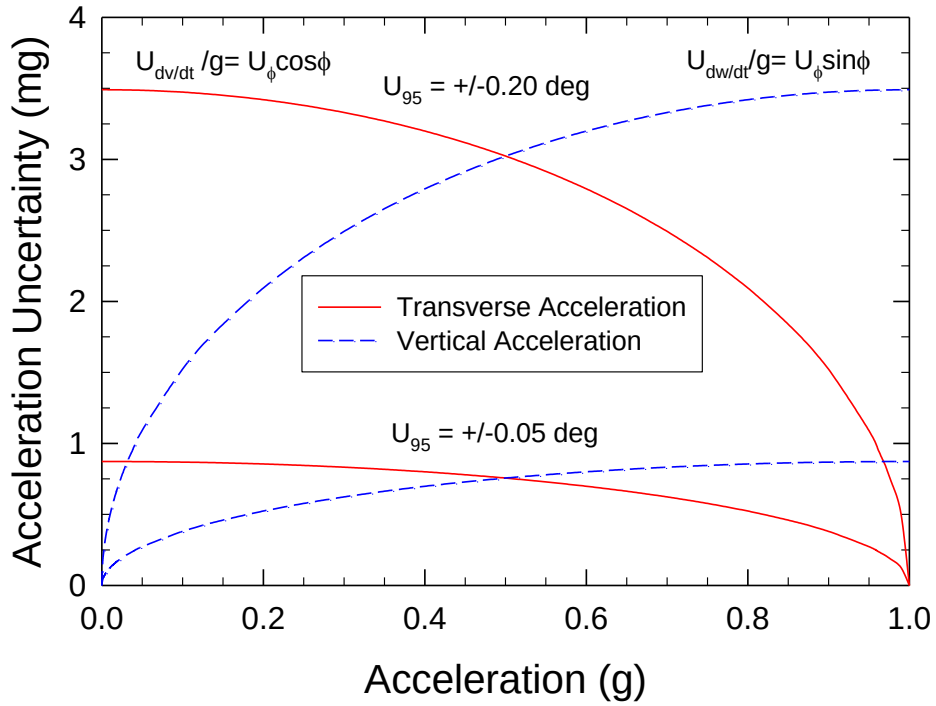

Figure A1. Expanded Uncertainty in Acceleration at the 95% Confidence Limit.

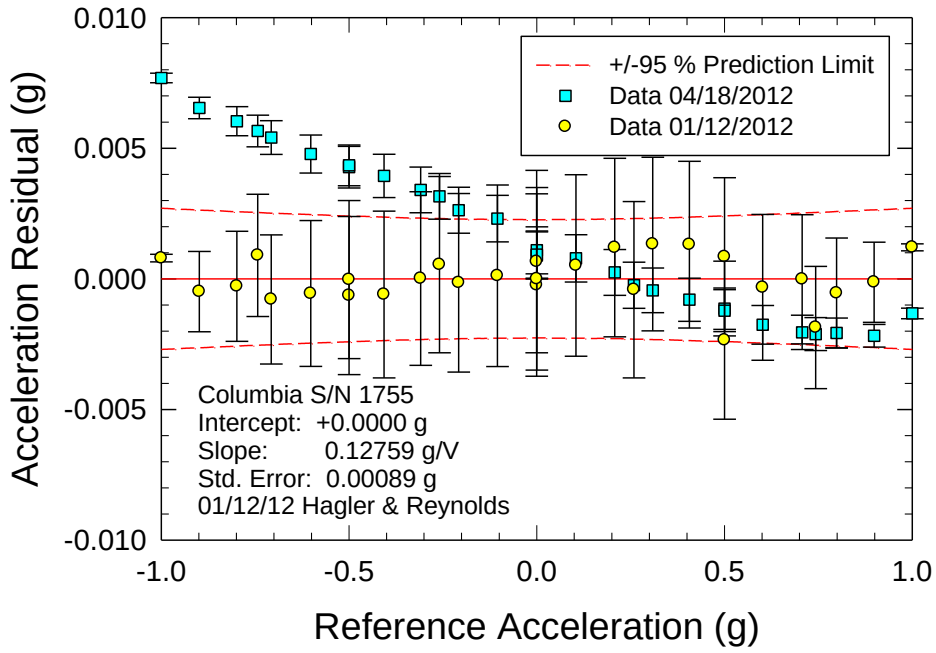

a. Longitudinal Acceleration

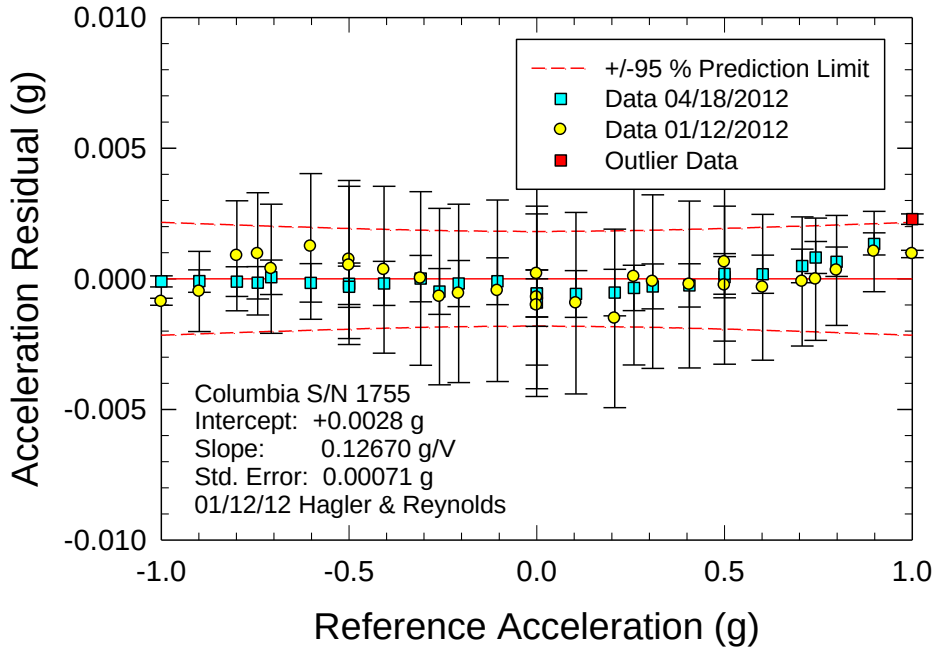

b. Transverse Acceleration

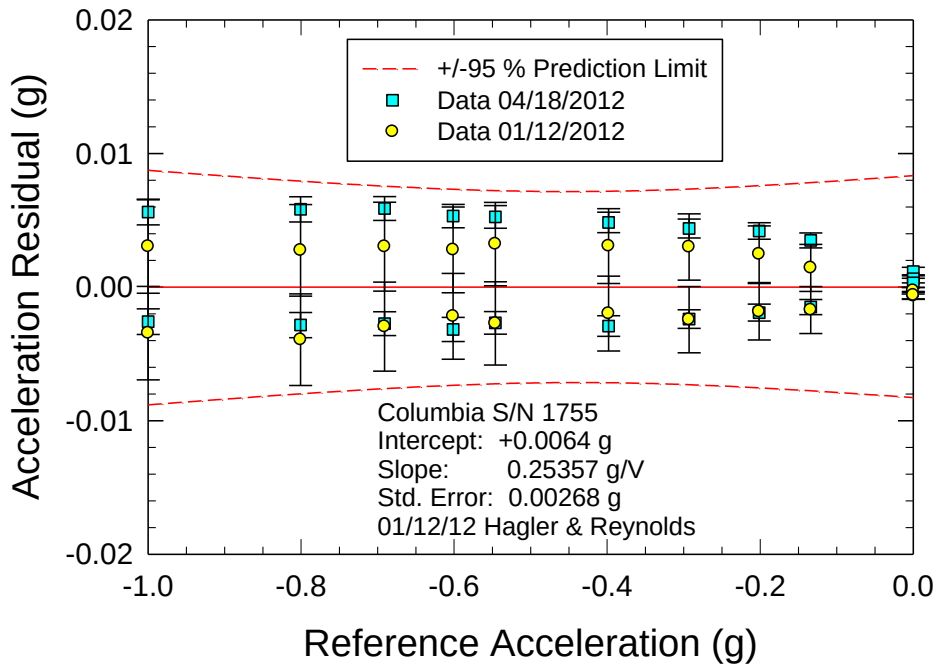

c. Vertical Acceleration

Figure A2. CG Accelerometer Calibration for Model 5720

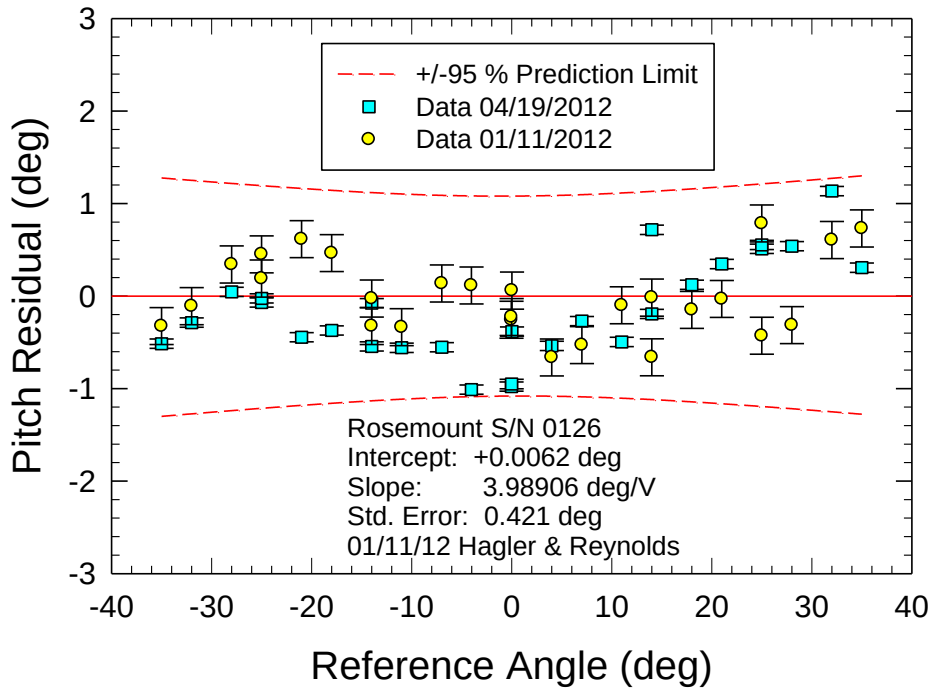

a. Pitch Angle

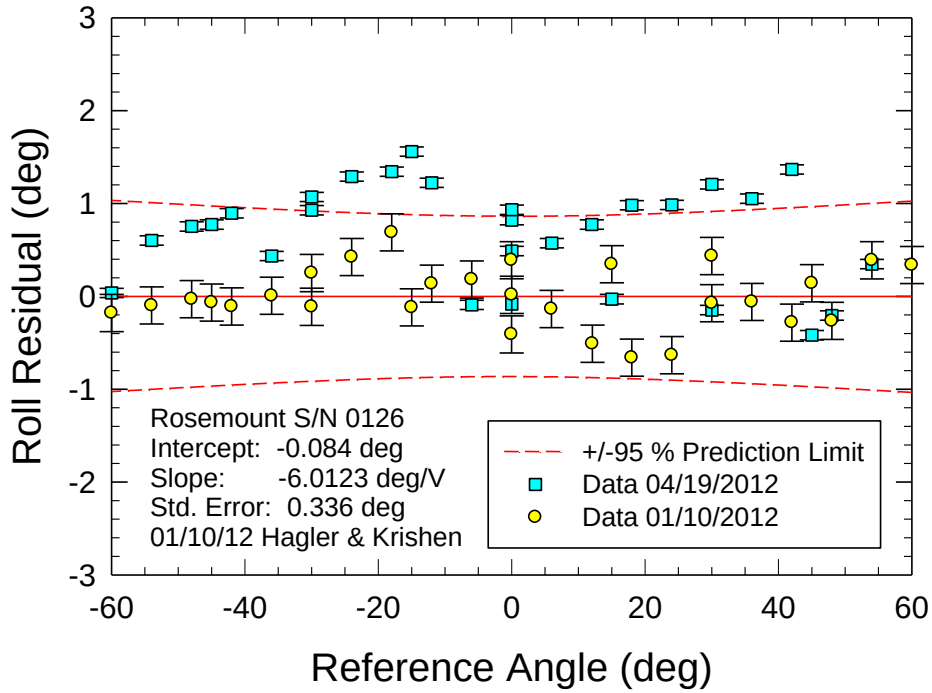

b. Roll Angle

Figure A3. Pitch and Roll Angle Calibration of Rosemount VG34-0803-3 SN 126 for Model 5720

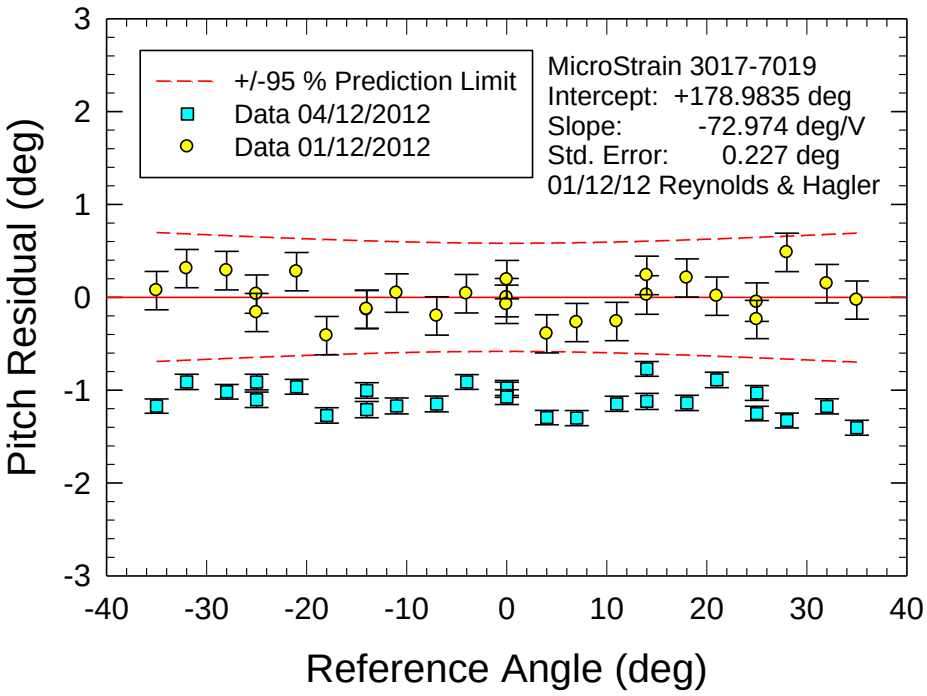

a. Pitch Angle

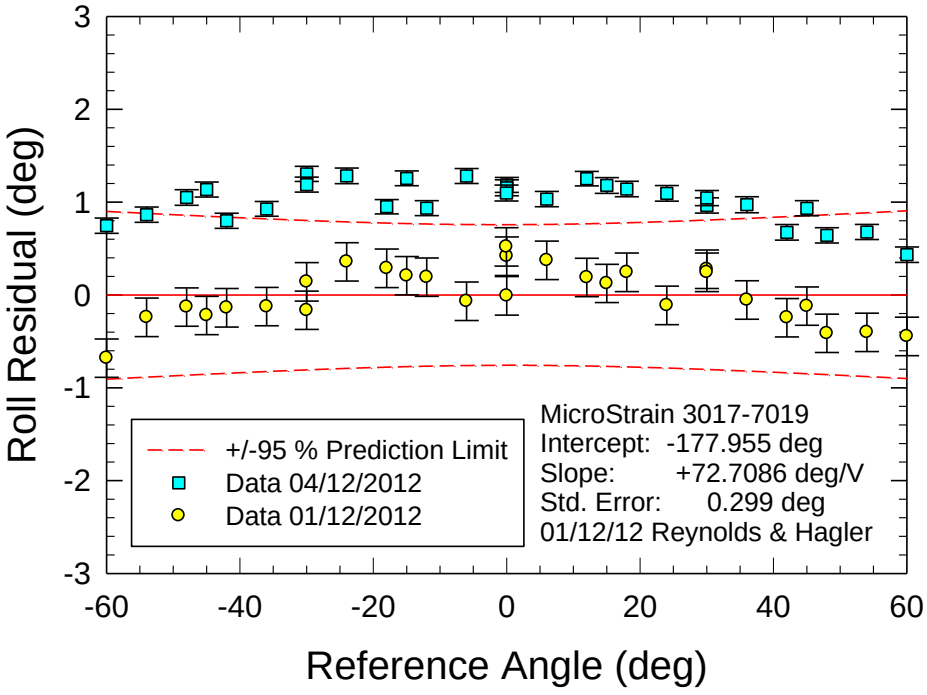

b. Roll Angle

Figure A4. Pitch and Roll Angle Calibration of MicroStrain 3DM-GX1 SN 3017-7019 for Model 5720

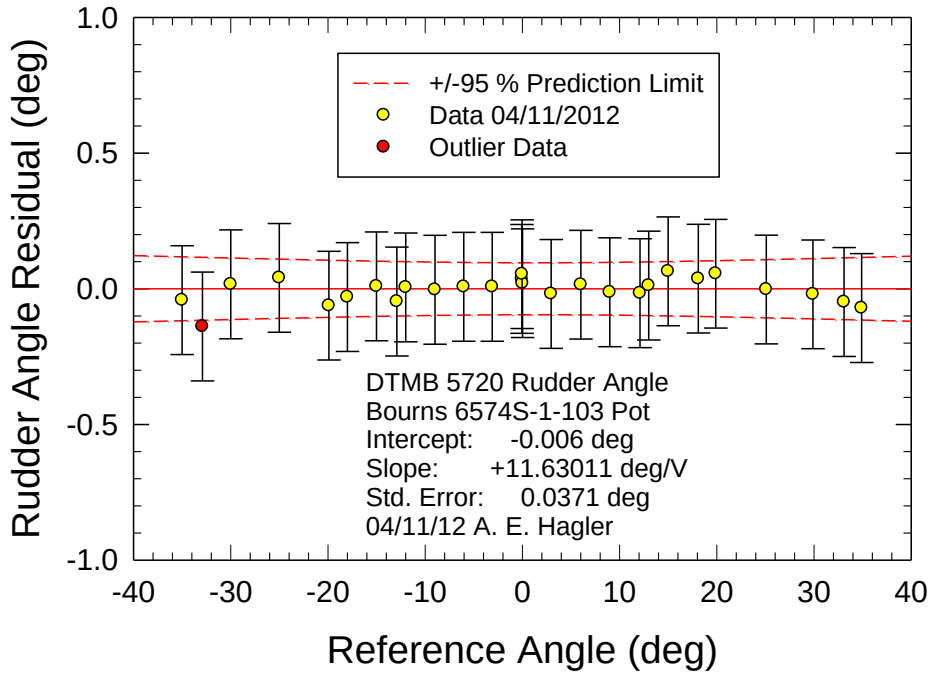

Figure A5. Steering Angle Calibration for Model 5720

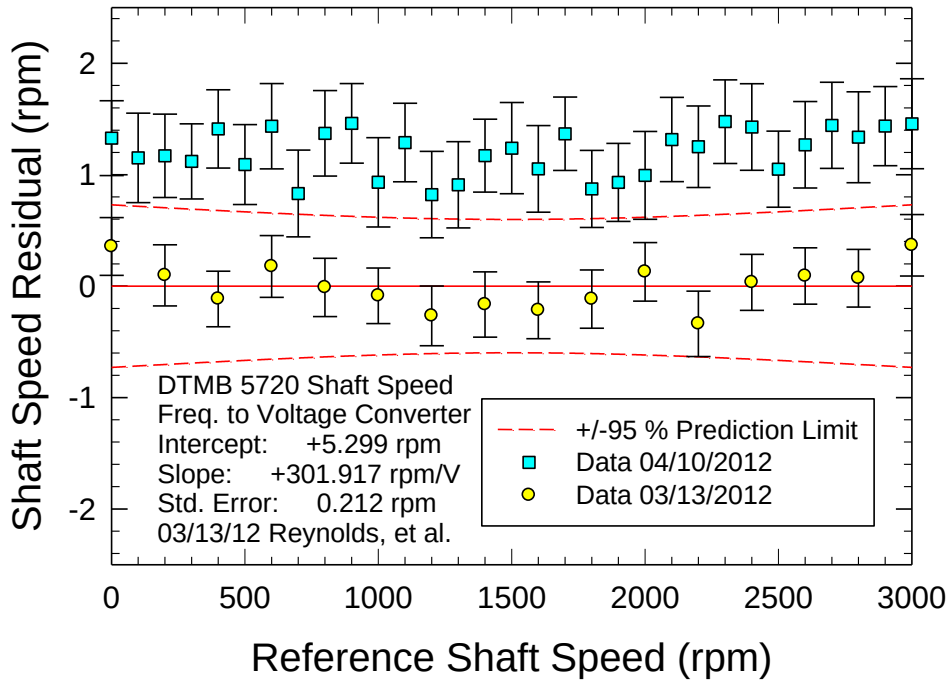

Figure A6. Shaft Speed Calibration of Frequency to Voltage Converter for Model 5720

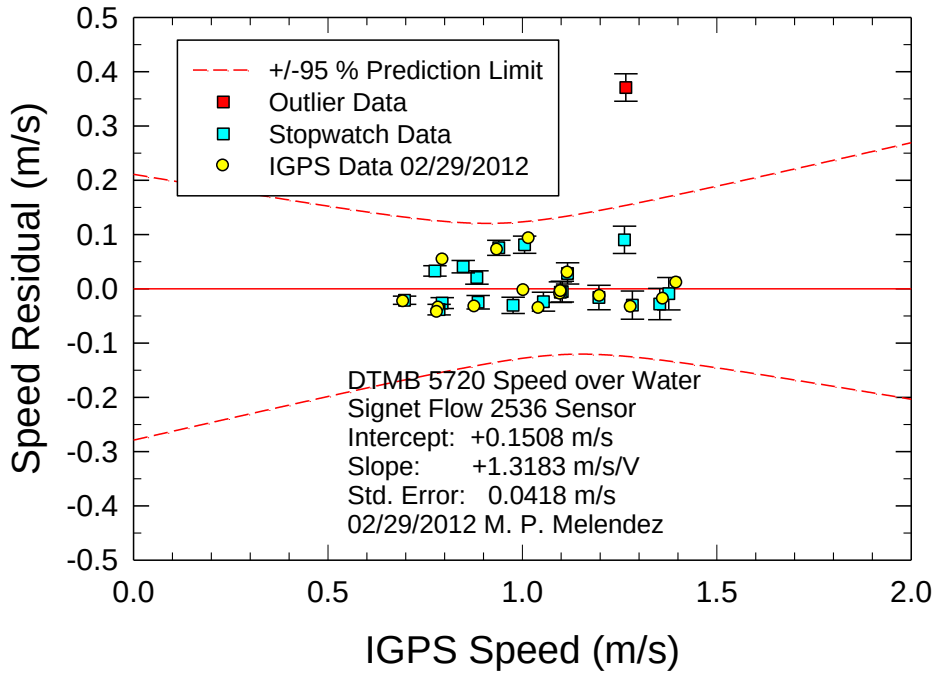

a. Calibration by Stopwatch

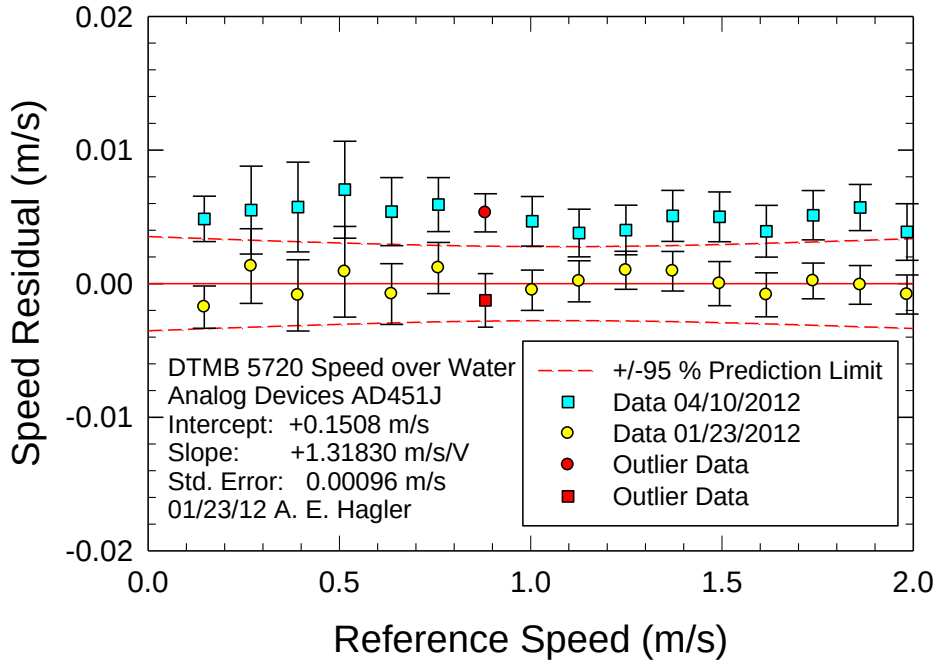

b. Calibration by Function Generator

Figure A7. Model Speed Calibration of Signet 2536 Paddlewheel Flow Sensor for Model 5720

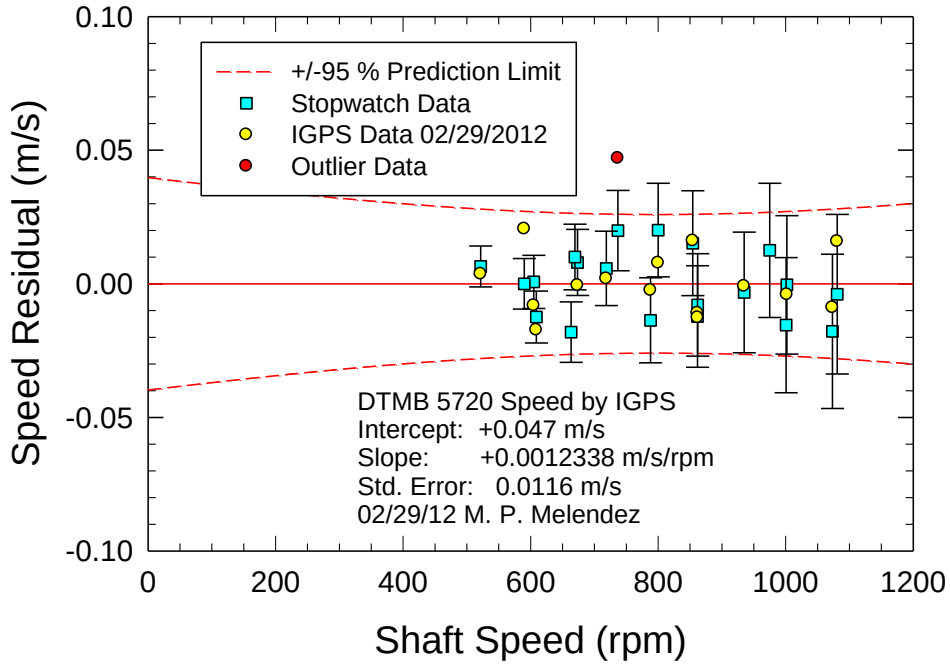

Figure A8. Model Speed Calibration of Model 5720 from Propeller Shaft Speed by Stopwatch

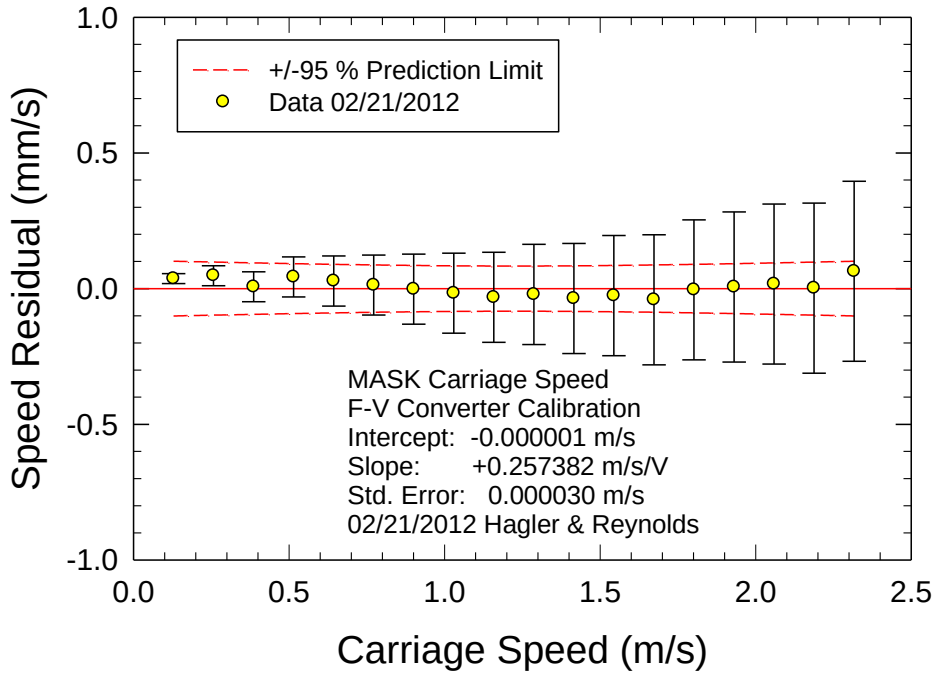

Figure A9. MASK Carriage Speed Calibration of Frequency to Voltage Converter

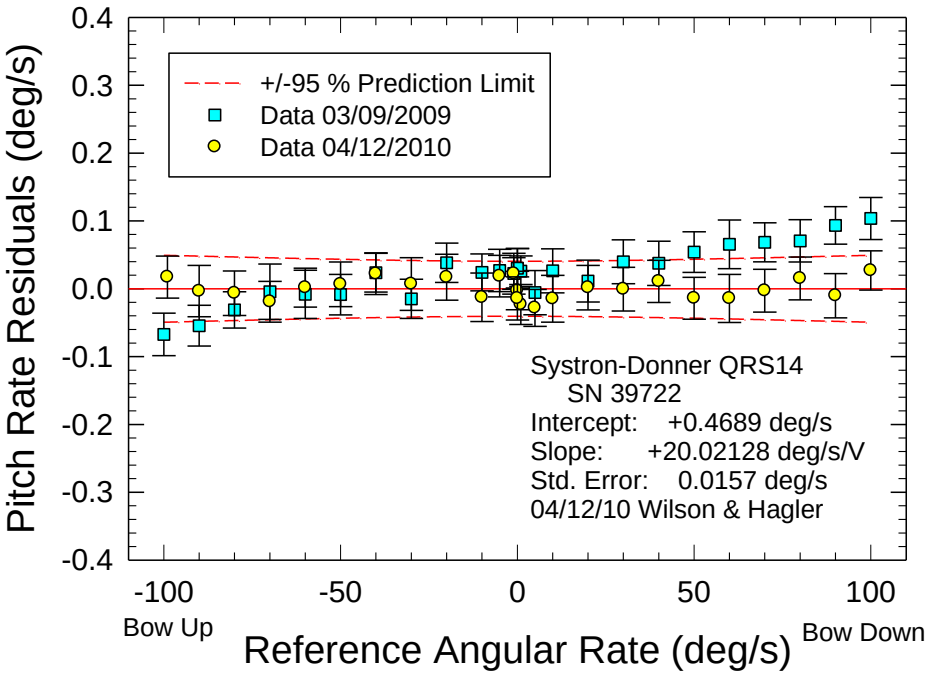

a. Pitch Rate

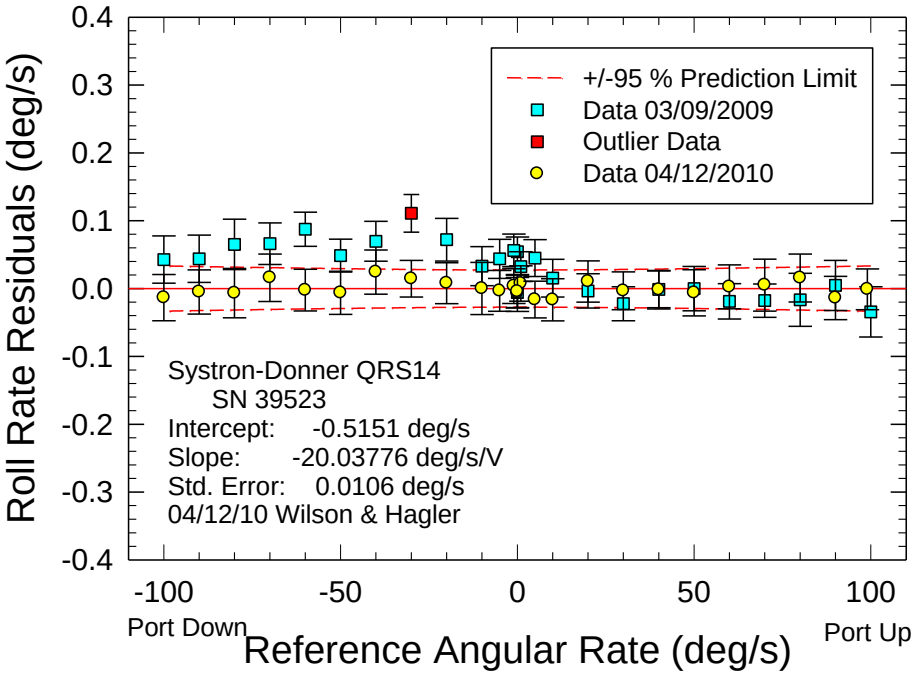

b. Roll Rate

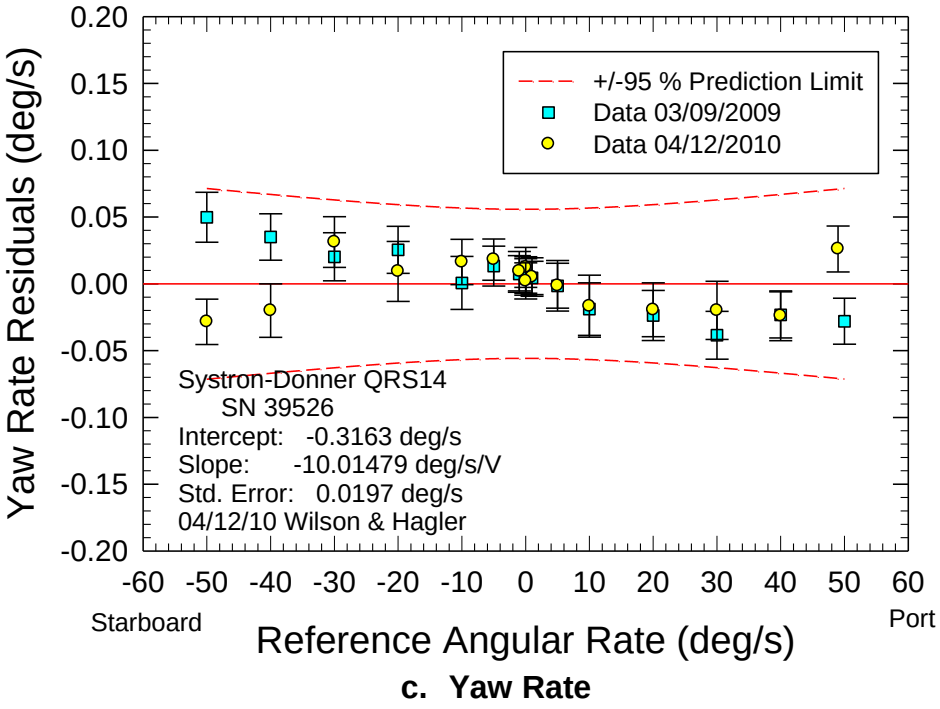

Figure A10. Systron-Donner Rate Sensors Calibration for DTMB #5720

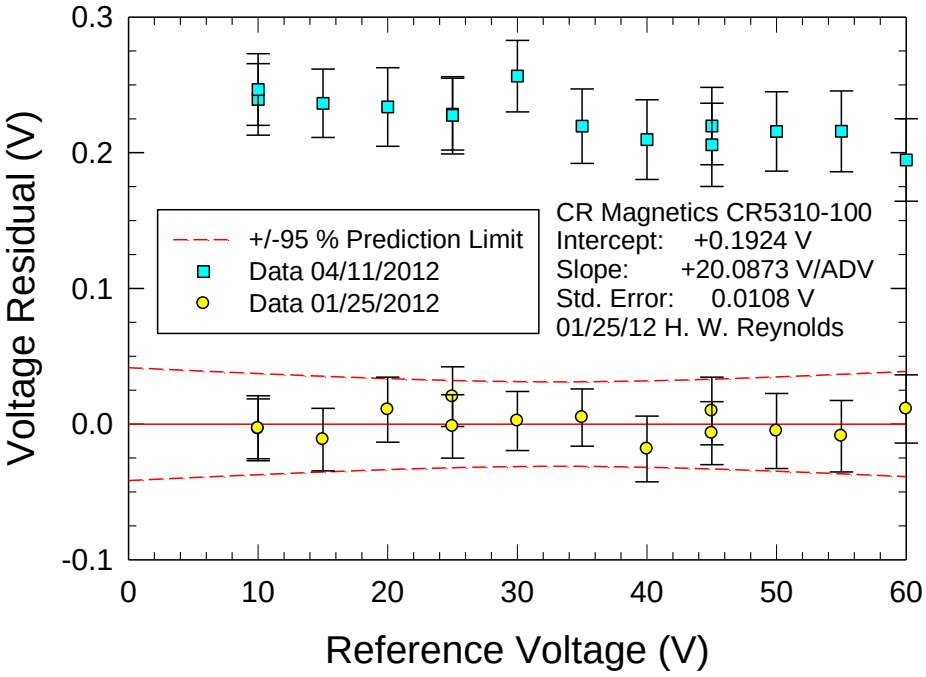

Figure A11. Propulsion Battery Monitor Calibration for Model 5720

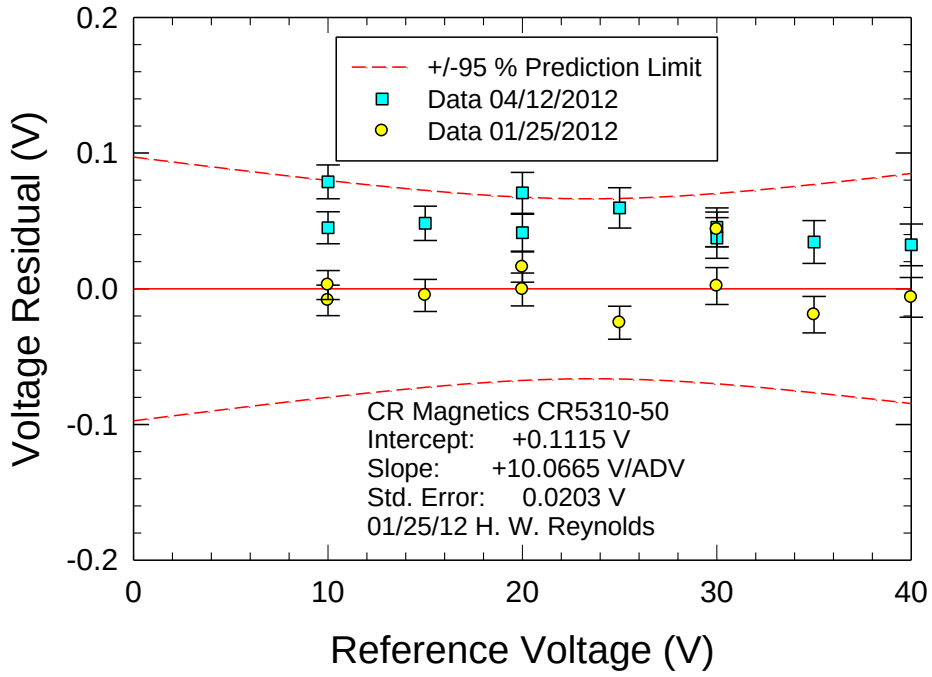

Figure A12. Electronics Battery Monitor Calibration for Model 5720

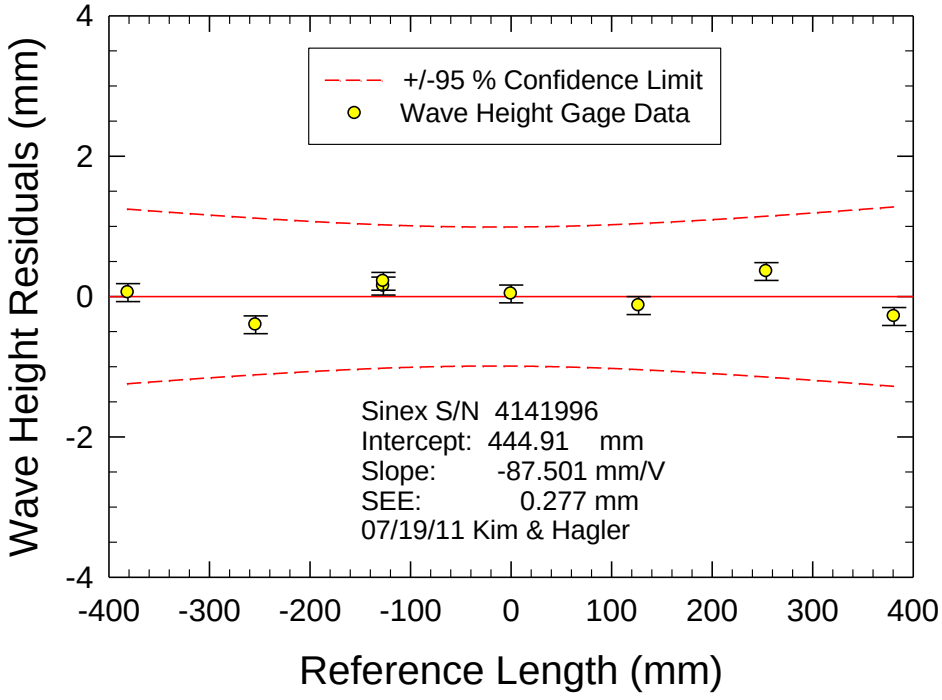

Figure A13. MASK Bridge Probe BP1 Calibration

This page intentionally left blank

APPENDIX B: DATA CD FILE SRUCTURE

The CD that accompanies this report contains the following file structure:

- (1) Data Sets
    - Model *.tmq* Files
    - Tracker *.ttq* Files
    - Bridge Waves *.twq* Files
- (2) Analysis
    - Roll Decay Results
    - Irregular Wave Spectra Analysis
    - RAO Results
    - Statistical Uncertainty Analysis
    - Statistical Summary.xls
- (3) Supporting Documentation
    - Run Summary.xls
    - Coordinate System Definition.xls
- (4) Video
    - Full Scale
    - Model Scale

The (1) Data Sets folder contains the *.tmq*, *.ttq*, and *.twq* files described in the Data Interpretation section of this report. The (2) Analysis folder contains the roll decay results, the wave spectra analysis, RAO results, and statistical uncertainty analysis results outlined in the Experimental Results and Data Analysis section of this report. In addition, it contains the statistical summary also referenced in the Experimental Results and Data Analysis section. The (3) Supporting Documentation contains a Run Summary Microsoft Excel file that summarizes the runs numbers associated with each regular and irregular wave condition. The Coordinate System Definition file contains the plots and tables provided in the Data Interpretation section of this report. Finally, the (4) Video folder contains a processed video file for each regular wave and irregular wave condition. The video file has been processed to contain plots of specified data channels (roll, pitch, heading, RPM, etc), time-synchronized and displayed in real time. These videos are provided in both full scale and model time. The synchronized data is only provided in full-scale units.

This page intentionally left blank

APPENDIX C: EXAMPLE DATA SETS

TESTTITLE:	23rd Scale R\V Melville								
TESTNAME:	m5720_Melville								
MODELNUMBER:	5720								
TESTCOMMENTS:	Scripps 23rd Scale R\V Melville Model Seakeeping Runs								
DATADIRECTORY:	C:\Users\HanyokLW\Desktop\m_5720_Melville_May_23\m5720-Melville\t01\Analysis\Post Test\(8) TMQ Processing\(2) TMQ Files\m57								
RUNNUMBER:	252								
COMMENTS:	Final TMQ created on 25-May-2012 11:18:58								
SAMPLERATE:	24								
HEADERFILE:	m5720 Melville-t01-Header 04-18-12_post-cal.hdr								
DATE:	3/6/2012								
TIME:	9:04:31 AM								
CHANNELNAMES:	Time MDL	Shaft Speed	Rudder Angle	Roll Angle Gyro	Pitch Angle Gyro	Roll Rate S/D	Pitch Rate S/D	Yaw Rate S/D	Accel Vert CG
UNITS:	ms	RPM	deg	deg	deg	deg/s	deg/s	deg/s	g
GAIN:	1	116.685997	11.66861	-6.0123	3.9891	-20.03776	20.02128	-10.01479	0.2535
OFFSET:	0	-0.3338	-3.6689	0.084	0.006	-0.5151	0.4689	-0.3163	0.0063
MAXIMUM:	32729766	160.3355	-0.78442	4.2307	4.1439	3.1904	2.7909	0.35712	0.098675
MINIMUM:	32670976	135.6763	-7.7389	-5.083	-3.7801	-3.0087	-2.8179	-0.40466	-0.097838
MEAN:	32700359.15	149.0163	-4.3554	-0.53228	0.13602	-0.0095767	0.016739	0.0017294	0.0002054
STDDEV:	16985.2576	5.5908	1.5918	2.1361	2.2359	1.486	1.5139	0.15581	0.052671
SSA:	33970.5152	11.1816	3.1837	4.2723	4.4717	2.972	3.0279	0.31161	0.10534
SDA:	67941.0303	22.3632	6.3673	8.5446	8.9435	5.9439	6.0557	0.62322	0.21068
Count Time	Time MDL	Shaft Speed	Rudder Angle	Roll Angle Gyro	Pitch Angle Gyro	Roll Rate S/D	Pitch Rate S/D	Yaw Rate S/D	Accel Vert CG
0	32670976	160.097044	-2.72841	-4.596576	2.852223	-1.026601	1.616538	-0.076185	-0.03246
0.199828	32671024	159.408485	-2.667733	-4.717423	3.099547	-0.73789	1.357704	-0.094353	-0.022092
0.399651	32671056	160.150571	-2.717908	-4.835264	3.332909	-0.336787	1.039173	-0.122335	-0.004296
0.599479	32671102	159.260067	-2.870767	-4.871939	3.475719	0.026295	0.724399	-0.150318	0.005514
0.799307	32671148	160.075146	-2.714408	-4.811215	3.576643	0.329212	0.279373	-0.198556	0.017758
0.99913	32671196	159.430382	-2.611724	-4.67714	3.638474	0.764576	-0.107207	-0.233847	0.030991
1.198958	32671228	160.031351	-2.586053	-4.572526	3.516807	1.149385	-0.465816	-0.21025	0.045593
1.398786	32671274	159.20654	-2.707407	-4.226218	3.340489	1.467343	-0.770988	-0.248882	0.051017
1.598609	32671322	159.778311	-2.700405	-3.818584	3.199275	1.787808	-1.165917	-0.264752	0.06169
1.798437	32671352	159.213839	-2.743579	-3.448226	2.87895	2.091979	-1.395527	-0.259949	0.068813
1.998265	32671400	159.82454	-2.714408	-2.98588	2.551445	2.348518	-1.6577	-0.262873	0.078548
2.198088	32671430	159.260067	-2.611724	-2.393068	2.22753	2.529432	-1.922377	-0.268929	0.077711
2.397916	32671476	159.162744	-2.724909	-1.934329	1.783543	2.654359	-2.086027	-0.218811	0.083364
2.597744	32671524	159.228438	-2.882436	-1.365566	1.31243	2.790985	-2.22922	-0.213173	0.084277
2.797567	32671556	159.444981	-2.74708	-0.870152	0.824164	2.858253	-2.230055	-0.192082	0.086127
2.997395	32671602	159.965658	-2.731911	-0.308603	0.350658	2.827753	-2.316054	-0.201061	0.081818
3.197223	32671648	159.384154	-2.672401	0.269179	-0.049847	2.774272	-2.330665	-0.161803	0.0787
3.397046	32671680	159.853737	-2.700405	0.698457	-0.56125	2.645585	-2.252181	-0.143635	0.072286
3.596874	32671728	158.688296	-2.72841	1.216116	-1.045926	2.460492	-2.15491	-0.084747	0.067799
3.796702	32671774	159.622595	-2.764583	1.718744	-1.413322	2.268715	-2.048454	-0.088924	0.061994
3.996525	32671822	159.094619	-2.995621	2.07828	-1.865287	2.054375	-1.789204	-0.064909	0.051778
4.196353	32671852	159.11165	-3.48687	2.437815	-2.263	1.757308	-1.662292	-0.067206	0.043438
4.39618	32671900	158.598272	-3.6689	2.755265	-2.493171	1.440603	-1.49405	-0.094353	0.036771
4.596004	32671930	159.622595	-4.139145	2.913388	-2.806315	1.061644	-1.259848	-0.082241	0.02805
4.795832	32671976	158.642067	-4.420358	3.221819	-3.061618	0.688116	-1.049025	-0.049665	0.019076
4.995659	32672024	159.260067	-4.552214	3.298777	-3.164138	0.363055	-0.824424	-0.077021	0.008379

Figure C1. Example .tmq model and carriage data file.

Relative Time	Relative Wave Heading	Global X	Global Y	Local X	Local Y	Avg Model Speed	N Global X	N Global Y	W Global X	W Global Y	S Global X	S Global Y	E Global X	E Global Y
sec	deg	m	m	m	m	kts	m	m	m	m	m	m	m	m
0	179.991306	790.215063	1687.647548	83.144964	103.798303	7.948508	821.193324	1599.84861	781.563324	1743.77861	902.993324	1698.70861	736.323324	1674.92861
0.199826	180.047199	790.216414	1686.852549	83.146051	103.817572		821.193404	1599.03386	781.563404	1742.96386	902.993404	1697.89386	736.323404	1674.11386
0.399653	180.072792	790.056325	1686.004469	82.985699	103.783759		821.193483	1598.219106	781.563483	1742.149106	902.993483	1697.079106	736.323483	1673.299106
0.599479	180.060719	790.139598	1685.16418	83.068708	103.757739		821.193563	1597.404356	781.563563	1741.334356	902.993563	1696.264356	736.323563	1672.484356
0.799305	180.101461	790.07614	1684.316408	83.004987	103.724235		821.193643	1596.589606	781.563643	1740.519606	902.993643	1695.449606	736.323643	1671.669606
0.999132	180.138949	789.958759	1683.443575	82.887342	103.665671		821.193723	1595.774852	781.563723	1739.704852	902.993723	1694.634852	736.323723	1670.854852
1.198958	180.178943	790.176347	1682.543272	83.104666	103.579636		821.193803	1594.960102	781.563803	1738.890102	902.993803	1693.820102	736.323803	1670.040102
1.398784	180.210969	789.896222	1681.649091	82.824278	103.499723		821.193883	1594.145353	781.563883	1738.075353	902.993883	1693.005353	736.323883	1669.225353
1.598611	180.234742	789.96352	1680.720017	82.891313	103.384917		821.193963	1593.330599	781.563963	1737.260599	902.993963	1692.190599	736.323963	1668.410599
1.798437	180.415166	790.352522	1679.8024	83.280051	103.281569		821.194043	1592.515849	781.564043	1736.445849	902.994043	1691.375849	736.324043	1667.595849
1.998263	180.35729	790.01821	1678.837362	82.945475	103.130799		821.194122	1591.701099	781.564122	1735.631099	902.994122	1690.561099	736.324122	1666.781099
2.198089	180.448779	789.690659	1677.84987	82.61766	102.957575		821.194202	1590.886345	781.564202	1734.816345	902.994202	1689.746345	736.324202	1665.966345
2.397916	180.43276	790.090542	1676.874291	83.017281	102.796265		821.194282	1590.071595	781.564282	1734.001595	902.994282	1688.931595	736.324282	1665.151595
2.597742	180.46657	790.145641	1675.893993	83.072115	102.630235		821.194362	1589.256845	781.564362	1733.186845	902.994362	1688.116845	736.324362	1664.336845
2.797568	180.476997	789.992802	1674.936049	82.919013	102.486559		821.194442	1588.442091	781.564442	1732.372091	902.994442	1687.302091	736.324442	1663.522091
2.997395	180.571589	789.907124	1673.934885	82.833071	102.299663		821.194522	1587.627341	781.564522	1731.557341	902.994522	1686.487341	736.324522	1662.707341
3.197221	180.609257	790.162276	1672.931267	83.08796	102.110314		821.194602	1586.812592	781.564602	1730.742592	902.994602	1685.672592	736.324602	1661.892592
3.397047	180.66757	790.105706	1671.947039	83.031126	101.940354		821.194682	1585.997842	781.564682	1729.927842	902.994682	1684.857842	736.324682	1661.077842
3.596874	180.72859	790.528478	1670.983687	83.453634	101.791271		821.194761	1585.183088	781.564761	1729.113088	902.994761	1684.043088	736.324761	1660.263088
3.7967	180.673554	790.107324	1670.014768	83.032217	101.63662		821.194841	1584.368338	781.564841	1728.298338	902.994841	1683.228338	736.324841	1659.448338
3.996526	180.737067	789.905128	1669.036094	82.829758	101.472214		821.194921	1583.553588	781.564921	1727.483588	902.994921	1682.413588	736.324921	1658.633588
4.196353	180.793185	790.157941	1668.049951	83.082307	101.300339		821.195001	1582.738834	781.565001	1726.668834	902.995001	1681.598834	736.325001	1657.818834
4.396179	180.774604	790.18978	1667.106588	83.113882	101.171245		821.195081	1581.924084	781.565081	1725.854084	902.995081	1680.784084	736.325081	1657.004084
4.596005	180.793638	790.160196	1666.199582	83.084034	101.078507		821.195161	1581.109334	781.565161	1725.039334	902.995161	1679.969334	736.325161	1656.189334
4.795832	180.835324	790.179165	1665.328071	83.102741	101.021264		821.195241	1580.29458	781.565241	1724.22458	902.995241	1679.15458	736.325241	1655.37458
4.995658	180.883832	789.925241	1664.427573	82.848552	100.935035		821.195321	1579.479831	781.565321	1723.409831	902.995321	1678.339831	736.325321	1654.559831
5.195484	180.896941	790.246877	1663.541763	83.169925	100.863493		821.1954	1578.665081	781.5654	1722.595081	902.9954	1677.525081	736.3254	1653.745081
5.39531	180.884935	790.260942	1662.697842	83.183727	100.83384		821.19548	1577.850327	781.56548	1721.780327	902.99548	1676.710327	736.32548	1652.930327
5.595137	180.885193	790.368023	1661.859031	83.290544	100.809297		821.19556	1577.035577	781.56556	1720.965577	902.99556	1675.895577	736.32556	1652.115577
5.794963	180.93299	790.128541	1661.067398	83.050798	100.831933		821.19564	1576.220827	781.56564	1720.150827	902.99564	1675.080827	736.32564	1651.300827
5.994789	181.011772	790.211204	1660.276158	83.133198	100.854962		821.19572	1575.406073	781.56572	1719.336073	902.99572	1674.266073	736.32572	1650.486073
6.194616	181.024692	789.803293	1659.479686	82.725023	100.872757		821.1958	1574.591323	781.5658	1718.521323	902.9958	1673.451323	736.3258	1649.671323
6.394442	180.904079	789.598499	1658.679646	82.519965	100.886985		821.19588	1573.776573	781.56588	1717.706573	902.99588	1672.636573	736.32588	1648.856573
6.594268	180.943787	789.665035	1657.928625	82.586238	100.950233		821.195959	1572.96182	781.565959	1716.89182	902.995959	1671.82182	736.325959	1648.04182
6.794095	180.980702	789.500583	1657.191005	82.421522	101.026881		821.196039	1572.14707	781.566039	1716.07707	902.996039	1671.00707	736.326039	1647.22707
6.993921	181.088941	790.29596	1656.475571	83.216636	101.125716		821.196119	1571.33232	781.566119	1715.26232	902.996119	1670.19232	736.326119	1646.41232
7.193747	180.979757	789.63417	1655.756062	82.554583	101.220475		821.196199	1570.51757	781.566199	1714.44757	902.996199	1669.37757	736.326199	1645.59757
7.393574	181.041384	790.023888	1655.030333	82.944037	101.309014		821.196279	1569.702816	781.566279	1713.632816	902.996279	1668.562816	736.326279	1644.782816
7.5934	180.945317	789.73424	1654.234037	82.654125	101.326986		821.196359	1568.888066	781.566359	1712.818066	902.996359	1667.748066	736.326359	1643.968066
7.793226	180.9768	789.59294	1653.534743	82.512562	101.441961		821.196439	1568.073316	781.566439	1712.003316	902.996439	1666.933316	736.326439	1643.153316
7.993053	180.981367	789.818705	1652.821776	82.738063	101.543262		821.196519	1567.258562	781.566519	1711.188562	902.996519	1666.118562	736.326519	1642.338562

Figure C2. Example .ttq tracker data file.

FILENAME:	C:\Users\HanyokLW\Desktop\m_5720_Melville_May_23\m5720-Melville\t01\Analysis\Post Test\(8) TMQ								
DATE:	3/6/2012								
TIME:	04:30.9								
NUMSAMPL	2832								
CMDSTARTT	32670966								
CHANNELNA	BP 1	BP 3	BP 4	BP 5	BP 6	BP 8			
UNITS:	m	m	m	m	m	m			
MEAN:	0.23814	-0.86419	0.51801	-0.23884	-0.0074778	0.26749			
STDDEV:	1.2706	1.318	0.92813	1.0193	1.3714	0.97185			
Count Time	BP 1	BP 3	BP 4	BP 5	BP 6	BP 8			
0	-0.591276	-2.054907	1.386668	-1.628472	2.04664	1.115193			
0.099912	-0.598646	-1.997815	1.337574	-1.655464	2.035589	1.07589			
0.199828	-0.594961	-1.891613	1.254114	-1.667733	2.014101	1.025532			
0.299739	-0.572237	-1.808125	1.236932	-1.684297	2.025766	0.939556			
0.399651	-0.586977	-1.727706	1.133835	-1.685523	1.977265	0.924817			
0.499563	-0.572851	-1.614752	1.089038	-1.68675	1.957005	0.826559			
0.599479	-0.556268	-1.566868	1.028284	-1.695338	1.929992	0.7805			
0.69939	-0.534772	-1.419536	0.939915	-1.687364	1.87658	0.709263			
0.799302	-0.526174	-1.337276	0.898186	-1.674481	1.843427	0.636797			
0.899218	-0.520647	-1.228618	0.785271	-1.664666	1.744582	0.598107			
0.99913	-0.480111	-1.102772	0.759496	-1.656691	1.712044	0.486952			
1.099042	-0.474584	-1.027264	0.660696	-1.613135	1.634074	0.467915			
1.198958	-0.427907	-0.875635	0.5846	-1.60332	1.532774	0.372113			
1.298869	-0.405182	-0.823454	0.542871	-1.564672	1.505761	0.307016			
1.398781	-0.377545	-0.669983	0.431183	-1.533386	1.351048	0.253588			
1.498693	-0.338238	-0.555187	0.408477	-1.48431	1.309301	0.159015			
1.598609	-0.30323	-0.485204	0.313358	-1.446889	1.198792	0.120325			
1.69852	-0.263923	-0.336031	0.250764	-1.422351	1.090739	-0.000041			
1.798432	-0.246112	-0.28692	0.183873	-1.343828	1.021978	-0.034432			
1.898348	-0.173641	-0.13836	0.108392	-1.315609	0.883842	-0.117952			
1.99826	-0.150916	-0.051188	0.069731	-1.247515	0.823062	-0.200243			
2.098171	-0.107311	0.047033	-0.024161	-1.190464	0.657913	-0.24446			
2.198088	-0.047122	0.158146	-0.050548	-1.153657	0.586082	-0.367283			
2.297999	-0.02624	0.225674	-0.127871	-1.035873	0.474959	-0.392461			
2.397911	0.040705	0.347836	-0.197215	-1.00704	0.316563	-0.483351			
2.497827	0.081239	0.383442	-0.223603	-0.913795	0.267449	-0.552746			
2.597739	0.134058	0.493941	-0.308903	-0.85429	0.07897	-0.603104			
2.69765	0.189948	0.583568	-0.326086	-0.772087	0.014506	-0.685395			
2.797562	0.237239	0.618559	-0.386226	-0.681909	-0.11749	-0.714873			
2.897478	0.298041	0.723533	-0.430411	-0.631605	-0.242734	-0.786724			
2.99739	0.331207	0.748089	-0.464162	-0.511981	-0.322546	-0.822957			

Figure C3. Example .twq bridge wave file.

This page intentionally left blank

APPENDIX D: IRREGULAR WAVE ROLL AND PITCH RAOs

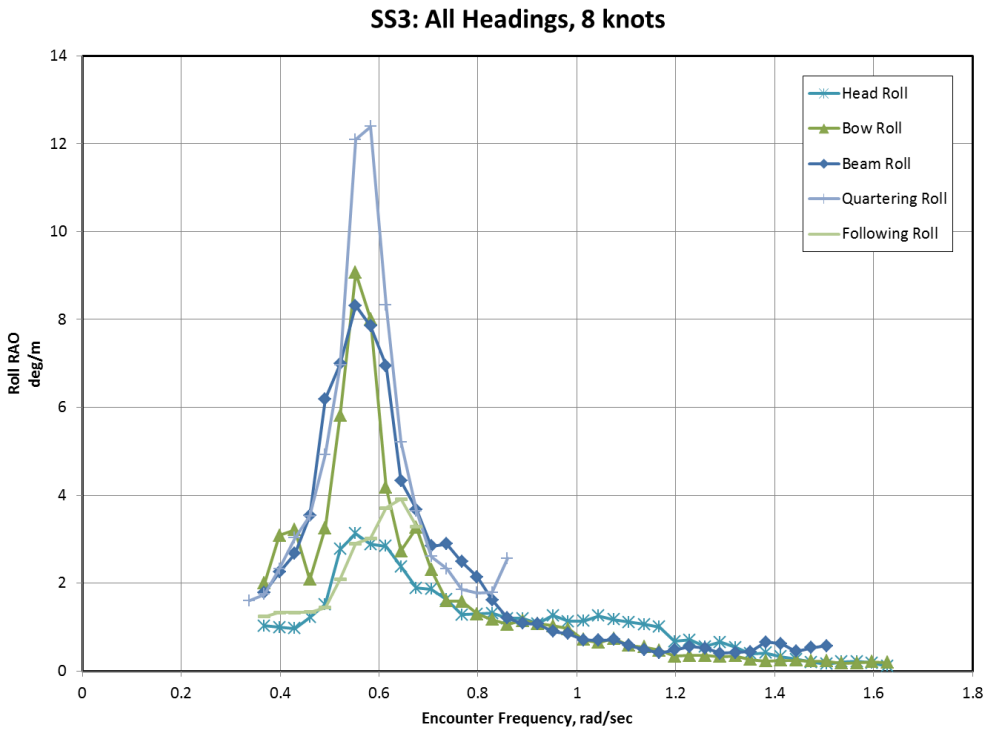

Figure D1. Roll RAOs, SS3, all headings, 8 knots

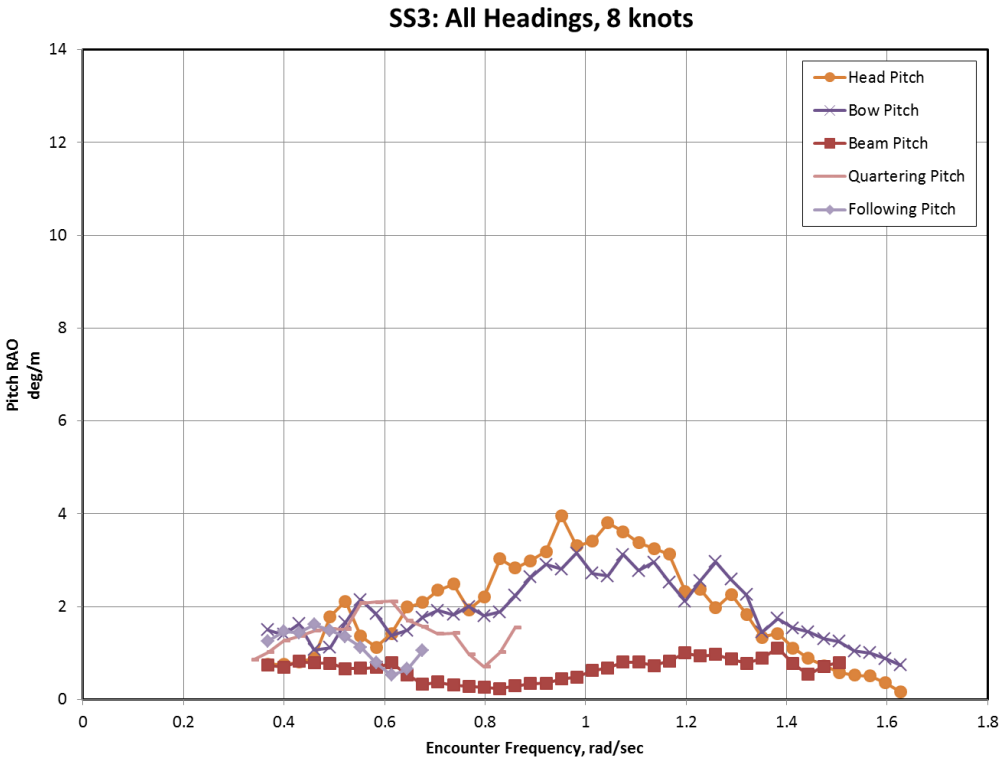

Figure D2. Pitch RAOs, SS3, all headings, 8 knots.

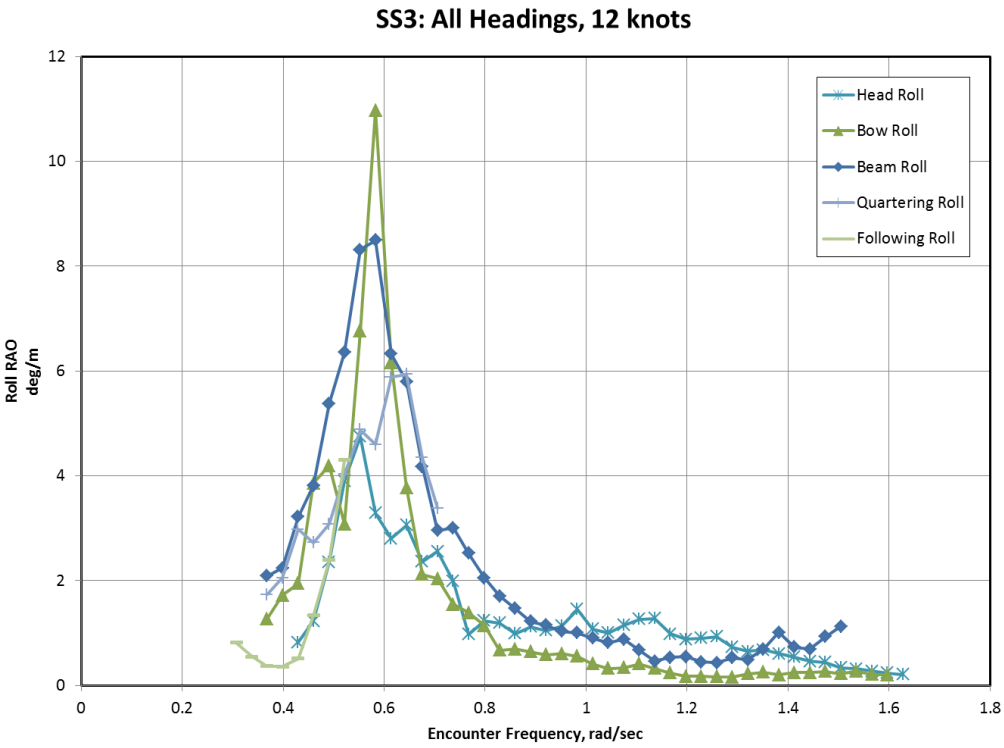

Figure D3. Roll RAOs, SS3, all headings 12 knots.

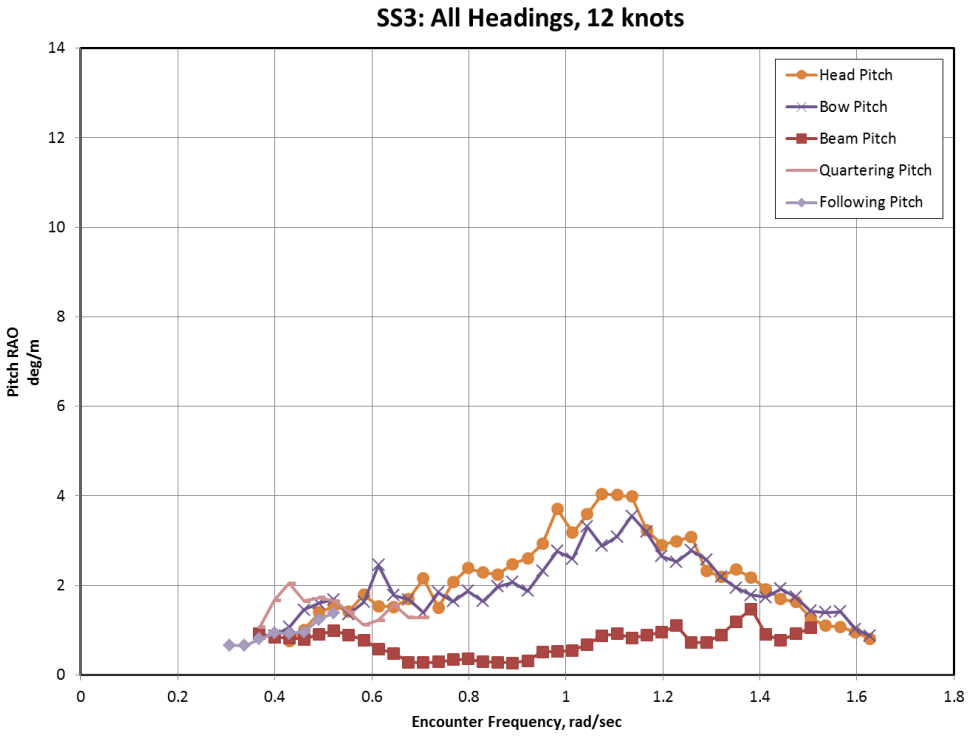

Figure D4. Pitch RAOs, SS3, all headings, 12 knots.

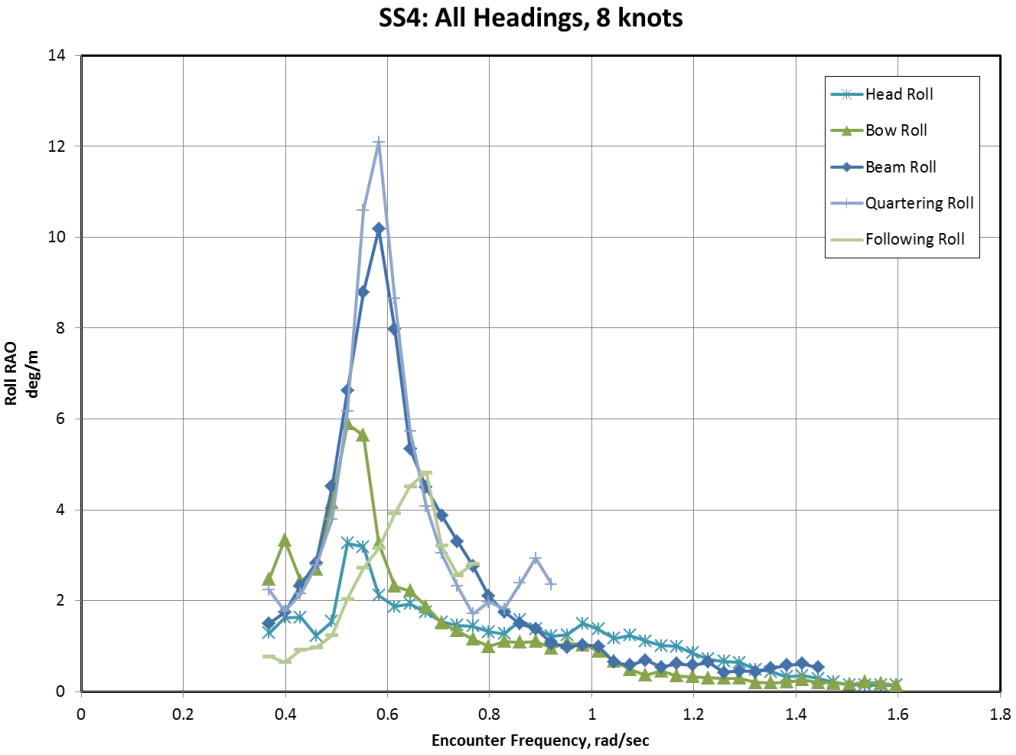

Figure D5. Roll RAOs, SS4, all headings, 8 knots.

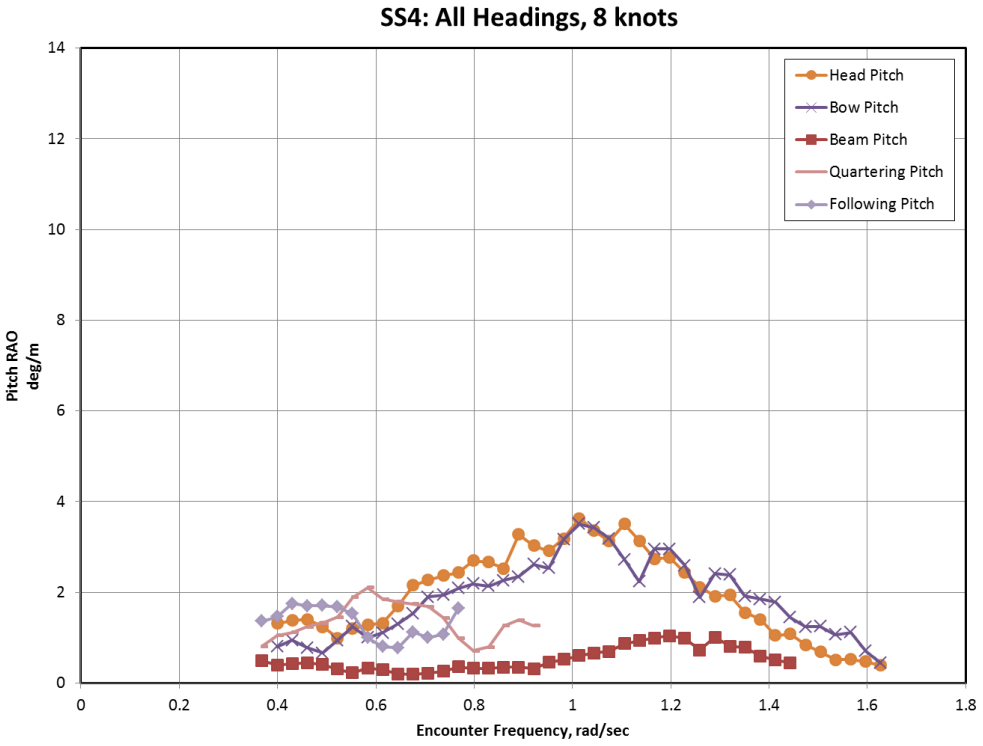

Figure D6. Pitch RAOs, SS4, all headings, 8 knots.

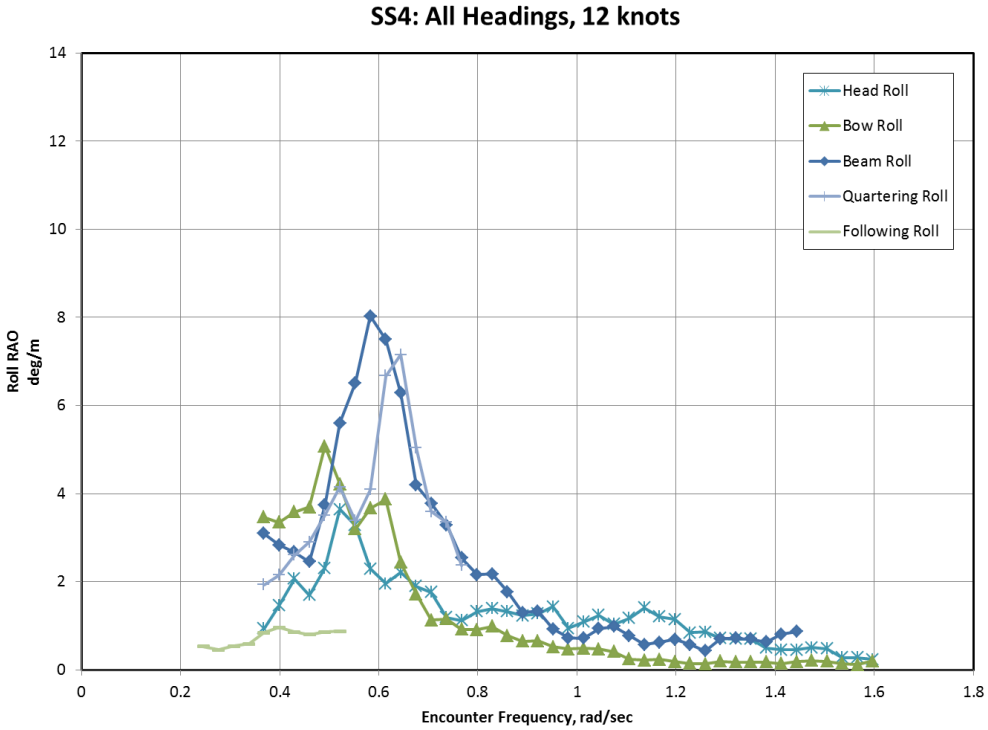

Figure D7. Roll RAOs, SS4, all headings, 12 knots.

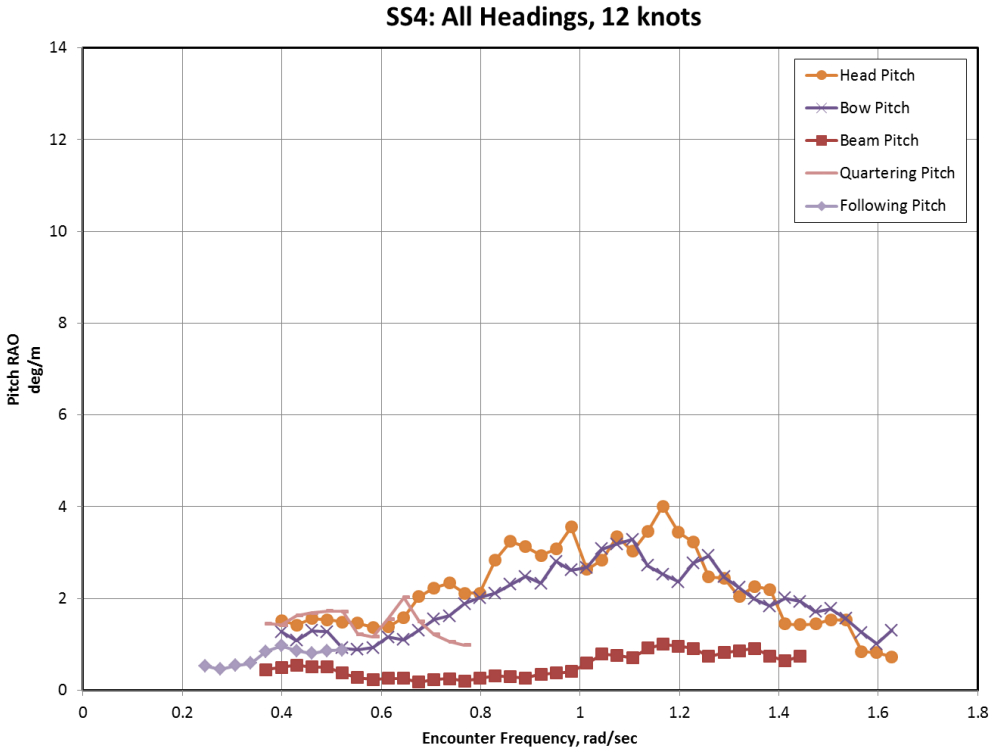

Figure D8. Pitch RAOs, SS4, all headings, 12 knots.

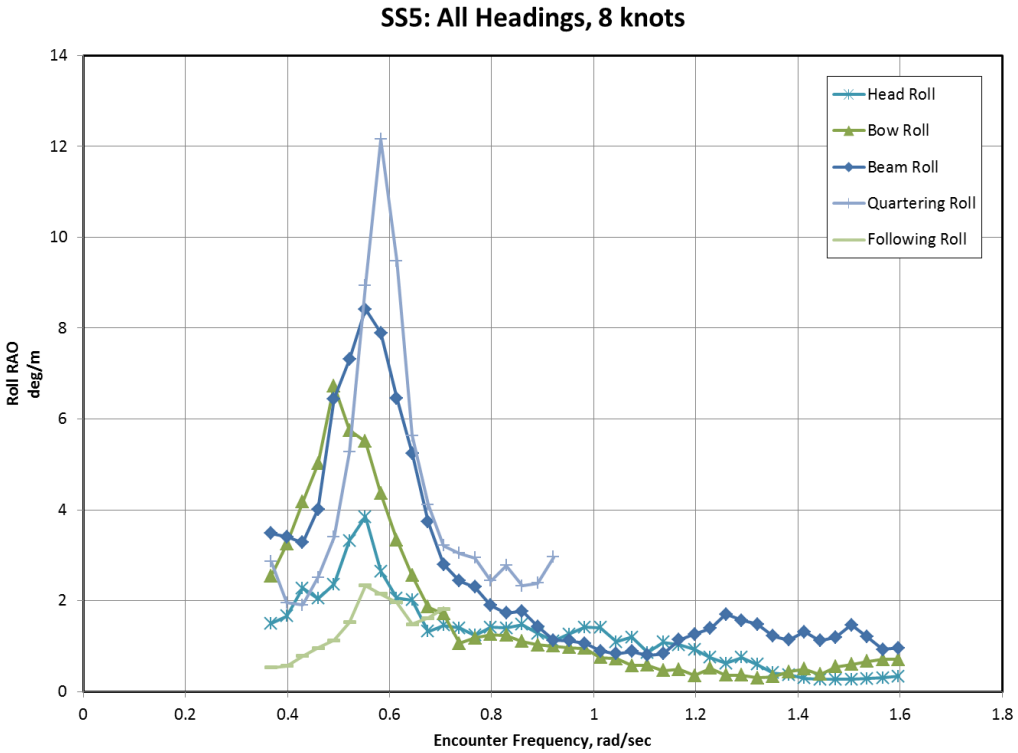

Figure D9. Roll RAOs, SS5, all headings, 8 knots.

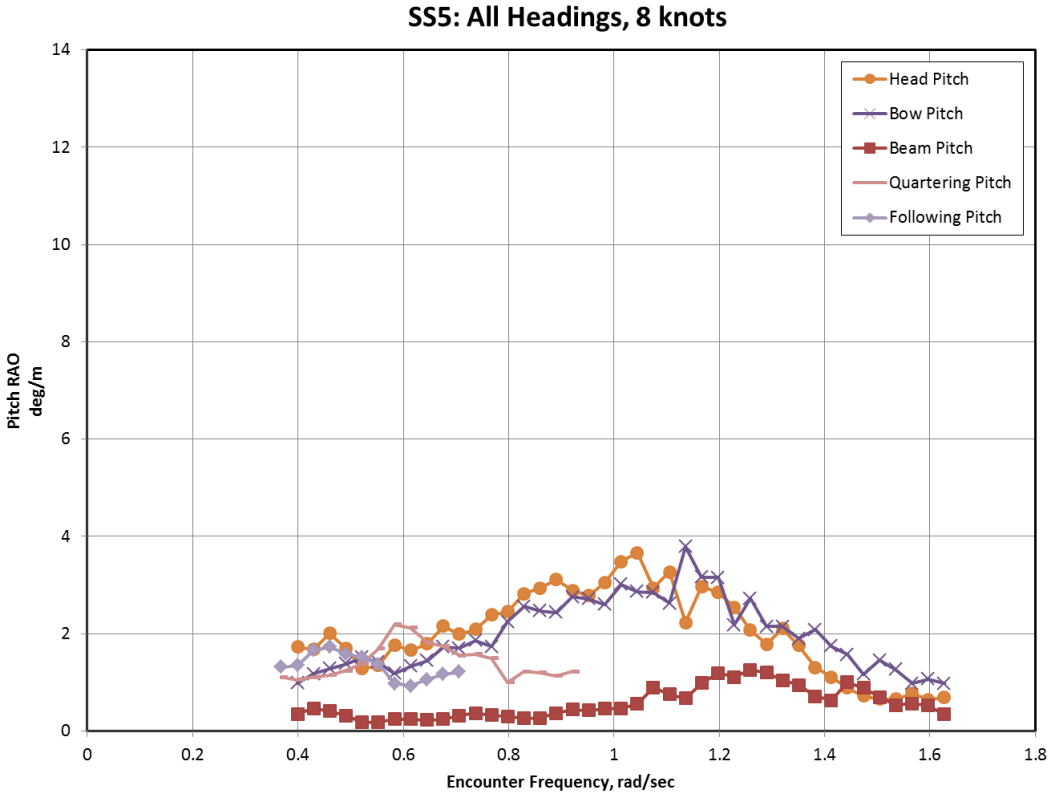

Figure D10. Pitch RAOs, SS5, all headings, 8 knots.

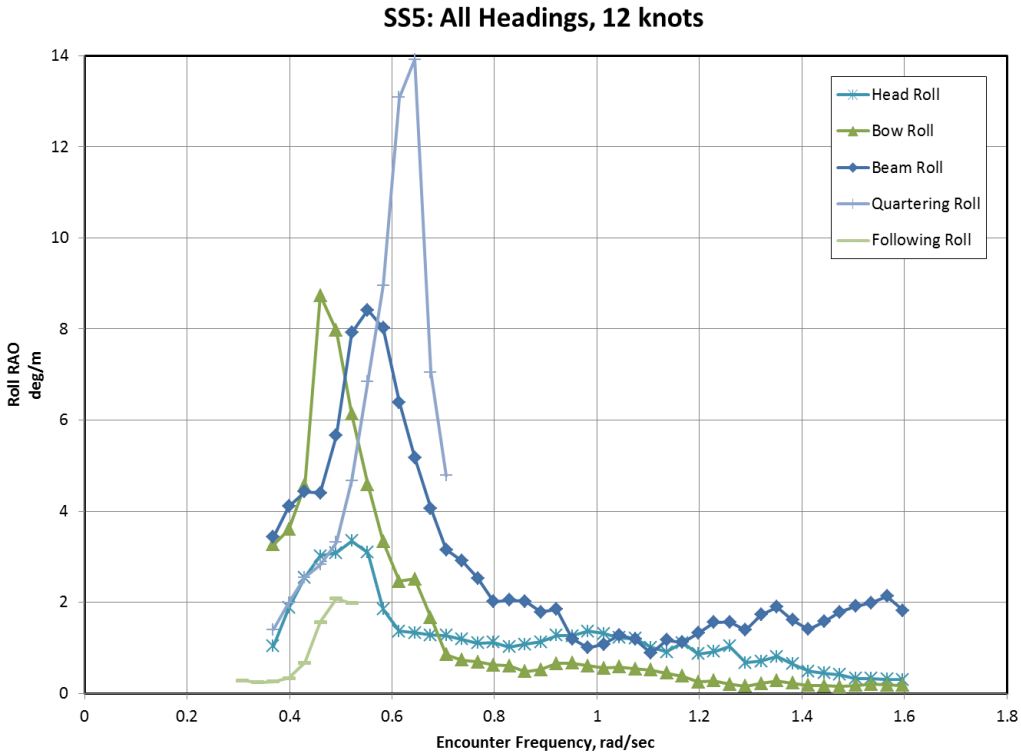

Figure D11. Roll RAOs, SS5, all headings, 12 knots.

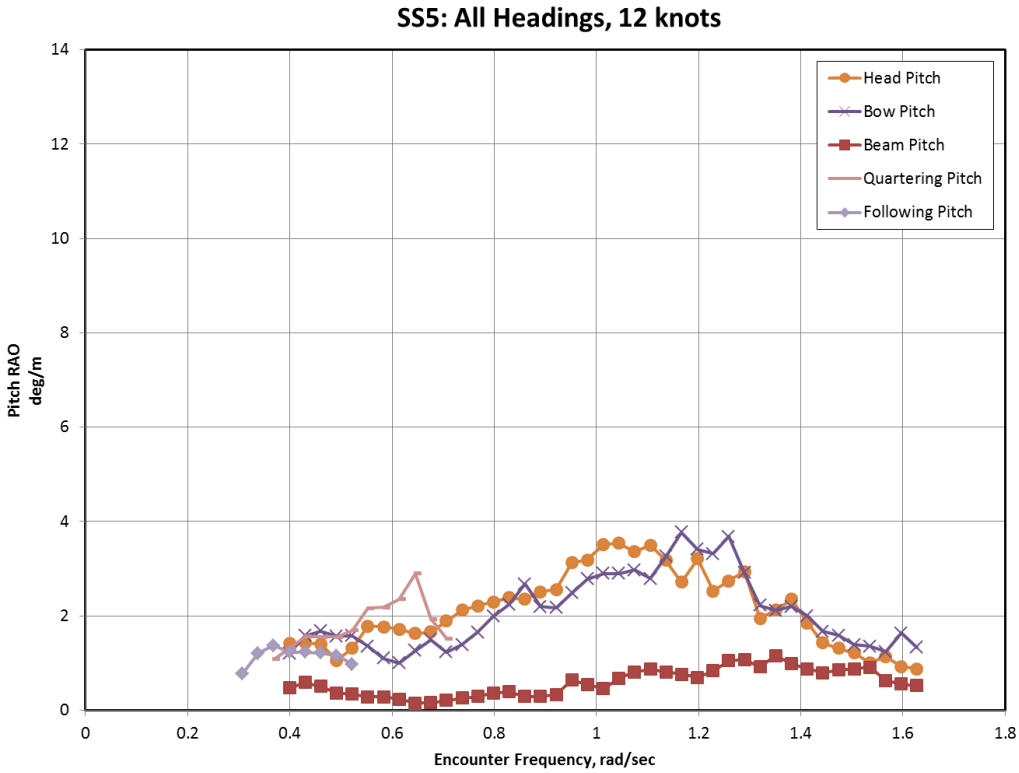

Figure D12. Pitch RAOs, SS5, all headings, 12 knots.

APPENDIX E: STATISTICAL UNCERTAINTY ANALYSIS

General Considerations

Statistical uncertainty differs from measurement uncertainty and is determined from a finite number of experimental records, while probabilistic concepts, such as variance, are defined for an infinite data set. As a result, the calculation of such quantities on any real-world data set is only an estimate of the actual quantity. The estimate is a random number, and as with any random number has its own distribution, mean value, and variance. The assessment of statistical uncertainty is a means of determining the variations in the data. It is typically performed using the boundaries of the confidence interval, where the true value is contained with a given confidence probability, such as 95%, which is used for most engineering applications.

There is a principal difference in the statistical uncertainty between a set of independent data points and a record of a stochastic process. The size of the sample of independent data points is defined by the number of points. In contrast, the size of a sample of records is not dependent on the number of points each individual record is comprised of (provided the time step is reasonable, with at least 7-10 points between local peaks), for the same reason that the amount of useful measured information cannot depend on a sampling rate. Thus, a method for assessment of statistical uncertainty must include the consideration of dependent continuous data within each record. The account for dependency is determined based on well-established statistical methods. For example, see Priestly (1981) and their adaptation for numerical simulation of ship motion data, such as from Belenky and Weems (2012). Specifics of the assessment of statistical uncertainty for results of a model test are the limited by the length of the record, due to the physical size of the MASK basin. This fact, since the length of the record cannot be manipulated, is an important consideration when comparing experimental data with a numerical simulation. The following sections details the process applied to determine the statistical uncertainty to a set of experimental data collected in the MASK basin.

Estimate of the Autocorrelation Function

The statistical significance of a record depends on, but is not completely defined by, its length. However, understanding how much statistical information a record contains is dependent on how fast or slow the autocorrelation function, R_j^*, dies out.

$$R_j^* = \frac{1}{N-j}\sum_{i=1}^{N-j}(x_i - m_X^*)(x_{i+j} - m_X^*) \tag{E.1}$$

where N is a number of points in a record and mX^* is an estimate of the mean value, obtained from the same record.

Figure E1 shows the autocorrelation functions estimated for two different records in the same ensemble, or irregular wave condition. The chosen records are of the similar length. The plot shows that the difference between the two records grows bigger with time. This "statistical noise" results from the decreasing amount of data available for the autocorrelation estimates with larger time difference. This "statistical noise" may be reduced by averaging estimates of autocorrelation function over a set of records (an ensemble).

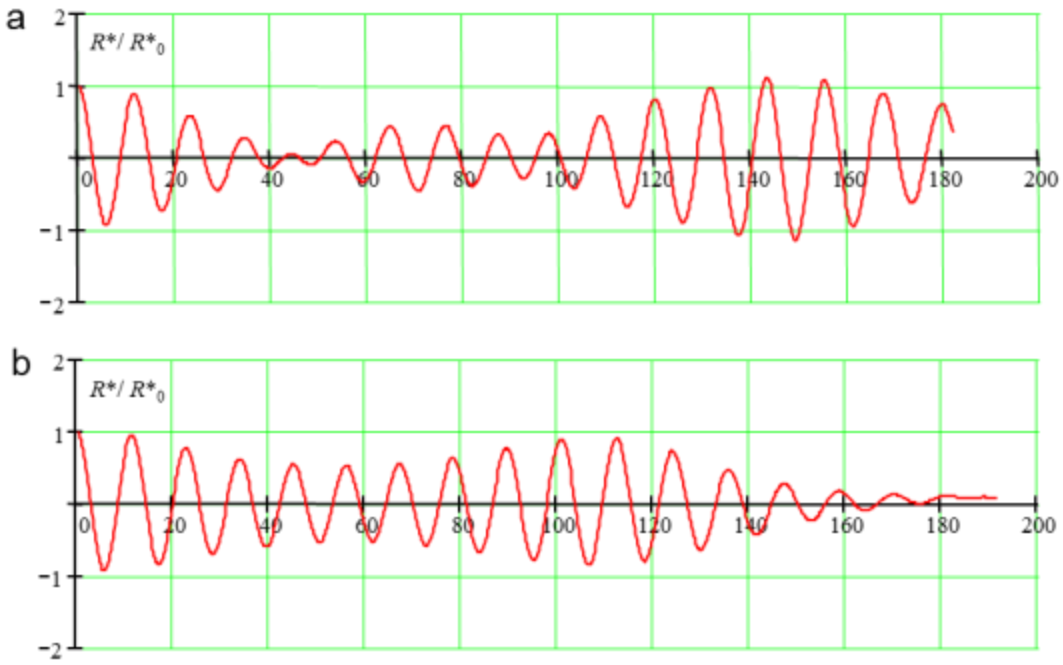

Figure E1. Autocorrelation Function Estimated on Two Records of the Similar Length (a) Run 669 duration 911 s, (b) Run 672, duration 959 s

The availability of several sample records can significantly decrease the statistical uncertainty, as the different records are independent of each other. Since the records may have different lengths, their relative statistical significance will differ, so the averaging should be performed with weights according to length (or number of points) of each record:

$$W_j = \frac{N_j}{\sum_{i=1}^{N_R} N_i} \tag{E.2}$$

where N_j is a number of points in the record j, while N_R is the total number of records. The weighted average estimate for the data set is expressed as:

$$R_a^*(\tau_i) = \sum_{j=1}^{N_R} \begin{cases} R_j^*(\tau_i) W_j & if \quad N_j \geq i \\ 0 & if \quad N_j < i \end{cases} \tag{E.3}$$

The result of averaging is shown in Figure E2. The level of "statistical noise" has decreased but has not been completely eliminated. It seems, this "statistical noise" begins somewhere between 40s and 80s, where the estimate of the autocorrelation function starts to grow again, but there are no physical reasons why the dependence becomes stronger with time.

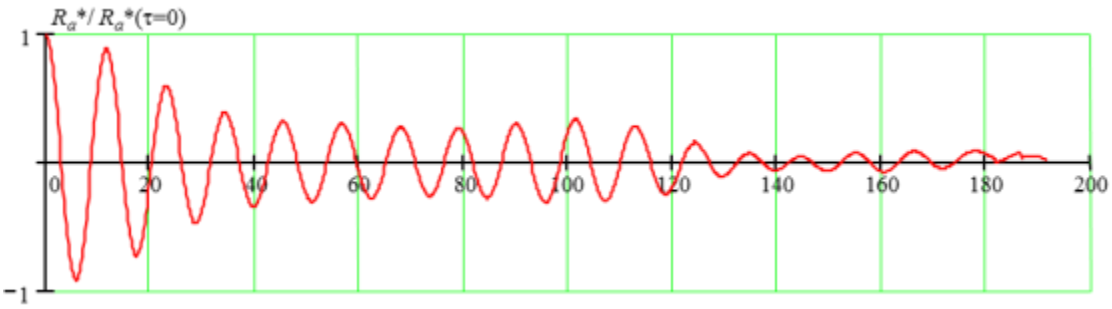

Figure E2. Estimate of Autocorrelation Function Averaged over the Ensemble

Averaged Spectrum

The direct time-domain computation (E.1) is not the only way to estimate the autocorrelation function. If a spectrum is known, it can also be evaluated using the known relation between the autocorrelation function, R, and the spectral density, $s(\omega)$.

$$R(\tau)=\int_0^{\infty} s(\omega)\cos\omega\tau\, d\omega \;; \qquad s(\omega)=\frac{2}{\pi}\int_0^{\infty} R(\tau)\cos\omega\tau\, d\tau \tag{E.4}$$

The evaluation of the spectral density for a time series is a standard procedure. For this numerical example, it was performed using a Fast Fourier Transform (FFT). The finite length of the sample record introduces statistical uncertainty into the estimated spectra; see Figure E3. This is a well-known issue that is typically resolved by smoothing the spectrum evaluated over a measured or simulated time series.

The averaging of the record spectra estimates over the ensemble has an effect similar to ensemble averaging of the estimate of autocorrelation function; see Figure E4.

$$R_a^*(\omega_i)=\sum_{j=1}^{n} S_j^*(\omega_i)W_j \tag{E.5}$$

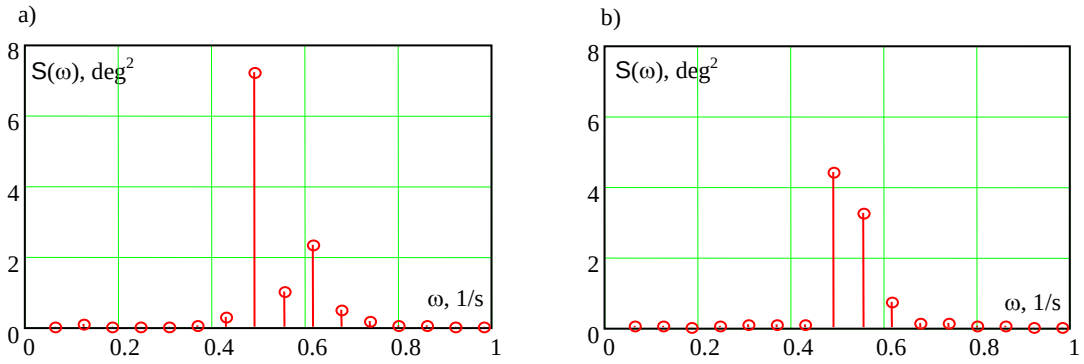

Figure E3. Spectra Estimated for Two Records of the Similar Length, (a) Run 669 duration 911 s, (b) Run 672, duration 959 s

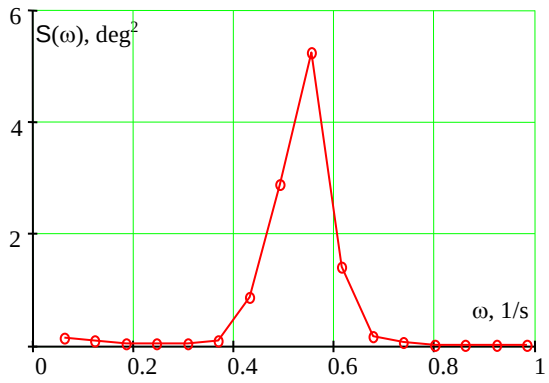

Figure E4. Estimate of the Spectrum Averaged over the Ensemble

As can be seen from Figure E4, the averaged spectrum is not smooth, but is "smoother" than the spectra estimated over individual records; see Figure E3 (a) or (b). This is an expected result, as the non-smoothness of a spectrum is equivalent to the "statistical noise" of the autocorrelation function.

Cut-Off Procedure for Estimate of Autocorrelation Function

Belenky & Weems (2012) describes a procedure for cutting-off an estimate of the autocorrelation function envelope. The envelope of the ensemble-averaged autocorrelation function is evaluated using the Hilbert transform:

$$E_R(\tau) = \sqrt{\left(R_a^*(\tau)\right)^2 + \left(Q_a^*(\tau)\right)^2} \tag{E.6}$$

Here Q_a^* is the result of Hilbert transform of the ensemble-averaged autocorrelation function, and is defined as follows:

$$Q_a^*(\tau) = \int_0^\infty \left(C_I(\omega)\cos(\omega\tau) - C_R(\omega)\sin(\omega\tau)\right)d\omega \tag{E.7}$$

where C_R and C_I are the real and imaginary parts of the Fourier coefficients of R_a^*. The Hilbert transform produces a complimentary function to R_a^* by shifting it 90 degrees. Numerically, the transformation was performed using a combination of direct and inverse FFT. The results are shown in Figure E5.

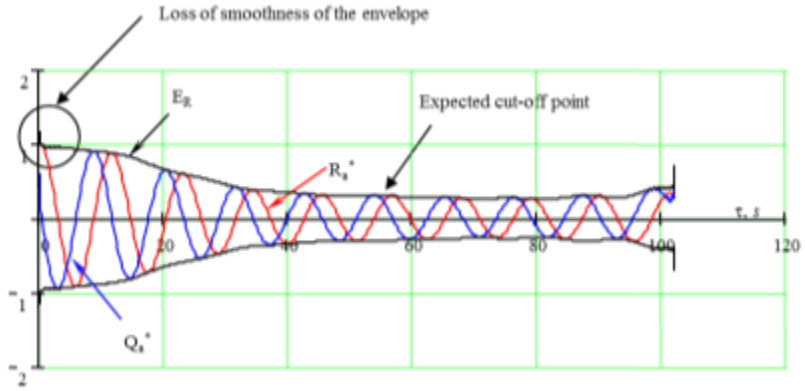

Figure E5. Ensemble-averaged Autocorrelation Function, its Hilbert Transform and the Envelope

The envelope loses it smoothness close to zero. This effect was not further studied here, as the objective was to find the minimum of the envelope and use it as a cut-off point. To avoid the influence of this non-smoothness, the minimum was searched by checking a local minimum among specified number of points of the envelope. For additional reliability, the search for the minimum can be repeated for a different number of points to see if it yields the same result. For the present numerical example, 10- and 12-point searches were used.

To avoid negative values for the variance of the mean that had been traced to an abrupt cut-off of the autocorrelation function, a power function was applied beyond the cut-off point:

$$R_C(\tau) = \begin{cases} R_a^*(\tau) & \tau < \tau_c \\ R_a^*(\tau)\, f_{cut}(\tau) & \tau \geq \tau_c \end{cases} \tag{E.8}$$

weere τ_c is the time corresponding to the cut-off point. The function f_{cut} was taken in the following form:

$$f_{cut}(\tau) = C_1 \exp\left(\psi \cdot \left(-\mu + \sqrt{\mu^2 - 1}\right) \cdot t\right) + C_2 \exp\left(\psi \cdot \left(-\mu - \sqrt{\mu^2 - 1}\right) \cdot t\right) \tag{E.9}$$

where C_1, C_2, μ, ψ are parameters of the cut-off function defined, as:

$$C_1 = \frac{\mu + \sqrt{\mu^2 - 1}}{2\sqrt{\mu^2 - 1}} \quad ; \quad C_2 = \frac{-\mu + \sqrt{\mu^2 - 1}}{2\sqrt{\mu^2 - 1}} \quad ; \quad \psi = -\frac{\ln(d)}{T_d} \quad ;$$
$$\mu = 1.000001 \quad ; \quad d = 0.001 \quad ; \quad T_d = \tau_c \tag{E.10}$$

The result of the cut-off procedure is shown in Figure E6. The automatic search for the cut-off point was found to be unreliable for short duration records, especially when the measured motions were small, therefore for this analysis, a manual setting of the cut-off point was used.

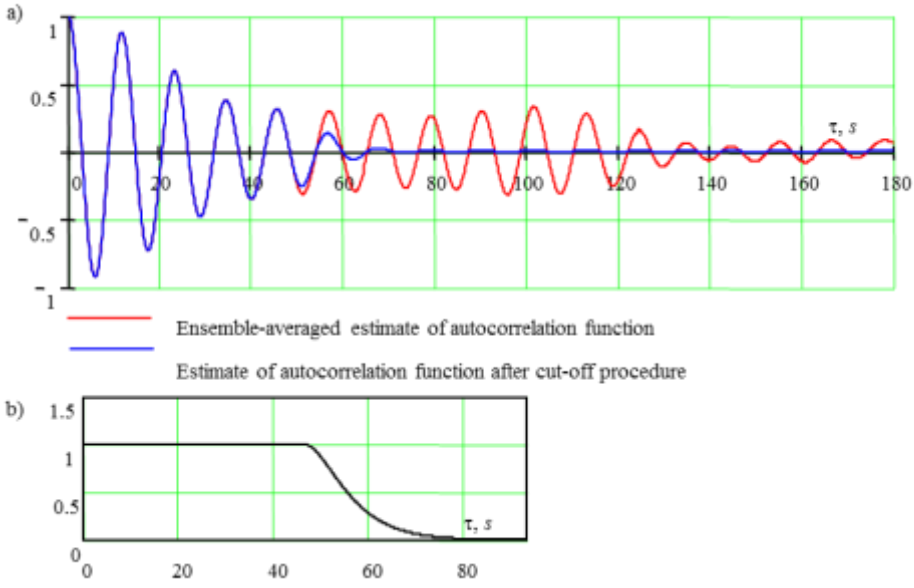

Figure E6. Result of the Cut-Off Procedure Applied to the Ensemble-Average Estimate of Autocorrelation Function; (a) Estimates of Autocorrelation Function, (b) Cut-off function

Comparison of Spectra

In principle, the spectrum evaluated with FFT can be smoothed. However, an attempt to use a low pass filter (when applicable) returned a trivial result, due to the limited duration of record and related frequency resolution. As a result, the ensemble-averaged spectrum (when available) was only used for visual comparison with the spectrum calculated from autocorrelation function with the cosine Fourier transform (E.4). Using the accepted frequency set and rectangles method for numerical integration, the spectral density was calculated as follows:

$$s(\omega_j) = \frac{2}{\pi} \sum_{i=1}^{N} R(\tau_i) \cos(\omega_j \tau_i) \Delta\tau \tag{E.11}$$

here $\Delta\tau$ is the time-step for the autocorrelation function. In this example, the time-step is equal to the time-step of the time series. Using the method of rectangles, the estimate of power spectrum can be evaluated:

$$S_{C0}(\omega_i) = \int_{\omega_i - 0.5\Delta\omega}^{\omega_i + 0.5\Delta\omega} s(\omega_i) d\omega = s(\omega_i) \Delta\omega \tag{E.12}$$

Figure E7 compares the two methods for estimating the spectra. This comparison was used as a "quality" check during statistical processing.

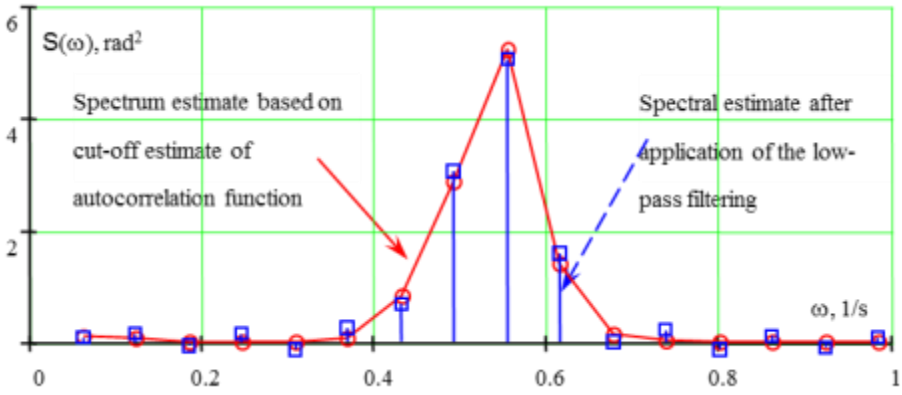

Figure E7 Spectral Estimates Calculated from Cut-off Autocorrelation Function (red) and Evaluated with FFT (blue)

Calculation of Autocorrelation Function from Spectrum

The cosine Fourier transform (E.4) also allowed for the evaluation of the autocorrelation function from the spectrum. Using the accepted frequency set and rectangles method for numerical integration, the autocorrelation function was calculated as follows:

$$R(\tau_i) = \sum_{j=1}^{N_\omega} S(\omega_j) \cos(\omega_j \tau_i) \tag{E.13}$$

Figure E8 shows the normalized autocorrelation function, as calculated from the averaged spectrum and estimated from the time-domain, with a further application of ensemble averaging and the cut-off procedure. The autocorrelation function calculated from spectrum exhibits self-

repeating behavior caused by insufficient frequency resolution of the spectrum estimate. As a result, only its first part was used for comparison.

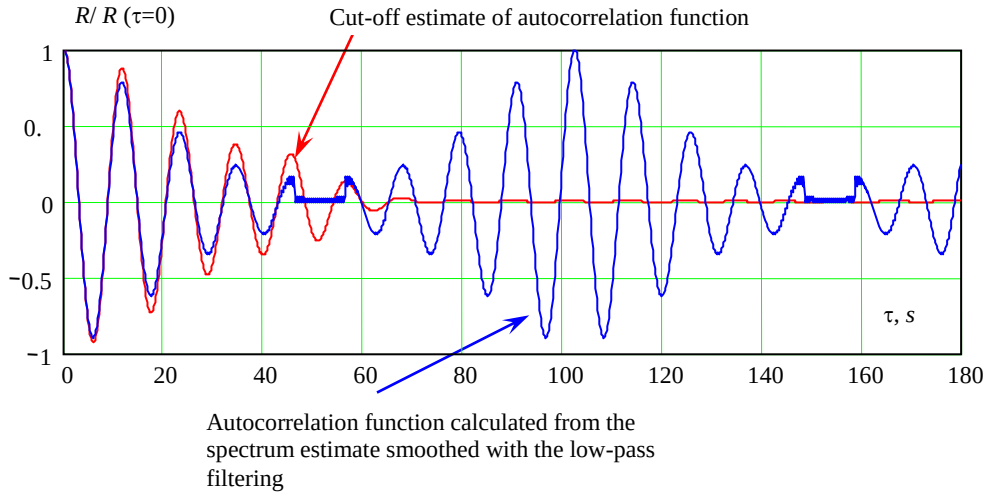

Figure E8 Comparison of Autocorrelation Function Calculated with Two Different Methods: Time-Domain Estimate with Cut-off Procedure (Red) and FFT-based Spectrum w (Blue)

Statistical Uncertainty of the Average and Variance of a Record

Estimates of the average and the variance of the record are expressed with well-known formulae. The variance can be estimated using the true value of the average m_X (if known), or its estimate m_X^* .

$$m_X^* = \frac{1}{N}\sum_{i=1}^{N} x_i \tag{E.14}$$

$$V_X^* = \frac{1}{N}\sum_{i=1}^{N}\left(x_i - m_X\right)^2 = \frac{1}{N}\sum_{i=1}^{N}\left(x_i - m_X^*\right)^2 \tag{E.15}$$

where N is a number of data points available.

These estimates are random numbers, as they are a sum and a sum of squares of a set of random numbers x_i. As for any other random number, they have their own mean values and variances.

The mean value of the average is equal to itself, as the average is an unbiased estimate:

$$m\left(m_X^*\right) = m_X^* \tag{E.16}$$

The mean value of the variance is not equal to itself, as the variance estimate is slightly biased. This bias can be removed with another well-known formula:

$$m\left(V_X^*\right) = \frac{N}{N-1}V_X^* \tag{E.17}$$

The evaluation of the variance of the mean and the variance of the variance is more complex as the variance of estimates bears information on statistical uncertainty. The variance of the mean for a set of dependent data points x_i is expressed as (Priestley 1981):

$$V\left(m_X^*\right)=\frac{1}{N}\sum_{i=-N}^{N}R\left(\tau_{|i|}\right)\left(1-\frac{|i|}{N}\right) \tag{E.18}$$

Here the dependency is defined by the autocorrelation function $R(\tau)$, and symbol $|i|$ is used as "absolute value of *i*." The variance of the variance is expressed as (Belenky and Weems, 2012).

$$V\left(V_X^*\right)=\frac{2}{N}\sum_{i=-N}^{N}\left(R\left(\tau_{|i|}\right)\right)^2\left(1-\frac{|i|}{N}\right) \tag{E.19}$$

The Normal distribution is assumed for the mean value estimates, based on the Central Limit Theorem. It is completely defined with the mean value and the variance, and the confidence interval can be calculated as:

$$\text{Mean value}\quad m_X^*\pm\Delta m_X^*\quad \Delta m_X^*=K_\beta\sqrt{V\left(m_X^*\right)} \tag{E.20}$$

$$K_\beta=Q_N\left(1-0.5(1-\beta)\right);\quad Q_N=\Phi^{-1} \tag{E.21}$$

Here Q_N is the inverse function to normal cumulative distribution function with zero mean and unity variance, and β is an accepted confidence probability. Numerical results for β=0.95 are shown in Figure E9.

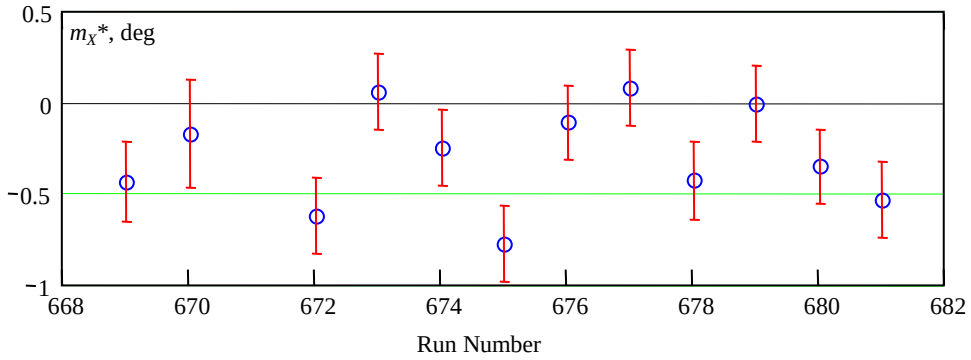

Figure E9. Mean Value Estimates of Each Record with Confidence Intervals

However, use of the normal distribution for variance, may formally lead to negative values of the estimate (which is impossible since the variance is a positive value by definition), because the normal distribution allows for negative values. However, the zero-truncated normal distribution does not have these limitations. It is defined as:

$$f\left(v;k,p_1,p_2\right)=\begin{cases}0 & v<0\\ \dfrac{k}{\sqrt{2\pi p_2}}\exp\left(-\dfrac{\left(v-p_1\right)^2}{2p_2}\right) & v\geq 0\end{cases} \tag{E.22}$$

where v is the random variable, k is a normalizing factor needed to make sure that the area under the PDF equals 1. The parameters p_1 and p_2 took the place of mean value and variance: the truncated normal distribution no longer have direct used of the mean value and the variance as parameters.

As a result, the norm factor k as well as the parameters p_1 and p_2 need to be found form the following system of algebraic equations

$$\begin{cases} \int_0^\infty f(v;k,p_1,p_2)dv = 1 \\ \int_0^\infty f(v;k,p_1,p_2)v dv = m\left(V_\phi^*\right) \\ \int_0^\infty f(v;k,p_1,p_2)\left(v - m\left(V_\phi^*\right)\right)^2 dv = V\left(V_\phi^*\right) \end{cases} \quad \text{(E.23)}$$

Examples of these distributions are shown in Figure E10. Once the distribution has been accepted, in principal further calculation of the boundaries of confidence interval V_{Low}^* and V_{Up}^* does not provide any difficulties.

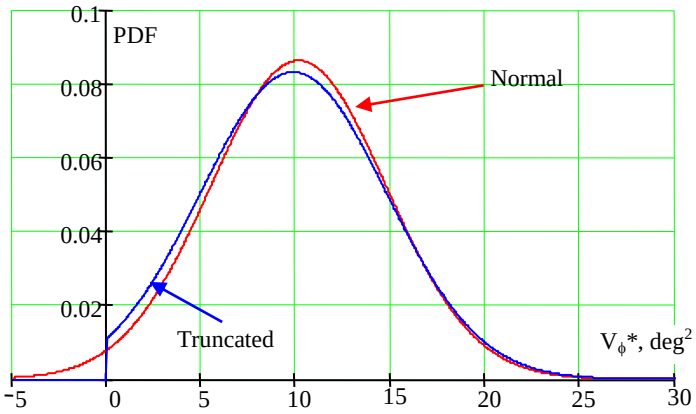

Figure E10. Use of Truncated Normal Distribution for the Estimate of Variance

$$V_{Low}^* = Q_T\left(0.5(1-\beta)\right);\ \ V_{Up}^* = Q_T\left(0.5(1+\beta)\right) \quad \text{(E.24)}$$

where β is the confidence probability, while Q_T is an inverse function to CDF of truncated normal distribution F:

$$F(v;k,p_1,p_2) = \begin{cases} 0 & v < 0 \\ \int_0^v \frac{k}{\sqrt{2\pi p_2}} \exp\left(-\frac{(z-p_1)^2}{2p_2}\right) dz & v \geq 0 \end{cases} \quad \text{(E.25)}$$

Figure E11 shows the results of these calculations the estimates of variance with confidence interval.

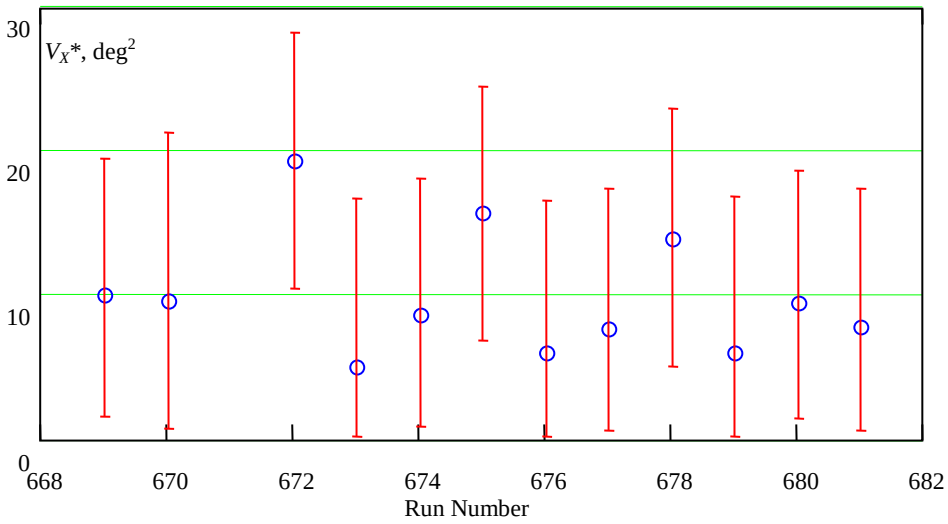

Figure E11. Variance Estimates of Each Record with Confidence Intervals

Statistical Uncertainty of Average and Variance of an Ensemble

The next step is calculating estimates of the entire ensemble of records with their corresponding confidence intervals. The estimate of the mean value is expressed as a weighted average, with the statistical weight W_i defined by (E.2):

$$m_{AX}^{*} = \sum_{i=1}^{N_R} W_i m_{Xi}^{*} \tag{E.26}$$

where m_{Xi}^{*} is the mean value estimate of record number, *i*, defined by formula (E.14).

Evaluation of the confidence interval required the variance of the mean. This can be calculated by applying the variance operator to both sides of (E.26) and taking into account that the random values m_{Xi}^{*} are deemed independent (as they were estimated over independent records) and weights W_i are deterministic numbers. The variance of the mean of the ensemble can be expressed as:

$$V\left(m_{AX}^{*}\right) = \sum_{i=1}^{N_R} W_i^2 V\left(m_{Xi}^{*}\right) \tag{E.27}$$

$V\left(m_{Xi}^{*}\right)$ is the variance of the mean of record number *i*

The results of the calculations for the numerical example are given in Figure E12; the width of the confidence interval for the ensemble is narrower than for any of the records. This is expected, as the ensemble contains more statistical information.

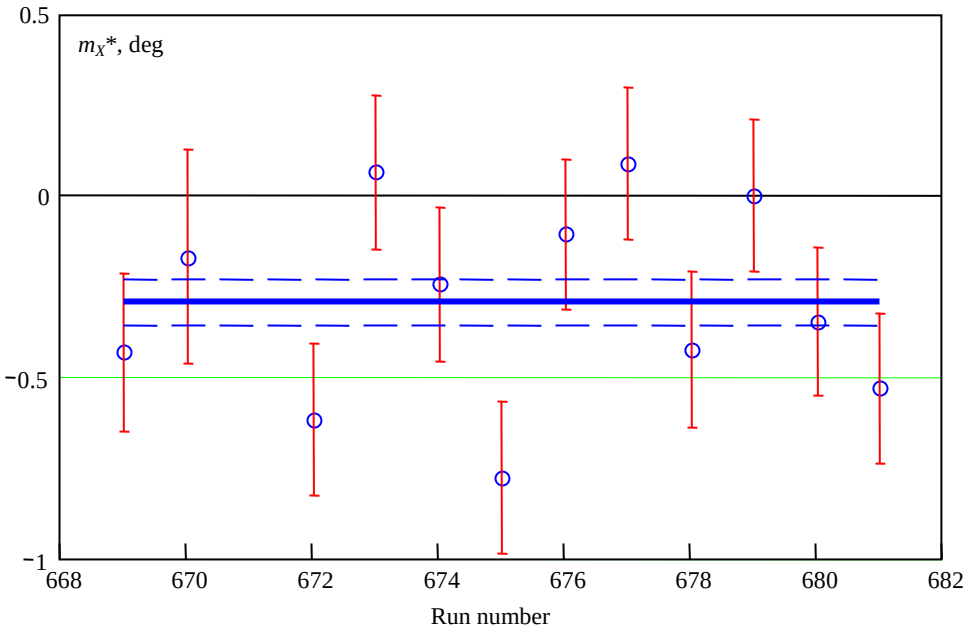

Figure E12. Mean Value and Confidence Interval for Ensemble and Records

The variance estimate of the ensemble can be expressed in a similar way, but it is more convenient to consider the estimate of the second raw moment. The estimate of second raw moment is defined as:

$$\alpha^*_{2i} = \frac{1}{N_i}\sum_{j=0}^{N_i} x^2_{ij} \qquad \text{(E.28)}$$

i

The estimate of the second raw moment relates to the estimate of the variance and mean value in the same way that true values do:

$$V^*_X = \alpha^*_2 - \left(m^*_X\right)^2 \qquad \text{(E.29)}$$

Consider the estimate of second initial moment for the ensemble:

$$\alpha^*_{2A} = \sum_{i=1}^{N_R} W_i \alpha^*_{2i} \qquad \text{(E.30)}$$

Finally, the estimate of the variance of the ensemble is expressed as:

$$V^*_A = \sum_{i=1}^{N_R} W_i \left(V^*_{Xi} + m^2_{Xi}\right) - \left(m^*_{AX}\right)^2 \qquad \text{(E.31)}$$

If the mean value estimates are zero or close to zero (in comparison with the variance estimates), then:

$$V^*_A = \sum_{i=1}^{N_R} W_i V^*_{Xi} \qquad \text{(E.32)}$$

The evaluation of the confidence interval for the variance estimate requires the evaluation of the variance of the variance. This can be done by applying the variance operator to both parts of (E.32):

$$V\left(V_{AX}^{*}\right)=V\left(\sum_{i=1}^{N_R} W_i V_{Xi}^{*}\right)=\sum_{i=1}^{N_R} W_i^{2} V\left(V_{Xi}^{*}\right) \tag{E.33}$$

Formula (E.33) is only applicable if the mean values are small in comparison with the variances. Figure E13 shows the results of calculating the confidence interval for the variance estimate of the ensemble together with estimates of each individual record. As for the mean values, it shows a dramatic decrease of the width of the confidence interval, once the statistical data of all the records are included.

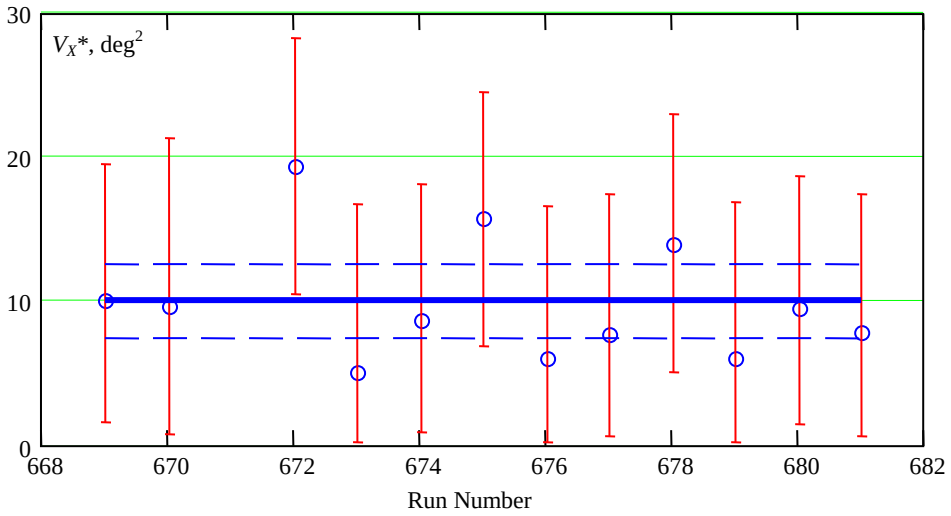

Figure E13. Mean Value and Confidence Interval for Ensemble and Records

REFERENCES

Armitage, P. (1971), Statistical Methods in Medical Research, Oxford: Blackwell Scientific Publications, pp. 289-291.

Belenky, V. and K. M. Weems (2012) "Probabilistic Properties of Parametric Roll", Chapter 6 of *Parametric Resonance in Dynamical Systems*, Fossen, T. I.; Nijmeijer, H. (Eds.) Springer, NY. ISBN 978-1-4614-10423-0

Carroll, R. J., C. H. Spiegelman, and J. Sacks, (1988), "A Quick and Easy Multiple-Use Calibration-Curve Procedure," *Technometrics*, 30(2), pp. 137-141.

The Glosten Associates (2010), "*R/V Melville Trim and Stability Book: Revision B*," File No. 06110, January.

Gust, J. C., R. M. Graham, and M. A. Lombardi (2009), "Stopwatch and Timer Calibrations," *NIST Special Publication 960-12*, National Institute of Standards and Technology, U. S. Department of Commerce, Washington, DC.

ITTC(2008a), "Guide to the Expression of Uncertainty in Experimental Hydrodynamics", ITTC Procedure 7.5-02-01-01, Revision 01, *Proc. 25th International Towing Tank Conference.*

ITTC (2008b), "Uncertainty Analysis - Instrument Calibration," ITTC Procedure 7.5-01-03-01, *Proc. 25th International Towing Tank Conference*.

ITTC (2008c), "The Specialist Committee on Uncertainty Analysis: Final Report and Recommendations to the 25th ITTC," *Proc. 25th International Towing Tank Conference*, Vol. II, pp. 433-471,.

JCGM (2008), "Evaluation of Measurement Data – Guide to the Expression of Uncertainty in Measurement," JCGM 100.

Kleinbaum, D. G., L. L. Kupper, and K. E. Muller (1988), *Applied Regression Analysis and Other Multivariable Methods*, Second Edition, Boston: PWS-Kent Publishing Company, pp. 266-269.

Moose, R. E. (1986), "The National Geodetic Survey Gravity Network," *NOAA Technical Report NOS 121 NGS 39*, National Oceanic and Atmospheric Administration, U. S. Department of Commerce, Washington, DC.

NATO STANAG 4194 (1983), "Standardized Wave and Wind Environments and Shipboard Reporting of Sea Conditions," 6 April.

NIST (2012), "Specifications, Tolerances, and Other Technical Requirements for Weighing and Measuring Devices," *NIST Handbook 44*, Tina Butcher, Steve Cook, Linda Crown, and Rick Harshman (Editors), National Institute of Standards and Technology, U. S. Department of Commerce, Washington, DC.

Park, J. T., J. M. Crum, and F. Rodriguez (2010), "Wheel #2 Diameter Measurements at David Taylor Model Basin Carriage #1 for Carriage Speed and Position," *Technical Report NSWCCD-50-TR—2010/040*, Naval Surface Warfare Center Carderock Division, West Bethesda, Maryland USA.

Park, J. T. and M. J. Dipper (2011), "User Calibration of Instrumentation," Procedure Number 00-5500-114-04, Naval Surface Warfare Center Carderock Division, West Bethesda, Maryland USA.

Pierce, R. D. (1985), "Extreme Value Estimates for Arbitrary Bandwidth Gaussian Processes Using the Analytic Envelope," *Ocean Engineering*, 12.

Priestley, M. B. (1981). *Spectral Analysis and Time Series*, Vol. 1, Academic Press, New York.

Ross, S. M. (2004), *Introduction to Probability and Statistics for Engineers and Scientists*, Third Edition, Amsterdam, Elsevier Academic Press.

Scheffe, H. (1973), "A Statistical Theory of Calibration," *The Annals of Statistics*, 1(1), pp. 1-37.

Initial Report Distribution

Number of Copies	Office	Individual	Type
1	ONR 331	P. Hess	Electronic
1	DTIC		Electronic

Number of Copies	NSWCCD Code	Individual	Type
1	3452 (Library)	(pdf only)	Electronic
1	50	J. Etxegoien	Electronic
1	504	A. Reed	Electronic
1	505	T. Fu	Electronic
1	5500	M. Dipper	Electronic
1	551	T. Smith	Electronic
1	552	D. Hayden	Electronic
1	5510	C. Bassler	Electronic
1	5510	V. Belenky	Electronic
1	5510	W. Belknap	Electronic
1	5510	B. Campbell	Electronic
1	5510	M. Hughes	Electronic
1	5510	A. Silver	Electronic
1	5520	L. Hanyok	Electronic
1	5520	M. Melendez	Electronic
1	5520	C. Turner	Electronic
1	5520	J. Park	Electronic
1	5620	L. Minnick	Electronic
1	5820	R. Hurwitz	Electronic
1	2202	H. Tomaszek	Electronic

Total Copies

22

This page intentionally left blank